



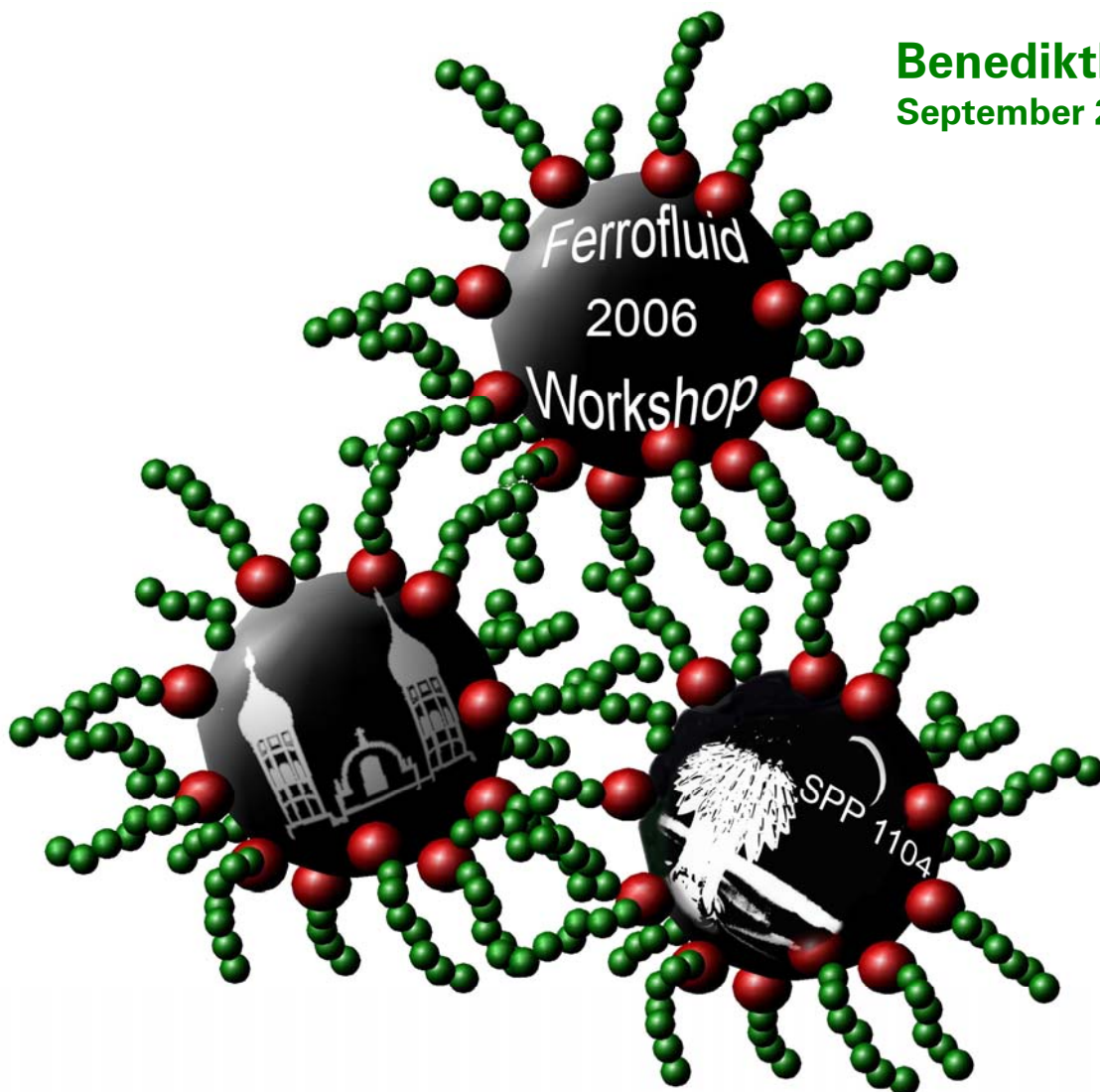
TECHNISCHE
UNIVERSITÄT
DRESDEN

7th German Ferrofluid Workshop

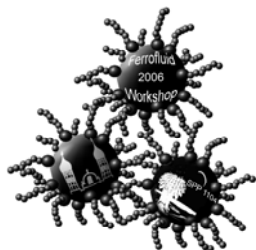
and

Final Colloquium of SPP1104

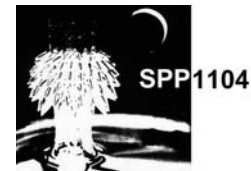
Benediktbeuern
September 25th – 29th



Book of Abstracts



Preliminary Program of the joined
7th German Ferrofluid Workshop
and the
Final Colloquium of DFG priority program SPP1104



Monday, September 25th - Tuesday, September 26th

Special Program for the Final Colloquium of SPP1104

Tuesday, September 26th

17:45 - ???

Get together of the 7th Germany Ferrofluidworkshop

and

1. Postersession (Poster group 1)

Wednesday, September 27th

Synthesis

- | | | |
|---------------|---|---|
| 9:00 - 9:25 | Buske, N. | <i>Entwicklungstrends von Dispersionen mit magnetischen Nano und Mikroteilchen</i> |
| 9:25 - 9:50 | Feyen, M.; Gelbrich, T.; Kaiser, A.; Schmidt, A.M. | <i>Magnetic Polymer Hybrids for Thermosensitive Magnetic Fluids</i> |
| 9:50 - 10:15 | Holzapfel, V.; Lorenz, M.; Mailänder, V.; Schrezenmeier, H.; Landfester, K. | <i>Synthesis and biomedical applications of fluorescent functionalized magnetic nanoparticles as obtained in the miniemulsion process</i> |
| 10:15 - 10:40 | Matoussevitch, N.; Bönnemann, H.; Behrens, S.; Bolle, J.; Dinjus, E. | <i>Synthesis and Properties of Co, Fe, Fe/Co Nanoparticles and Magnetic Fluids. Surface modification for biomedical Application</i> |
| 10:40 - 11:30 | <i>Coffee & Posters (Poster group 1)</i> | |

Structure and Dynamics

- | | | |
|---------------|--|---|
| 11:30 - 11:55 | Märkert, C.; Wagner, J.; Hempelmann, R. | <i>Rodlike Magnetic Core Shell Particles as Model System for Lyotropic Liquid Crystals</i> |
| 11:55 - 12:20 | Wiedenmann, A.; Keiderling, U.; Habicht, K.; Russina, M.; Gähler, R. | <i>Microsecond dynamics of field-induced ordering in magnetic colloids studied by new time-resolved Small Angle Neutron Scattering techniques</i> |
| 12:20 - 12:45 | Heinrich, D.; Goni, A. R.; Thomsen, C. | <i>Dynamics of clustering in ionic ferrofluid from Raman scattering</i> |
| 12:45 - 14:00 | Lunch | |

Medical Applications 1

- 14:00 - 14:25 Müller, R.; Dutz, S.; Hergt, R.; Hilger, I.; Kettering, M.; Steinmetz, H.; Zeisberger, M.; Gawalek, W. *Loss investigations on dextran coated iron oxide nanoparticles*
- 14:25 - 14:50 Zeisberger, M.; Müller, R.; Steinmetz, H.; Hergt, R.; Gawalek, W. *Temperature limited heating by magnetic nanoparticles*
- 14:50 - 15:15 Kettering, M.; Winter, J.; Zeisberger, M.; Bremer-Streck, S.; Bergemann, C.; Alexiou, C.; Hergt, R.; Kaiser, W. A.; Hilger, I. *Magnetic enhancement of cellular nanoparticle uptake in tumour cells: Combination of magnetically based labelling and magnetic heating*
- 15:15 - 16:05 *Coffee & Posters (Poster group 1)*

Medical Applications 2

- 16:05 - 16:30 Lang, C.; Schüler, D. *Magnetosomes - Production, characterization and application*
- 16:30 - 16:55 Wiekhorst, F.; Eberbeck, D.; Steinhoff, U.; Jurgons, R.; Seliger, C.; Alexiou, C.; Trahms, L. *Quantification of magnetic nanoparticles in tissue demonstrated by magnetorelaxometry tomography*
- 16:55 - 17:20 Aurich, K.; Heister, E.; Nagel, S.; Weitschies, W. *Determination of binding parameters of antigen/antibody systems based on magneto-optical relaxation measurements*
- 17:20 - 17:45 Schwalbe, M.; Vetterlein, M.; Pachmann, K.; Höffken, K.; Clement, J. H. *Quantitative magnetic assisted depletion of tumor cells from peripheral blood*
- 18:00 - 19:30 *Guided tour through the cloister*

Thursday, September 28th

Basics 1

- 9:00 - 9:25 Ryskin, A.; Pleiner, H. *Magnetic Field Driven Sedimentation Instability in Ferrofluids*
- 9:25 - 9:50 Gollwitzer, C.; Turanov, A.; Krekhova, M.; Richter, R. *Magnetic kicks to a ferrogel ball. How a ferrogel sphere elongates in a uniform pulsed magnetic field*
- 9:50 - 10:15 Leschhorn, A.; Embs, J. P.; Lücke, M. *Magnetization of rotating ferrofluids: the effect of polydispersity*
- 10:15 - 11:30 *Coffee & Posters (Poster group 2)*

Free Surface Phenomena

- 11:30 - 11:55 Beetz, A.; Richter, R.; Rehberg, I. *Response of a ferrofluid to travelling stripe forcing*
- 11:55 - 12:20 Lange, A.; Knieling, H.; Matthies, G.; Rehberg, I.; Richter, R. *Maximal growth rate at the Rosensweig instability: theory, experiment, and numerics*
- 12:20 - 12:45 Lavrova, O.; Matthies, G.; Tobiska, L. *Numerically resolved solitary pattern of the Rosensweig instability*
- 12:45 - 14:00 **Lunch**
- 14:00 - 16:05 **Coffee & Posters (Poster group 2)**

Rheology

- 16:05 - 16:30 Shahnazian, H.; Odenbach, S. *Controlled shear stress rheological investigations of ferrofluids*
- 16:30 - 16:55 Krauss, R.; Fischer, B.; Youyong, X.; Müller, A. H. E.; Richter, R. *Giant relaxation times in novel type of magnetorheological fluid*
- 16:55 - 17:20 Fahmi, A.; Mendoza, C.; Kancharla, V.; Pietsch, T.; Gindy, N. *Synthesis and rheological characterization of magnetorheological fluids in a varying external magnetic field*
- 17:20 - 17:45 Ilg, P.; Coquelle, E.; Hess, S. *Structural, dynamical, and viscous properties of ferrofluids from computer simulations*
- 17:45 - 18:05 Iskakova, L.; Zubarev, A. *Rheological properties of magnetic suspensions with chain-like aggregates*
- 19:00 - ??? **Conference Dinner**

Friday, September 29th

Basics 2

- 9:00 - 9:25 Berkov, D. V.; Gorn, N. L.; Schmitz, R.; Stock, D. *Numerical simulations of ferrofluid dynamics: Comparison of various ferrofluid models*
- 9:25 - 9:50 Ludwig, F.; Heim, E.; Schilling, M. *Charakterisierung magnetischer Nanoteilchen durch Analyse der Magnetisierungs- und Relaxationsdynamik mit Fluxgate-Magnetometern*
- 9:50 - 10:15 Cerda, J.; Holm, C.; Kantorovich, S. *Microstructure of ferrofluid monolayers: theory and computer simulations*
- 10:15 - 11:30 **Coffee & Posters (Poster group 2)**

Technical Applications

- | | | |
|---------------|--|--|
| 11:30 - 11:55 | Borin, D. | <i>Magnetorheological actuator for the control of primary mirror elements of extra-large telescope</i> |
| 11:55 - 12:20 | Guldbakke, J. M.; Hesselbach, J. | <i>Development of a Linear Guide and a Foam Damper based on Magnetically Controllable Fluids</i> |
| 12:20 - 12:45 | Zimmermann, K.; Zeidis, I.; Naletova, V. A.; Böhm, V.; Kolev, E.; Popp, J. | <i>Locomotion of Mobile Robots based on Ferrofluid</i> |
| 12:45 - 13:00 | <i>Closing</i> | |

Poster group 1

Technical Applications

- 1 Borin, D. *Magnetorheological actuator for the control of primary mirror elements of extra-large telescope*
- 2 Guldbakke, J. M.; Hesselbach, J. *Development of a Linear Guide and a Foam Damper based on Magnetically Controllable Fluids*
- 3 Uhlmann, E.; Bayat, N.; Hipper, M. *Multidimensional Magnetofluidic Positioning Systems*
- 4 Zimmermann, K.; Zeidis, I.; Naletova, V. A.; Böhm, V.; Kolev, E.; Popp, J. *Locomotion of Mobile Robots based on Ferrofluid*

Basics

- 5 Bohlius, S.; Pleiner, H.; Brand, H. R. *Pattern Formation in Isotropic Ferrogels - Nonlinear Analysis Using the Energy Method*
- 6 Engler, H.; Odenbach, S. *Parametric modulation of thermal and thermomagnetic convection in magnetic fluids*
- 7 Groh, C.; Busse, F.; Rehberg, I.; Richter, R. *Flip of hexagonal surface pattern under broken symmetry*
- 8 Haase, W.; Galaymetdinov, Y. *Magnetic and optical properties of some Ferrofluids and of paramagnetic Metallomesogens doped with Ferrofluids*
- 9 Heinrich, D.; Goni, A. R.; Thomsen, C. *Dynamics of clustering in ionic ferrofluid from Raman scattering*
- 10 Ivanov, A. O.; Kantorovich, S. S.; Reznikov, E. N.; Holm, C.; Pshenichnikov, A. F.; Lebedev, A. V.; Chremos, A.; Camp, P. J. *Magnetic properties of polydisperse ferrocolloid suspensions: A critical comparison between experiment, theory and computer simulation*
- 11 Knieling, H.; Richter, R. *Growth behaviour of solitary spikes on the surface of magnetic fluids*
- 12 Mekhonoshin, V. *Faraday instability on a ferrofluid in a vertical magnetic field: non-linear planform selection*
- 13 Ryskin, A.; Pleiner, H. *Effects of Sedimentation in the Thermal Convection of Ferrofluids*
- 14 Schmitz, R. *Effect of Hydrodynamic Interaction on the Short-Time Dynamics of Ferrofluids*
- 15 Beetz, A.; Richter, R.; Rehberg, I. *Response of a ferrofluid to travelling stripe forcing*
- 16 Lange, A.; Knieling, H.; Matthies, G.; Rehberg, I.; Richter, R. *Maximal growth rate at the Rosensweig instability: theory, experiment, and numerics*
- 17 Lavrova, O.; Matthies, G.; Tobiska, L. *Numerically resolved solitary pattern of the Rosensweig instability*
- 18 Märkert, C.; Wagner, J.; Hempelmann, R. *Rodlike Magnetic Core Shell Particles as Model System for Lyotropic Liquid Crystals*
- 19 Wiedenmann, A.; Keiderling, U.; Habicht, K.; Russina, M.; Gähler, R. *Microsecond dynamics of field-induced ordering in magnetic colloids studied by new time-resolved Small Angle Neutron Scattering techniques*
- 20 Berkov, D. V.; Gorn, N. L.; Schmitz, R.; Stock, D. *Numerical simulations of ferrofluid dynamics: Comparison of various ferrofluid models*

- 21 Cerda, J.; Holm, C.; Kantorovich, S. *Microstructure of ferrofluid monolayers: theory and computer simulations*
- 22 Ludwig, F.; Heim, E.; Schilling, M. *Charakterisierung magnetischer Nanoteilchen durch Analyse der Magnetisierungs- und Relaxationsdynamik mit Fluxgate-Magnetometern*
- 23 Gollwitzer, C.; Turanov, A.; Krekhova, M.; Richter, R. *Magnetic kicks to a ferrogel ball. How a ferrogel sphere elongates in a uniform pulsed magnetic field*
- 24 Leschhorn, A.; Embs, J. P.; Lücke, M. *Magnetization of rotating ferrofluids: the effect of polydispersity*
- 25 Ryskin, A.; Pleiner, H. *Magnetic Field Driven Sedimentation Instability in Ferrofluids*

Poster group 2

Medical Applications

- 26 Heim, E.; Harling, S.; Schwoerer, A.; Ludwig, F.; Menzel, H.; Schilling, M. *Supermagnetische Nanoteilchen als Sonden für die Hydrogel-Charakterisierung mittels Fluxgate-Magnetrelaxometrie*
- 27 Aurich, K.; Heister, E.; Nagel, S.; Weitschies, W. *Determination of binding parameters of antigen/antibody systems based on magneto-optical relaxation measurements*
- 28 Eberbeck, D.; Bergemann, C.; Wiekhorst, F.; Steinhoff, U.; Trahms, L. *Agglutination of functionalised MNP as a tool for quantification of biomolecules*
- 29 Kettering, M.; Winter, J.; Zeisberger, M.; Bremer-Streck, S.; Bergemann, C.; Alexiou, C.; Hergt, R.; Kaiser, W. A.; Hilger, I. *Magnetic enhancement of cellular nanoparticle uptake in tumour cells: Combination of magnetically based labelling and magnetic heating*
- 30 Kettering, M.; Zeisberger, M.; Dutz, S.; Hergt, R.; Müller, R.; Kaiser, W. A.; Hilger, I. *Magnetic nanoparticles for combined hyperthermia and chemotherapeutic treatment of tumours*
- 31 Lang, C.; Schüler, D. *Magnetosomes - Production, characterization and application*
- 32 Müller, R.; Dutz, S.; Hergt, R.; Hilger, I.; Kettering, M.; Steinmetz, H.; Zeisberger, M.; Gawalek, W. *Loss investigations on dextran coated iron oxide nanoparticles*
- 33 Rahn, H.; Odenbach, S. *X-ray tomography as a tool for the analysis of magnetic particle distribution in tumor tissue*
- 34 Schmidl, F.; Büttner, M.; Müller, T.; Prass, S.; Köttig, T.; Weber, P.; Mans, M.; Bocker, C.; Heinrich, J.; Wagner, K.; Röder, M.; Berkov, D. V.; Görnert, P.; Glöckel, G.; Weitschies, W.; Seidel, P. *Temperature dependent Néel relaxation (TMRX) measurements for characterization of nanoparticle distributions*
- 35 Schwalbe, M.; Vetterlein, M.; Liebert, T.; Pachmann, K.; Heinze, T.; Höffken, K.; Clement, J. H. *The modification of the dextran shell influences the interaction of magnetic nanoparticles with cells*
- 36 Schwalbe, M.; Buske, N.; Vetterlein, M.; Pachmann, K.; Höffken, K.; Clement, J. H. *Improvement of the separation of tumor cells from peripheral blood cells using magnetic nanoparticles*
- 37 Schwalbe, M.; Vetterlein, M.; Pachmann, K.; Höffken, K.; Clement, J. H. *Quantitative magnetic assisted depletion of tumor cells from peripheral blood*

- 38 Seliger, C.; Jurgons, R.; Kolb, S.; Wiekhorst, F.; Eberbeck, D.; Trahms, L.; Iro, H.; Alexiou, C. *Physiological and physical investigations concerning intraarterial Magnetic Drug Targeting*
- 39 Wiekhorst, F.; Eberbeck, D.; Steinhoff, U.; Jurgons, R.; Seliger, C.; Alexiou, C.; Trahms, L. *Quantification of magnetic nanoparticles in tissue demonstrated by magnetorelaxometry tomography*
- 40 Zeisberger, M.; Müller, R.; Steinmetz, H.; Hergt, R.; Gawalek, W. *Temperature limited heating by magnetic nanoparticles*

Rheology

- 41 Fahmi, A.; Mendoza, C.; Kancharla, V.; Pietsch, T.; Gindy, N. *Synthesis and rheological characterization of Magnetorheological fluids in a varying external magnetic field*
- 42 Ilg, P.; Coquelle, E.; Hess, S. *Structural, dynamical, and viscous properties of ferrofluids from computer simulations*
- 43 Iskakova, L.; Zubarev, A. *Rheological properties of magnetic suspensions with chain-like aggregates*
- 44 Iskakova, L.; Zubarev, A. *Optical birefringence in ferrofluids*
- 45 Iskakova, L.; Ivanov, A.; Kantorovich, S.; Zubarev, A. *Kinetics of internal structure formation in magnetic suspensions*
- 46 Krauss, R.; Fischer, B.; Youyong, X.; Müller, A. H. E.; Richter, R. *Giant relaxation times in novel type of magneto-rheological fluid*
- 47 Patzke, J.; Rathke, B.; Will, S. *Viscous Properties of a Magnetic-based Ferrofluid From Capillary Wave Spectroscopy*
- 48 Pop, L.; Odenbach, S.; Kammel, M.; Wiedenmann, A. *In situ SANS investigations of microstructure changes of cobalt based ferrofluids under shear and magnetic field influence*
- 49 Shahnazian, H.; Odenbach, S. *Controlled shear stress rheological investigations of ferrofluids*

Synthesis

- 50 Bolle, J.; Matoussevitch, N.; Bönnemann, H.; Franzreb, M.; Köster, R. *Synthesis and Characterisation of Polymer-Cobalt-Microspheres*
- 51 Buske, N. *Entwicklungstrends von Dispersionen mit magnetischen Nano und Mikroteilchen*
- 52 Feyen, M.; Gelbrich, T.; Kaiser, A.; Schmidt, A.M. *Magnetic Polymer Hybrids for Thermosensitive Magnetic Fluids*
- 53 Holzapfel, V.; Lorenz, M.; Mailänder, V.; Schrezenmeier, H.; Landfester, K. *Synthesis and biomedical applications of fluorescent functionalized magnetic nanoparticles as obtained in the miniemulsion process*
- 54 Kaiser, A.; Schmidt, A.M. *Hydrocarbon-based Thermoresponsive Magnetic Fluids*
- 55 Krekhova, M.; Lattermann, G. *Influence of the Gelator Type on Properties of Thermoreversible Ferrogels*
- 56 Matoussevitch, N.; Bönnemann, H.; Behrens, S.; Bolle, J.; Dinjus, E. *Synthesis and Properties of Co, Fe, Fe/Co Nanoparticles and Magnetic Fluids. Surface modification for biomedical Application*

Content

Synthesis

Authors	Title of abstract	Page
Bolle, J.; Matoussevitch, N.; Bönnemann, H.; Franzreb, M.; Köster, R.	<i>Synthesis and Characterisation of Polymer-Cobalt- Microspheres</i>	1
Buske, N.	<i>Entwicklungstrends von Dispersionen mit magnetischen Nano und Mikro-Teilchen</i>	2
Feyen, M.; Gelbrich, T.; Kaiser, A.; Schmidt, A.M.	<i>Magnetic Polymer Hybrids for Thermosensitive Magnetic Fluids</i>	3
Holzapfel, V.; Lorenz, M.; Mailänder, V.; Schrezenmeier, H.; Landfester, K.	<i>Synthesis and biomedical applications of fluorescent functionalized magnetic nanoparticles as obtained in the miniemulsion process</i>	5
Kaiser, A.; Schmidt, A.M.	<i>Hydrocarbon-based Thermoresponsive Magnetic Fluids</i>	7
Krekhova, M.; Lattermann, G.	<i>Influence of the Gelator Type on Properties of Thermoreversible Ferrogels</i>	9
Matoussevitch, N.; Bönnemann, H.; Behrens, S.; Bolle, J.; Dinjus, E.	<i>Synthesis and Properties of Co, Fe, Fe/Co Nanoparticles and Magnetic Fluids. Surface modification for biomedical Application</i>	11

Basics

Authors	Title of abstract	Page
Beetz, A.; Richter, R.; Rehberg, I.	<i>Response of a ferrofluid to travelling stripe forcing</i>	13
Berkov, D. V.; Gorn, N. L.; Schmitz, R.; Stock, D.	<i>Numerical simulations of ferrofluid dynamics: Comparison of various ferrofluid models</i>	15
Bohlius, S.; Pleiner, H.; Brand, H. R.	<i>Pattern Formation in Isotropic Ferrogels - Nonlinear Analysis Using the Energy Method</i>	17
Cerda, J.; Holm, C.; Kantorovich, S.	<i>Microstructure of ferrofluid monolayers: theory and computer simulations</i>	18
Engler, H.; Odenbach, S.	<i>Parametric modulation of thermal and thermomagnetic convection in magnetic fluids</i>	20
Gollwitzer, C.; Turanov, A.; Krekhova, M.; Richter, R.	<i>Magnetic kicks to a ferrogel ball How a ferrogel sphere elongates in a uniform pulsed magnetic field</i>	22
Groh, C.; Busse, F.; Rehberg, I.; Richter, R.	<i>Flip of hexagonal surface pattern under broken symmetry</i>	24
Haase, W.; Galaymetdinov, Y.	<i>Magnetic and optical properties of some Ferrofluids and of paramagnetic Metallomesogens doped with Ferrofluids</i>	26
Heinrich, D.; Goñi, A. R.; Thomsen, C.	<i>Dynamics of clustering in ionic ferrofluid from Raman scattering</i>	27

Ivanov, A. O.; Kantorovich, S. S.; Reznikov, E. N.; Holm, C.; Pshenichnikov, A. F.; Lebedev, A. V.; Chremos, A.; Camp, P. J.	<i>Magnetic properties of polydisperse ferrocolloid suspensions: A critical comparison between experiment, theory and computer simulation</i>	28
Knieling, H.; Richter, R.	<i>Growth behaviour of solitary spikes on the surface of magnetic fluids</i>	30
Lange, A.; Knieling, H.; Matthies, G.; Rehberg, I.; Richter, R.	<i>Maximal growth rate at the Rosensweig instability: theory, experiment, and numerics</i>	32
Lavrova, O.; Matthies, G.; Tobiska, L.	<i>Numerically resolved solitary pattern of the Rosensweig instability</i>	34
Leschhorn, A.; Embs, J. P.; Lücke, M.	<i>Magnetization of rotating ferrofluids: the effect of polydispersity</i>	36
Ludwig, F.; Heim, E.; Schilling, M.	<i>Charakterisierung magnetischer Nanoteilchen durch Analyse der Magnetisierungs- und Relaxationsdynamik mit Fluxgate-Magnetometern</i>	37
Märkert, C.; Wagner, J.; Hempelmann, R.	<i>Rodlike Magnetic Core Shell Particles as Model System for Lyotropic Liquid Crystals</i>	39
Mekhonoshin, V.	<i>Faraday instability on a ferrofluid in a vertical magnetic field: non-linear planform selection</i>	41
Ryskin, A.; Pleiner, H.	<i>Magnetic Field Driven Sedimentation Instability in Ferrofluids</i>	43
Ryskin, A.; Pleiner, H.	<i>Effects of Sedimentation in the Thermal Convection of Ferrofluids</i>	45
Schmitz, R.	<i>Effect of Hydrodynamic Interaction on the Short-Time Dynamics of Ferrofluids</i>	47
Wiedenmann, A.; Keiderling, U.; Habicht, K.; Russina, M.; Gähler, R.	<i>Mikrosecond dynamics of field-induced ordering in magnetic colloids studied by new time-resolved Small Angle Neutron Scattering techniques</i>	48

Rheology

Authors	Title of abstract	Page
Fahmi, A.; Mendoza, C.; Kancharla, V.; Pietsch, T.; Gindy, N.	<i>Synthesis and rheological characterization of Magnetorheological fluids in a varying external magnetic field</i>	50
Ilg, P.; Coquelle, E.; Hess, S.	<i>Structural, dynamical, and viscous properties of ferrofluids from computer simulations</i>	51
Iskakova, L.; Zubarev, A.	<i>Rheological properties of magnetic suspensions with chain-like aggregates</i>	53
Iskakova, L.; Zubarev, A.	<i>Optical birefringence in ferrofluids</i>	55
Iskakova, L.; Ivanov, A.; Kantorovich, S.; Zubarev, A.	<i>Kinetics of internal structure formation in magnetic suspensions</i>	57
Krauss, R.; Fischer, B.; Youyong, X.; Müller, A. H. E.; Richter, R.	<i>Giant relaxation times in novel type of magneto-rheological fluid</i>	59
Patzke, J.; Rathke, B.; Will, S.	<i>Viscous Properties of a Magnetic-based Ferrofluid From Capillary Wave Spectroscopy</i>	61

Pop, L.; Odenbach, S.; Kammel, M.; Wiedenmann, A.	<i>In situ SANS investigations of microstructure changes of cobalt based ferrofluids under shear and magnetic field influence</i>	62
Shahnazian, H.; Odenbach, S.	<i>Controlled shear stress rheological investigations of ferrofluids</i>	64

Technical Applications

Authors	Title of abstract	Page
Borin, D.; Mikhailov, V.	<i>Magnetorheological actuator for the control of primary mirror elements of extra-large telescope</i>	66
Guldbakke, J. M.; Hesselbach, J.	<i>Development of a Linear Guide and a Foam Damper based on Magnetically Controllable Fluids</i>	67
Uhlmann, E.; Bayat, N.; Hipper, M.	<i>Multidimensional Magnetofluidic Positioning Systems</i>	69
Zimmermann, K.; Zeidis, I.; Naletova, V. A.; Böhm, V.; Kolev, E.; Popp, J.	<i>Locomotion of Mobile Robots based on Ferrofluid</i>	71

Medical Applications

Authors	Title of abstract	Page
Heim, E.; Harling, S.; Schworer, A.; Ludwig, F.; Menzel, H.; Schilling, M.	<i>Supermagnetische Nanoteilchen als Sonden für die Hydrogel-Charakterisierung mittels Fluxgate-Magnetrelaxometrie</i>	73
Aurich, K.; Heister, E.; Nagel, S.; Weitschies, W.	<i>Determination of binding parameters of antigen/antibody systems based on magneto-optical relaxation measurements</i>	75
Eberbeck, D.; Bergemann, C.; Wiekhorst, F.; Steinhoff, U.; Trahms, L.	<i>Agglutination of functionalised MNP as a tool for quantification of biomolecules</i>	77
Kettering, M.; Winter, J.; Zeisberger, M.; Bremer-Streck, S.; Bergemann, C.; Alexiou, C.; Hergt, R.; Kaiser, W. A.; Hilger, I.	<i>Magnetic enhancement of cellular nanoparticle uptake in tumour cells: Combination of magnetically based labelling and magnetic heating</i>	79
Kettering, M.; Zeisberger, M.; Dutz, S.; Hergt, R.; Müller, R.; Kaiser, W. A.; Hilger, I.	<i>Magnetic nanoparticles for combined hyperthermia and chemotherapeutical treatment of tumours</i>	81
Lang, C.; Schüler, D.	<i>Magnetosomes - Production, characterization and application</i>	83
Müller, R.; Dutz, S.; Hergt, R.; Hilger, I.; Kettering, M.; Steinmetz, H.; Zeisberger, M.; Gawalek, W.	<i>Loss investigations on dextran coated iron oxide nanoparticles</i>	85
Rahn, H.; Alexiou, Ch.; Hilger, I.; Odenbach, S.	<i>X-ray tomography as a tool for the analysis of magnetic particle distribution in tumor tissue</i>	87

Schmidl, F.; Büttner, M.; Müller, T.; Prass, S.; Köttig, T.; Weber, P.; Mans, M.; Bocker, C.; Heinrich, J.; Wagner, K.; Röder, M.; Berkov, D. V.; Görnert, P.; Glöckel, G.; Weitschies, W.; Seidel, P.	<i>Temperature dependent Néel relaxation (TMRX) measurements for characterization of nanoparticle distributions</i>	89
Schwalbe, M.; Vetterlein, M.; Liebert, T.; Pachmann, K.; Heinze, T.; Höffken, K.; Clement, J. H.	<i>The modification of the dextran shell influences the interaction of magnetic nanoparticles with cells</i>	91
Schwalbe, M.; Buske, N.; Vetterlein, M.; Pachmann, K.; Höffken, K.; Clement, J. H.	<i>Improvement of the separation of tumor cells from peripheral blood cells using magnetic nanoparticles</i>	92
Schwalbe, M.; Vetterlein, M.; Pachmann, K.; Höffken, K.; Clement, J. H.	<i>Quantitative magnetic assisted depletion of tumor cells from peripheral blood</i>	93
Seliger, C.; Jurgons, R.; Kolb, S.; Wiekhorst, F.; Eberbeck, D.; Trahms, L.; Iro, H.; Alexiou, C.	<i>Physiological and physical investigations concerning intraarterial Magnetic Drug Targeting</i>	94
Wiekhorst, F.; Eberbeck, D.; Steinhoff, U.; Jurgons, R.; Seliger, C.; Alexiou, C.; Trahms, L.	<i>Quantification of magnetic nanoparticles in tissue demonstrated by magnetorelaxometry tomography</i>	96
Zeisberger, M.; Müller, R.; Steinmetz, H.; Hergt, R.; Gawalek, W.	<i>Temperature limited heating by magnetic nanoparticles</i>	98

Abstracts

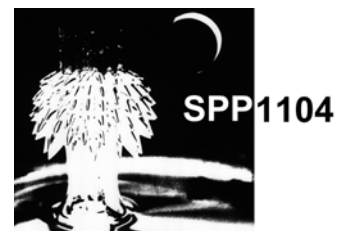
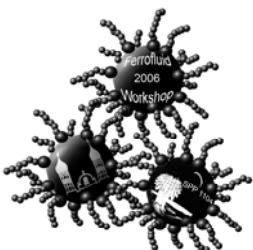
for the

7th German Ferrofluid Workshop

and the

Final Colloquium of SPP1104

*Kolloidale magnetische Flüssigkeiten:
Grundlagen, Entwicklung und Anwendung
neuartiger Ferrofluide*



Synthesis and Characterisation of Polymer-Cobalt-Microspheres

J.Bolle¹, N.Matoussevitch^{2,3}, H.Boenemann⁴, M.Franzreb¹, R.Köster¹

¹ Forschungszentrum Karlsruhe, ITC - WGT, Post Box 3640, D-76021 Karlsruhe, Germany,

² University of Heidelberg, D-69117 Heidelberg, Germany

³ Forschungszentrum Karlsruhe, ITC - CPV, Post Box 3640, D-76021 Karlsruhe, Germany

⁴ Max-Planck-Institut für Kohlenforschung, Kaiser-Wilhelm-Platz 1, D-45470 Mülheim an der Ruhr, Germany

An effective tool to achieve rapid, simple, and specific biological separation such as cell isolation, protein purification and immunoassays are magnetic polymer microspheres. Once functionalised, the magnetic microspheres can be linked to biomolecules and can be collected easily with the application of a magnetic field. Metallic (Co, Fe, FePt) particles are very promising to obtain microspheres with specific and improved magnetic properties as compared to magnetite (Fe₃O₄) microspheres.

For preparation of Cobalt-microspheres we have used the oil-in-water (o/w) emulsion – solvent evaporation method.

Therefore an oil phase (containing the monomer, homogeneously dispersed metallic particles, a radical starter and a cross-linker) and a water phase (consisting of an aqueous solution of surfactant and stabiliser) were mixed together at a suitable mixing speed and heating. During the following polymerisation the metallic particles (~10 nm) were integrated into the cross-linked particles (0.5 µm to 10 µm), converting them into magnetic ones.

This process of forming microspheres depends on many parameters. We have tried to find the optimal conditions of polymerisation by investigating the role and influence of some of them, such as:

- type and concentration of monomers
- surfactants and carrier-liquid of Cobalt-magnetic fluid (MF)
- temperature and time of polymerisation
- speed of mixing
- initial concentration of MF

Our resulting Cobalt-microspheres which were produced via the co-polymerisation of methylmethacrylate and divinylbenzene as well as

vinylacetate and divinylbenzene show high saturation magnetisation (33 Am²/kg, see Fig.1), improving functionalisation (functional groups 865 µmol/g) and good stability.

We investigated our Cobalt-microspheres by ESEM, SEM, measured magnetic properties by Alternating Gradient Magnetometer (AGM), determined the size distribution and functionalisation. The data will be presented.

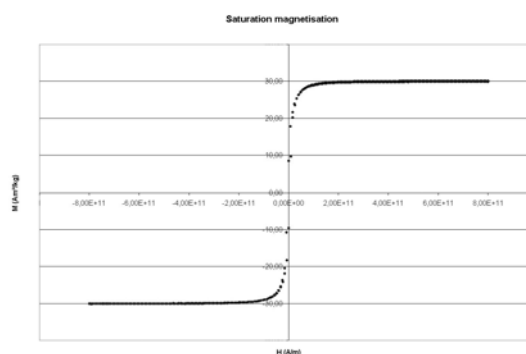


Fig.1. Magnetization of Cobalt-microspheres

Acknowledgments

The support of this work by Deutsche Forschungsgemeinschaft (SPP 1104, grant No. BO1135 and SPP1259, grant No. BE3709) is gratefully acknowledged.

We thank W. Habicht (ITC-CPV, FZK) for SEM measurements.

Entwicklungstrends von Dispersionen mit magnetischen Nano und Mikro-Teilchen

N. Buske

www.magneticfluids.de, Berlin

Dispersionen mit magnetischen Nano und Mikroteilchen haben wegen ihrer multifunktionalen Eigenschaften ein sich erfolgreich entwickelndes Anwendungspotential. Die vorteilhafte Kombination physikalischer, kolloidaler und (bio)chemischer Eigenschaften der Dispersionen ist das Ziel vieler gegenwärtiger Entwicklungen.

Dabei kann man auf eine Vielzahl stofflicher Zusammensetzungen zurückgreifen, die aber hinsichtlich der chemisch/physikalischen Eigenschaften zueinander passen müssen. Die Kernteilchenzusammensetzung, -größe und -konzentration, aber auch die chemische Zusammensetzung der Hüllen, sind besonders wichtige Parameter. Solche designten Dispersionen aus Kern/Hüll-Teilchen werden auch heute noch zeitaufwendig durch Trial and Error-Methoden entwickelt.

Hinsichtlich der **Kernteilchengröße** kann man aus physikalischer Sicht folgende Einteilung vornehmen:

a) Durchmesser: 2-15nm (für Magnetit). Die korrespondierenden Dispersionen haben superparamagnetisches Verhalten (keine Hysterese in der Magnetisierungskurve), die Langevin Theorie ist anwendbar und werden als magnetische Flüssigkeiten bzw. Ferrofluide bezeichnet. Zwar ist die magnetische Wechselwirkungskraft eines Teilchens zum äußeren Magnetfeld sehr gering, doch wird diese durch die hohe Teilchenkonzentration mit bis zu 10^{17} Nanoteilchen/ml wesentlich gesteigert.

Das kolloidale Verhalten der Dispersionen kann mit der DLVO-Theorie beurteilt werden. Die Dispersionen auf Wasser oder organischer Basis können kolloidal stabil hergestellt werden.

b) Durchmesser: ca. 16-100nm (für Magnetit). Diese Teilchen besitzen eine relative Magnetisierung und Koerzitiv-

feldstärke. Die kolloidale Stabilität ist eingeschränkt, könnte aber durch dickere Adsorptionsschichten verbessert werden.

Diese Dispersionen haben ein ferromagnetisches Verhalten, man findet eine Hysterese in der Magnetisierungskurve. Man kann sie somit als ferromagnetische Flüssigkeiten bezeichnen, ihr Anwendungspotential wird als bedeutend eingeschätzt. Es wird erwartet, dass Herstellverfahren von funktionalen Kern/Hüllteilchen mit enger Teilchengröße-Verteilung entwickelt werden, wobei die Sicherung der kolloidalen Stabilität der Dispersionen eine Herausforderung ist. Die physikalischen Eigenschaften dieser Dispersionen sind noch weitgehend unbekannt.

Diese Dispersionen haben auch einen deutlichen magnetorheologischen (MR) Effekt, sie werden darum auch als Nano-MR-Flüssigkeiten (nano-MRF) bezeichnet.

c) Teilchengröße im μm -Bereich.

Typisch werden als disperse Phase „Eisen-carbonylteilchen“ verwendet, die aus weichmagnetischen Eisenkernen mit einer Oxidschutzhaut bestehen.

Die korrespondierenden Dispersionen werden auch als MRF bezeichnet. Noch nicht optimal gelöste technische Anforderungen sind die niedrige Grundviskosität bei hohen Teilchenkonzentrationen, eine geringe Teilchensedimentation und die leichte Redispersierbarkeit des Sediments bei geringen Schubspannungen.

In diesem Beitrag werden die gegenwärtigen Machbarkeitsgrenzen und das Optimierungspotenzial der magnetischen Dispersionen anhand einzelner Anwendungen erläutert. Die Probleme bei der Herstellung/Charakterisierung der unter b) genannten Dispersionen werden vorrangig diskutiert werden.

Magnetic Polymer Hybrids for Thermosensitive Magnetic Fluids

M. Feyen¹, T. Gelbrich¹, A. Kaiser¹, A. M. Schmidt^{1*}

¹*Institute for Organic Chemistry and Macromolecular Chemistry, Heinrich-Heine University Düsseldorf, Universitätsstr. 1, D-40225 Düsseldorf*

**e-mail: schmidt.annette@uni-duesseldorf.de, phone: +49 211-8114820*

The combination of magnetic nanoparticles with stimuli-sensitive polymers is an interesting approach for the preparation of magnetic fluids with tailor-made properties.

Our work combines magnetic nanoparticles with thermosensitive polymeric shells to obtain magnetic fluids with thermoreversible dispersion properties [1-3]. The polymer chains are covalently end-grafted on the surface of the inorganic magnetic material. The resulting brush-like architecture is most suitable to sterically stabilize the hybrid particles in proper

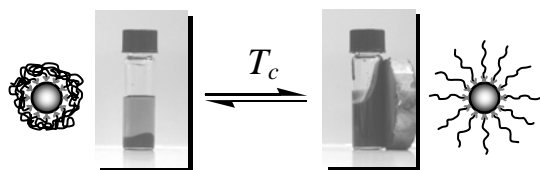


Fig. 1: Schematic behavior of the polymer brush shell in thermoreversible magnetic fluids and photographs of $\text{Fe}_3\text{O}_4@\text{PMEMA}_{43}$ in MeOH

organic solvents and in water without additional surfactants.

The polymers are selected to show a critical solution behaviour in the carrier medium. At a critical temperature T_c , the solubility of the polymer arms instantly changes leading to a collapsing or swelling of the shell (figure 1). Consequently, the hybrid particles precipitate or become well dispersible. The thermal transition is detectable in a shift of the hydrodynamic diameter (DLS) and in turbidity experiments (figure 2) [1]. The heat energy that is necessary to reach T_c can be provided by induction heating of the magnetic cores [4].

In order to obtain magnetic fluids for many different applications, we prepared hybrid materials consisting of Fe_3O_4 - or Co-cores and a shell composed of polystyrene (PS) [3], poly(ϵ -caprolactone) (PCL) [2], and different methacrylates [1].

The synthetic route is based on a grafting-from approach using a surface initiated ring opening polymerization and *atom transfer radical polymerization* (ATRP) [1-2]. These controlled mechanisms allow us to tailor the polymeric arm length via the molecular weight by the ratio of initiator to monomer [3]. We obtained hybrid particles

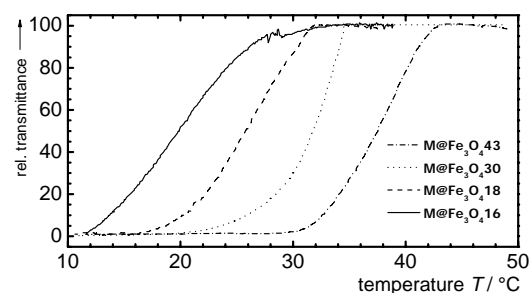


Fig. 2: Relative transmittance vs. temperature T of $\text{Fe}_3\text{O}_4@\text{PMEMA}$ suspensions in methanol in cloud point photometry experiments

with different shell thicknesses which have direct influence on the dispersion properties of the particles [1].

Thermoreversible behaviour of the prepared magnetic fluids was found in cyclohexene (PS), methanol and DMSO (PCL). Also first results of water-based magnetic fluids with thermal tailorable stability are received [5].

Depending on the nature of the core and the polymeric shell, the obtained magnetic

fluids are of high interest for many applications.

On the one hand they are of use as model systems for the investigation of stabilization and relaxation processes and on the other hand the swelling and collapsing of the polymer shell is useful for biomedical applications like drug delivery or targeting. Separation methods based on thermosensitive magnetic fluids would combine the advantage of small single cored particles with magnetic microspheres leading to an effective separation of biomolecules like DNA or proteins.

- [1] T. Gelbrich, M. Feyen, A. M. Schmidt, *Macromolecules* (2006) 39: 3460-3472
- [2] A. M. Schmidt *Macromol. Rapid. Commun.* (2005) 26: 93-97
- [3] A. Kaiser, A. M. Schmidt, *J. Phys. Cond. Matter*, accepted (2006)
- [4] A. M. Schmidt *J. Magnetism Magn. Mater.* (2006) 299C: 5-8
- [5] T. Gelbrich, A. M. Schmidt, *Magnetism Magn. Mater.*, submitted (2006)

Synthesis and biomedical applications of fluorescent functionalized magnetic nanoparticles as obtained in the miniemulsion process

V. Holzapfel¹, M. Lorenz², V. Mailänder²,
Hubert Schrezenmeier², K. Landfester¹

¹ University of Ulm, Department of Organic Chemistry III - Macromolecular Chemistry and Organic Materials, Albert-Einstein-Allee 11, 89081 Ulm, Germany

² Institute of Clinical Transfusion Medicine, Helmholtzstr. 10, 89081 Ulm, Germany

Purpose: As superparamagnetic nanoparticles are increasingly applied in the biomedical field, the route of interaction of nanoparticles with cells and tissues and the uptake of nanoparticles into cells is getting into focus. Some variables for this uptake are studied.

Materials and Methods: We therefore synthesized a series of magnetic polystyrene particles encapsulating magnetite nanoparticles (10 – 12 nm) in a hydrophobic poly(styrene-co-acrylic acid) shell by a three-step miniemulsion process. As a second reporter, a fluorescent dye (PMI) was integrated. By co-polymerization of hydrophilic acrylic acid, the amount of carboxyl groups on the surface was varied. The characterization of the latexes included dynamic light scattering, TEM, surface charge and SQUID measurements. For biomedical evaluation, the nanoparticles were incubated with different cell types. Further modification was introduced to the surface of our nanoparticles by covalently coupling lysine to carboxyl groups

Results: Finally polymerization of the monomer styrene yielded nanoparticles in the range of 45 to 70 nm. By the miniemulsion process a high amount of iron oxide was incorporated (typically 30-40% (w/w)). As hydrophilic magnetite particles are encapsulated in the composite particles, there are two interfaces between the polymer and the hydrophilic material, i.e. magnetite particles or the water phase. Therefore the carboxylic groups do not only tend to be arranged on the polymer/water-interface, but also inside the particle on the polymer/magnetite interface. This explains why about 30% less carboxylic groups are found on the surface of the particles compared to poly(styrene-co-acrylic acid) particles without magnetite (data also shown in Figure 1).

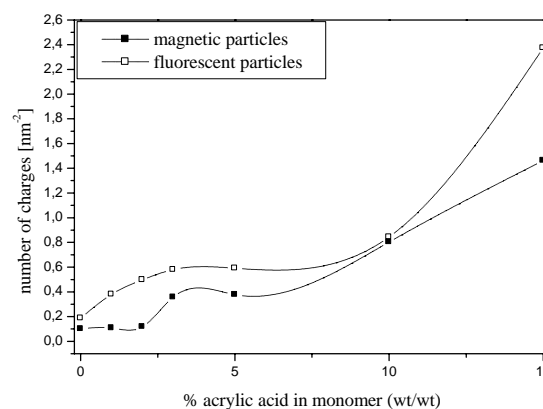


Figure 1. Surface charge density versus concentration of acrylic acid for the magnetic particles (the lines are guides to the eye). The comparison with the fluorescent particles without encapsulated magnetite(10) shows that in the case of the magnetite containing latexes the carboxylic group on the surface is reduced by about 30%.

Carboxyl groups enabled the uptake of nanoparticles into different cell lines as demonstrated by the detection of the fluorescent signal by FACS (see Figure 2) and laser scanning microscopy (Figure 3).

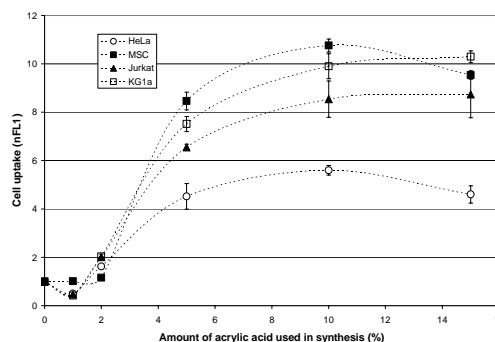


Figure 2. Uptake of VHMPM particles in different cell lines. Different cell lines show similar results for the uptake of particles with different acrylic acid contents by FACS. Lines are given as guides for the eye.

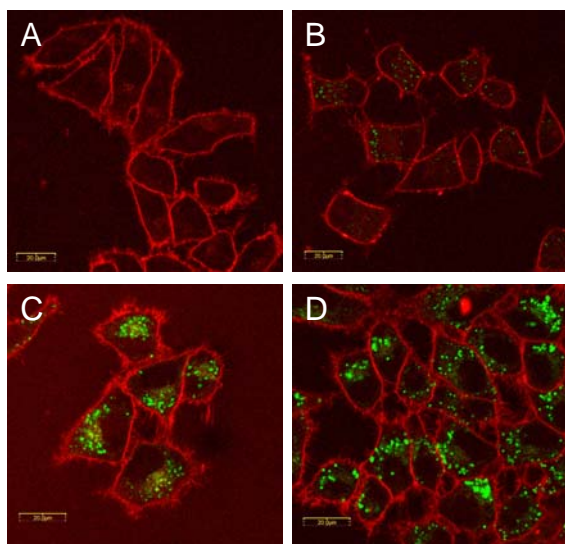


Figure 3. Laser scanning microscopy of HeLa cells. Cell membranes are stained with RH414 in red and the particles in green. A) untreated control, B) particles with 2% of acrylic acid, C) particles with 5% of acrylic acid, D) particles with 10% of acrylic acid.

The quantity of iron that is required for most biomedical applications (typically in the range of 5 to 30 pg/cell) is higher as can be achieved by functionalization of the nanoparticles with carboxyl groups. Further increase of uptake can be accomplished by transfection agents like poly-L-lysine or other positively charged polymers which are physically adsorbed on the particle surface.

The transfection functionality can also be grafted (and therefore covalently bond) onto the surface of the nanoparticles. Here, lysine was bound by the EDC coupling, using sulfo-NHS as catalyst. ζ -potential measurements of the latexes before and after coupling of lysine show that the coupling was successful: the ζ -potential after the coupling was more positive (before coupling: -47.5 mV; after coupling: -10.9 mV). In addition, the hydrodynamic diameter of the particles was more than doubled (before coupling: 68 nm; after coupling: 151 nm). Lysine functionalized nanoparticles show the same dependency of concentration with an even higher amount of measurable iron content in these cell cultures (up to 11 pg/cell, Figure 4). This means that the particles with coupled lysine are best suited for cell uptake.

Furthermore we demonstrate the subcellular localization of these nanoparticles as they are clustered in endosomal compartments (see Figure 5).

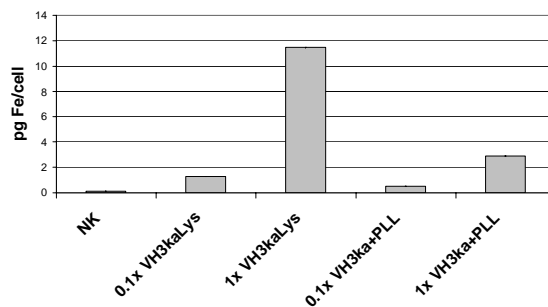


Figure 4. Iron uptake of lysine functionalized particles (VH3kaLys) and carboxyl functionalized particles with poly-L-lysine as transfection agent (VH3ka+PLL). Uptake depends on concentration of nanoparticles (0.1x equals 7.5 μg nanoparticles/ml, 1x equals 75 μg nanoparticles/ml).

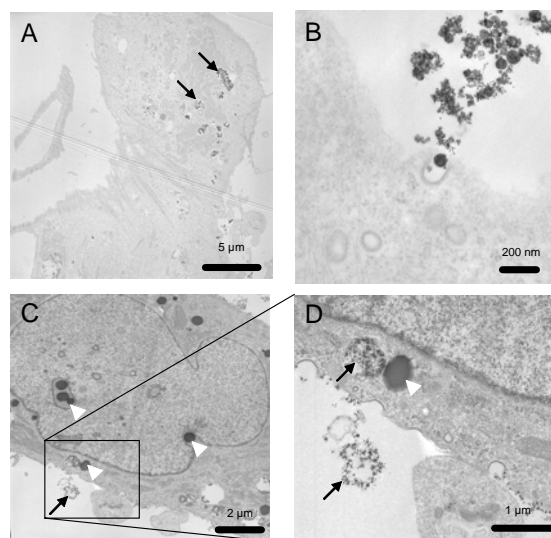


Figure 5. TEM studies of VH3ka (A and B) and VH3kaLys (C and D) in MSC. A and B were not counterstained with lead citrate. The dark spots in A (arrows) correspond to VH3kaLys in endosomes. C and D are counterstained with lead citrate and therefore cell organelles appear darker (white arrowheads), but still the iron containing VH3ka (black arrows) can be distinguished. D is a magnification of C.

References

- V. Holzapfel, A. Musyanovych, K. Landfester, M.R. Lorenz, V. Mailänder, *Macromol. Chem. Phys.* **2005**, *290*, 1025-1028.
- M.R. Lorenz, V. Holzapfel, A. Musyanovych, K. Nothelfer, P. Walter, H. Frank, K. Landfester, H. Schrezenmeier, V. Mailänder, *Biomaterials* **2006**, *27*, 2820-2828.
- V. Holzapfel, M. Lorenz, C.K. Weiss, H. Schrezenmeier, K. Landfester, V. Mailänder, *Journal of Physics: Condensed Matter* **2006**, accepted.

Hydrocarbon-based Thermoresponsive Magnetic Fluids

A. Kaiser¹, A. M. Schmidt^{1*}

¹Institute for Organic Chemistry and Macromolecular Chemistry, Heinrich-Heine University Düsseldorf, Universitätsstr. 1, D-40225 Düsseldorf

* e-mail: schmidt.annette@uni-duesseldorf.de, phone: +49 211-8114820

Motivation

We present results on the synthesis and characterization of novel thermoreversible magnetic fluids based on magnetite (Fe_3O_4) coated with a covalently anchored, polymeric shell of polystyrene (PS). The core-shell-particles referred to as Fe_3O_4 @PS form stable dispersions in toluene and benzene while in cyclohexane the shell shows a reversible volume transition at the Θ -temperature ($\sim 34^\circ\text{C}$). This behaviour is of interest for the investigation of basic nanomagnetic properties as well as for applications in responsive catalytic or separation systems.

Results

The synthesis is carried out by alkaline precipitation of Fe_3O_4 [1] with a following functionalization of the surface with 2-bromo-2,2-dimethylpropionic acid as initiator and a grafting-from *atom transfer radical polymerization* (ATRP) of styrene [2,3]. Dynamic light scattering (DLS) results combined with Gel Permeation Chromatography (GPC) experiments on the molecular weight of detached polymeric arms indicate a well defined architecture with adjustable shell thickness (s. fig. 1).

While by dispersion of the obtained magnetic polymer brush particles in toluene stable superparamagnetic fluids with magnetite contents up to 3 wt-% (according to VSM) are obtained, transferring the core-shell particles into cyclohexane leads to a thermoreversible dispersion. This can be attributed to the

occurrence of a intensively investigated Θ -temperature in the system PS/cyclohexane

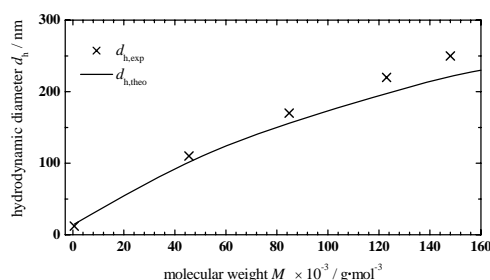
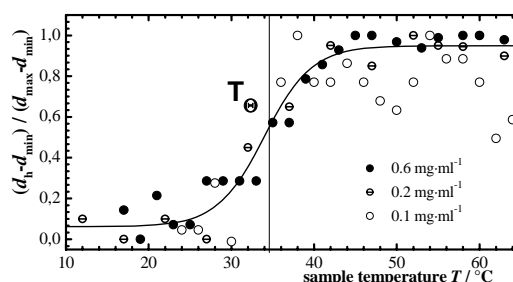


Fig. 1: Hydrodynamic diameter d_h (DLS) of Fe_3O_4 @PS-samples vs. molecular weight M_w in comparison with the theoretical model of Biver *et. al.* [3].

that is associated with a volume transition of the PS chains. [4]. We have shown that it is possible to explore the volume transition in the PS shell of diluted magnetic dispersions of the hybrid particles close to the Θ -temperature with means of DLS, and we found a concentration-



independent transition temperature and a swelling ratio close to 1.5 (s. fig. 2).

Fig. 2: Fe_3O_4 @PS in cyclohexane, hydrodynamic diameter measured at different concentrations and temperatures

This reversible shell expansion/collapse results in a less effective stabilization of the dispersion, and consequently may cause precipitation of the hybrid particles. Future experiments will show if the effect is of interest for the examination of relaxational processes and magnetic particle interactions, and applications in switchable catalytic systems will be investigated.

References

- [1] R. Massart, V. Cabuil, *J. Chem. Phys.* (1987) 84: 967–73
- [2] A. Kaiser, A. M. Schmidt, *J. Phys. Cond. Matter* (2006) accepted
- [2] C. R. Vestal, A. J. Zhang, *J. Am. Chem. Soc.* (2002) 124: 14312-14313
- [3] C. Biver et al., *Macromolecules* (1997) 30: 1787-1792
- [5] e. g. : G. Swislow, S. T. Sun, I. Nishio, T. Tanaka, *Phys. Rev. Lett.* (1980) 44: 796–798

Influence of the Gelator Type on Properties of Thermoreversible Ferrogels

M. Krekhova, G. Lattermann

Makromolekulare Chemie I, Universität Bayreuth, D-95447 Bayreuth, Germany

Thermoreversible ferrogels have been prepared by physical gelation of ferrofluids [1]. Therefore, ferrofluids (Finavestan A80B) with paraffine oil as liquid phase, containing magnetite nanoparticles, stabilized with oleic acid as a surfactant have been synthesised by the coprecipitation method. As gelators, triblock copolymers (poly(styrene-*block*-poly(ethylene-*stat*-butylene)-*block*-poly(styrene), SEBS) from the series KRATON G (1650, $M_w = 100000$; 1652, $M_w = 79000$) have been used. The results of phase transition investigations and of transmission electron microscopy (TEM) and rheological measurements of the ferrogels have been compared with those obtained for the pure gels obtained from paraffine oil and the same gelators. The gel-sol transitions T_{G-S} of both the pure gels and the ferrogels have been determined by the falling-ball method. So, a simple phase diagram has been established (Fig. 1). Below a critical gelator concentration (4 w% for G-1650 and 3w% for G-1652), two-phase systems of fluid and gel are formed. For gelator concentrations $4 \text{ w\%} > C_{\text{gelator}} < 10\text{w\%}$, the gel-sol transition temperature T_{G-S} is the same for ferrogels and pure gels.

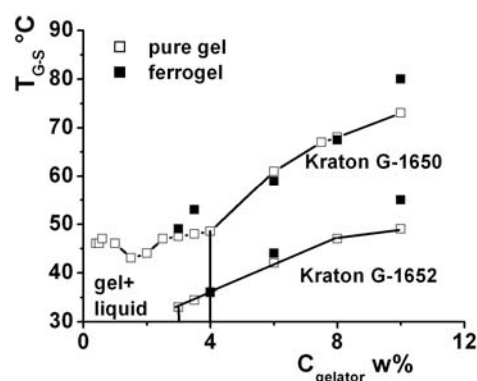


Fig. 1. Gel-sol transition temperature depending on gelator concentration.

The gels prepared with gelator G-1652 are softer and have lower T_{G-S} than those obtained using G-1650.

The structure of gels has been studied using TEM. It has been found that the typical diameters of the polystyrene micelles formed by aggregated polystyrene end-blocks were 17 ± 1.4 nm for gels with the gelator G-1650 and 11.2 ± 1.3 nm with the gelator G-1652, respectively. TEM micrographs demonstrate that the magnetite particles (7 ± 1 nm in diameter) are preferably located in the “free” paraffin phase between larger domains, formed by a several number of single SEBS micelles of the gelator (Fig. 2).

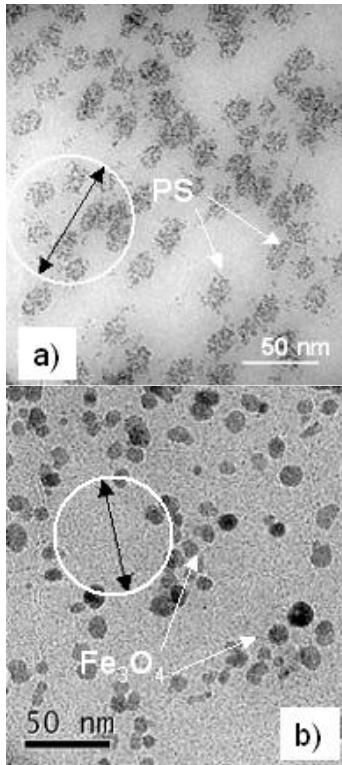


Fig. 2. TEM micrographs (cryo-cut) for a) pure gel, stained with RuO_4 and b) ferrogel. 5 w% KRATON G-1650. 22 w% magnetite concentration.

Therefore the magnetite particles make visible a “negative” picture of the structure of the micellar domains of the ferrogel, which was observed in the pure gel as a “positive” image. The size of the micellar domains is smaller for gels with the gelator G-1652.

Rheological investigations of pure gels and ferrogels with 4-10 wt% gelator demonstrate that the transition from gel to liquid occurred at temperatures 55-85 °C for gels with gelator G-1650 and 35-55 °C for G-1652, respectively.

Acknowledgments

Financial support from the DFG (Research Group FOR 608, project 5) is gratefully acknowledged.

References

- [1] G. Lattermann and M. Krekhova, *Macromol. Chem. Rapid Commun.*, 2006, in press.

Synthesis and Properties of Co, Fe, Fe/Co Nanoparticles and Magnetic Fluids.

Surface modification for biomedical Application

N. Matoussevitch^{a,b}, H. Bönemann^{a,c}, S. Behrens^a, J. Bolle^a
E. Dinjus^{a,b}

^aForschungszentrum Karlsruhe, ITC-CPV, Post Box 3640, D-76021 Karlsruhe, Germany,

^bUniversity of Heidelberg, D-69117 Heidelberg, Germany

^cMax-Planck-Institut für Kohlenforschung, Kaiser-Wilhelm-Platz 1, D-45470 Mühlheim, Germany,

During the last years the focus of our work was the development of Co, Fe and Fe/Co particles stabilising them in different carrier-liquids to produce stable metal magnetic fluids with high saturation magnetization.

We prepare Co, Fe and Fe/Co nanoparticles via thermolysis of the metal carbonyls in the presence of aluminum alkyls. Subsequent "smooth" air oxidation protects the metallic or alloyed particles against further oxidation. [1, 2].

The particles were fully characterized by electron microscopy (SEM, TEM, ESI), electron spectroscopy (MIES, UPS, and XPS) as well as by X-ray absorption spectroscopy (EXAFS).

Magnetic fluids (MFs) were obtained via peptisation of the metallic or bimetallic magnetic nanoparticles (**Fe, Co, and Fe/Co**) by using suitable surfactants in different carrier liquids, such as toluene, kerosene, mineral, vacuum and silicon oils. The resulting magnetic fluids show high saturation magnetisation values at low metal concentrations.

Each concrete application or system needs a magnetic fluid with special properties. For high vacuum seals, bearings, brakes, dampers and other technical equipment it is necessary to have long time stable magnetic fluids with high saturation magnetisation and low viscosity. In this respect our metallic and bimetallic magnetic fluids on the basis of mineral, vacuum and silicon

oils show very interesting and promising properties.

Our MFs were successfully tested in various technical applications, e.g. for brakes (W. Patzwaldt, Physiklabor, Reutlingen), positioning systems (N. Bayat, TU-Berlin), magnetic pump (R. Krauß, Uni-Bayreuth) and others.

In view of potential biomedical applications of these metallic core particles, several procedures for surface modification and the preparation of water based MFs will be presented.

Water-based MFs for biomedical applications may be obtained using bi- or polylayers around the particles with the help of suitable surfactants or phase transfer agents.

Alternatively, the particle surface may be modified by amino- or mercapto- groups. We succeeded to modify the surface of Co, Fe and Fe/Co-alloy particles by L-cysteine-ethyl ester. According to IR- and XANES-spectra SH is the anchoring group whereas the NH₂ –groups remain free for further coupling reactions in order to attach e.g. Biotin, Streptavidin, and/or antibodies, resp. linkers needed for various biomedical applications.

Surface-functionalisation using 3-aminopropyltrimethoxysilane (APTS) was also successfully carried out. Amino-modified particle surfaces are a good basis to form dendrimers increasing the amount of NH₂ –groups. Further, Amino-modification allows the metallic nanoparti-

cles to be easily coated by dextrans or silica. Preliminary tests using dextran coated Co particles for magnetic cell-separations already showed encouraging results.

Co-microspheres with improved magnetic properties as compared to magnetite were produced via the method of oil-in-water emulsion – solvent evaporation copolymerisation. Oil phase was formed from mixture of methylmethacrylate (or vinylacetate) and divinylbenzene and concentrated Co- magnetic fluid in dichloromethane which could be easily mixed in monomers. Water phase contains 2,5 % polyvinylalcohol (PVA 22000). PVA was employed as a stabilizer in the aqueous solution to stabilize the droplets.

Fig. 1 and Fig.2 displays obtained magnetic microspheres and the magnetisation curve.

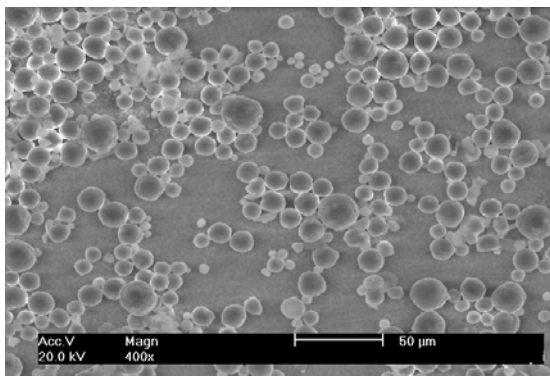


Fig. 1. SEM micrograph showing Co/poly(MMA-DVB) microspheres.

Magnetic Co particles were encapsulated in poly(vinylacetate-divinylbenzene) and poly(methylmetacrylate-divinylbenzene) microspheres resulting in spheres with a diameter of about 1-3 μ m and 5-15 μ m.

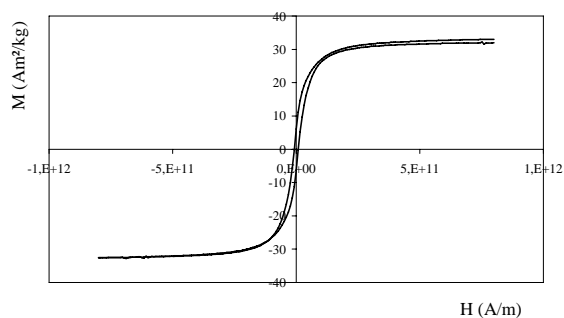


Fig.2 Magnetisation curve Co/poly(MMA-DVB)-microspheres

The saturation magnetisation was found to be 35 Am²/kg, which is higher than those reported in similar work with Fe₃O₄ magnetic fluid [3].

We have determined and compared the surface-functionalisation for different kind of modified metallic nanoparticles, e.g., by functionalisation with L-cysteine ethyl ester and APTS, dendrimers, dextran coating, as well as obtained particle-polymer microspheres. These modifications will allow the modified particles to be used directly for future biomedical applications including the binding of bioactive molecules.

Acknowledgements

The support of this work by Deutsche Forschungsgemeinschaft (SPP 1104, grant No. BO1135) is gratefully acknowledged. We thank S. Odenbach, L. Pop and T. Völker (T. U. Dresden) for magnetic measurements; B. Waßmuth (MPI, Muelheim/Ruhr) for IR-Spectra; W. Habicht (FZK Karlsruhe) for SEM, H. Modrow and N. Palina for XANES; V. Kempfer (TU-Clausthal) for MIES measurements.

References

- H. Bönnemann, W. Brijoux, R. Brinkmann, N. Matoussevitch, N. Waldöfner, DE 10227779.6 to Studiengesellschaft Kohle m.b.H (2002)
- [2] H. Bönnemann, R. A. Brand, W. Brijoux, H.-W. Hofstadt, M. Frerichs, V. Kempfer, W. Maus-Fridrichs, N. Matoussevitch, K. S. Nagabhushana, F. Voigts and V. Caps. "Air Stable Fe and Fe/Co Magnetic Fluids - Synthesis and Characterization" *Applied Organometallic Chemistry* 2005; 19; 790-796.
- [3] Yang C, Liu H, Guan Y, Xing J, Liu J and Shan G 2005 *J. Magn. Magn. Mater.* **293** 187

Response of a ferrofluid to travelling stripe forcing

Achim Beetz, Reinhard Richter and Ingo Rehberg

Experimentalphysik V, Universität Bayreuth, 95440 Bayreuth, Germany

Introduction

When a critical value of the vertical magnetic induction is surpassed, the surface of a ferrofluid exhibits an array of liquid crests. This Rosensweig instability [1] has mostly been investigated with respect to its static aspects (see [2], e.g.) or under temporal modulation of the magnetic field (see [3], e.g.) or the gravitational acceleration [4]. Both excitations are homogeneous in space. Recently these driving modes have been extended by a particularly simple mode of spatiotemporal forcing, namely a travelling stripe forcing [5]. We apply it for the first time to the surface of magnetic liquids in the advent of the Rosensweig instability. This kind of magnetic modulation is of high interest in the immediate vicinity of the instability, because there, critical scaling laws of standing and travelling waves have been measured [6]. We report on the amplitude of travelling waves as a function of the lateral driving velocity.

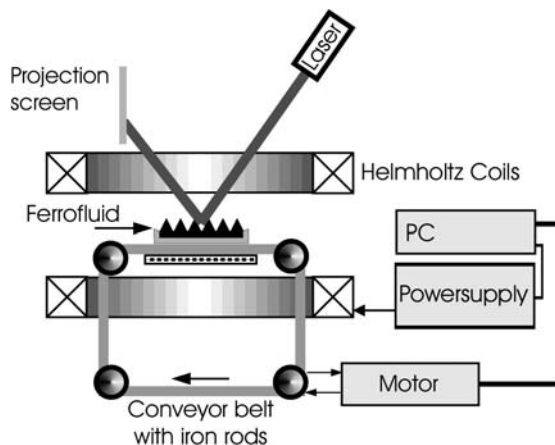


Figure 1: *The experimental setup*

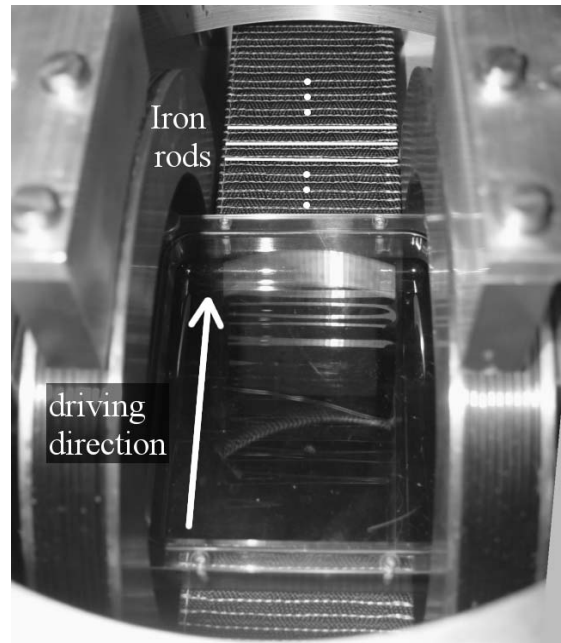


Figure 2: *The band under the ferrofluid*

Experimental setup

The Ferrofluid container is placed inside a Helmholtz pair of coils with a constant magnetic field applied perpendicular to the surface. The modulation of the magnetic field is realized with a "conveyor belt", which harbours periodically placed iron rods with the same wavelength as the surface pattern. It is driven by a eletromotor which allows to vary the velocity. Because of the higher suszeptibility of the iron, the magnetic field strength varies along the driving direction. Figure 2 shows a picture of the experiment, which unveils that the iron rods attract the fluid. The ferrofluid we use is mark APG 512A from Ferrotec Co.

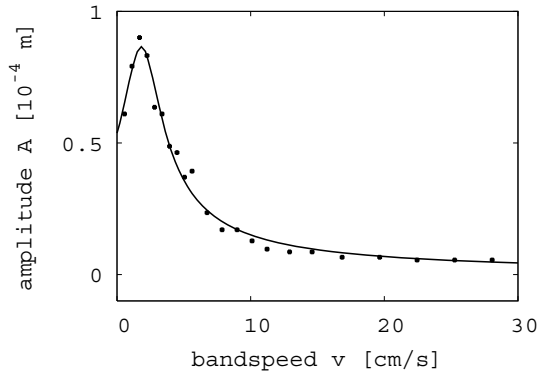


Figure 3: Amplitude of the stripes versus the driving velocity at $B = 15.6$ mT. The solid lines displays a fit by Eq. (1) with $A_0 = 1.7$, $v_c = 3.1$ and $\delta = 0.8$

Experimental results

Currently we observe the dynamics of travelling waves. For this we are measuring the amplitude of the fluid waves in dependency of the driving velocity. This is done with a laser reflected on the surface. The wavelength is fixed, so there exists a native propagation velocity corresponding to the dispersion relation. If driving is done with this velocity, the system is in resonance and the amplitude is maximal. Now we can shift the propagation velocity by varying bias magnetic induction via the Helmholtz coils. At the critical induction for the Rosensweig instability ($B_c = 15.8$ mT) the velocity is predicted to be zero [6]. For figure 3 B has been selected to be slightly smaller than B_c .

The amplitude of the travelling waves passes through a maximum and decays for higher band velocities. The response to the spatio-temporal driving can well be described by the behaviour of a damped harmonic oscillator

$$A(v) = \frac{A_0 v_c^2}{\sqrt{(v^2 - v_c^2)^2 + v^2 \delta^2}}. \quad (1)$$

Here A denotes the amplitude, A_0 the amplitude at zero velocity, v the driving velocity, v_c the critical driving velocity and δ the

damping. A fit by Eq. (1) is shown in figure 3 as the solid line.

Measuring the amplitude for different magnetic inductions leads to the dispersion relation of the ferrofluid for subcritical fields.

Further Issues

In future works we want to investigate a stripe hexagon transition in a tilted magnetic field triggered by the periodically modulation similar to [5]. Also the the hexagon square transition under such a driving force is an interesting subject.

Acknowledgments

We thank Christopher Groh and Klaus Oetter for technical assistance with the setup. Financial support by *Deutsche Forschungsgemeinschaft* under grant Ri 1054/1-4 is gratefully acknowledged.

References

- [1] M. D. Cowley and R. E. Rosensweig, *J. Fluid Mech.* **30**, 671 (1967).
- [2] C. Gollwitzer, R. Richter, and I. Rehberg, *The Surface Topography of the Rosensweig Instability — a Quantitative Comparison between Experiment and Numerical Simulation*, *J. Fluid Mech.*, 2006, accepted.
- [3] T. Mahr and I. Rehberg, *Europhys. Lett.* **43**, 23 (1998).
- [4] H. Ko, J. Lee, and K. J. Lee, *Phys. Rev. E* **67**, 026218 (2003).
- [5] D. G. Miguez *et al.*, *Phys. Rev. Lett.* **93**, 048303 (2003).
- [6] B. Reimann, R. Richter, I. Rehberg, and A. Lange, *Phys. Rev. E* **68**, 036220 (2003).

Numerical simulations of ferrofluid dynamics: Comparison of various ferrofluid models

D.V. Berkov¹, N.L. Gorn¹, R. Schmitz², D. Stock¹

¹INNOVENT e.V., Prüssingstr. 27B, D-07745, Jena, Germany

²Institute of Theoretical Physics C, RWTH Aachen, 52056 Aachen, Germany

Introduction

We present a general methodology for numerical simulations of the ferrofluid dynamics analyzing the applicability of various ferrofluid models. We discuss three types of models which can be used to study remagnetization processes in ferrofluids:

- (i) the simplest ‘*rigid dipoles*’ model with magnetic moments ‘firmly attached’ to ferrofluid particles (not allowed to move with respect to particles themselves);
- (ii) the model with *discrete orientations* of particle moments relative to particles;
- (iii) the model where magnetic moments can continuously rotate relative to particles (*‘flexible moments’* model), i.e., internal magnetic degrees of freedom are taken into account rigorously.

Validity of various ferrofluid models

Three models listed above are described by very different systems of stochastic equations of motions: (i) the ‘*rigid dipoles*’ model uses the equations only for the translational and rotational particles motion; (ii) the model with *discrete* moment orientations within a particle should (in addition to the equations mentioned above) contain the rule to calculate the probability of the moment to ‘jump’ between these orientations; (iii) finally, the ‘*flexible moments*’ model includes the Landau-Lifshitz-Gilbert equations of motion for magnetic moments with respect to particles.

To find out, for which physical parameters of ferrofluid particles and external conditions these models can be applied, we compared thermal energy kT and three characteristic energy scales of a ferrofluid:

- Demagnetizing (self-interaction) particle energy $E_{\text{dem}} \sim M_S^2 V_m$;
- Single-particle uniaxial anisotropy energy $E_{\text{an}} \sim KV_m = \frac{\beta}{2} M_S^2 V_m = \frac{\beta}{2} E_{\text{dem}}$, (here $\beta = 2K/M_S^2$ is the reduced anisotropy constant);
- Maximal magnetodipolar interaction energy $E_{\text{dip}}^{\text{max}} \approx \frac{\mu^2}{r_{\text{min}}^3} = \frac{(M_S V_{\text{mag}})^2}{(2R_{\text{part}})^3}$ between particles.

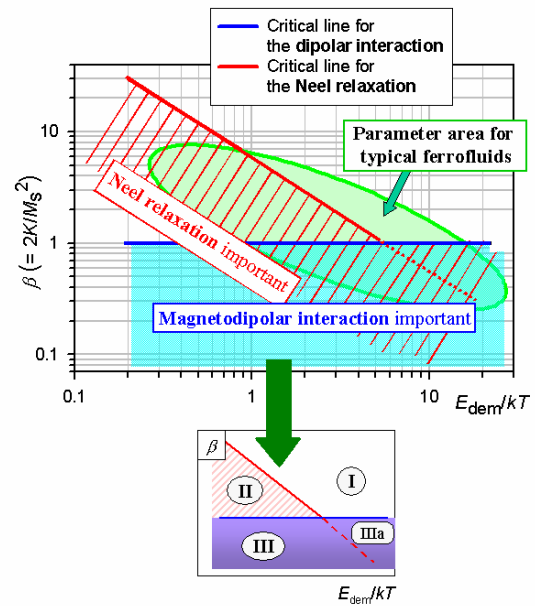


Fig.1 ‘Phase diagram’ showing the validity regions of various ferrofluid models

Basing on the above mentioned comparison, we have composed the ‘phase diagram’ in co-ordinates ‘particle size - anisotropy’ where the validity regions of each model mentioned above and the area of typical ferrofluid parameters are shown (Fig. 1). The main result of this analysis is

that for most ferrofluids only the ‘flexible moments’ model provides adequate physical results.

Physical applications

Using Langevin dynamics simulations we have studied remagnetization processes of various kinds in ferrofluids in frames of the models listed above.

Equilibrium magnetization. Here we could show analytically (and confirm our result by numerical simulations) that equilibrium magnetization properties of a ferrofluid (like the field dependence of the magnetization $M(\mathbf{H})$) are the same for all ferrofluid models discussed in the previous Section.

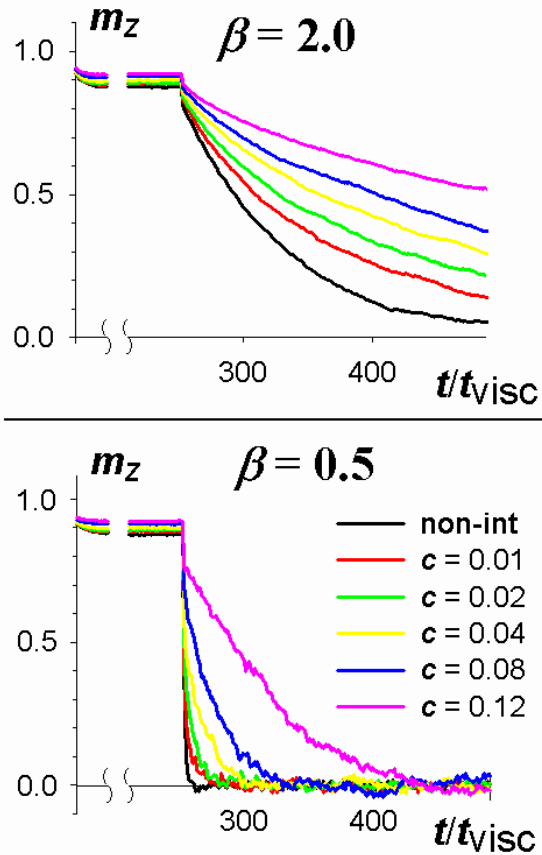


Fig. 2 Magnetization time dependence of a ferrofluid after an external field has been switched off for high (upper panel) and low (lower panel) single particle anisotropy values.

Magnetization relaxation. In contrast to the equilibrium (time-independent) properties, relaxation of a ferrofluid magnetization after an external magnetizing field is switched off, occurs very differently for models

with rigid and flexible moments (Fig. 2, upper panel shows the relaxation of a ferrofluid with the high single particle magnetic anisotropy which is equivalent to the ‘rigid dipole’ case). We have demonstrated that the influence of the magnetodipolar interparticle interaction is also very different for various ferrofluid models.

AC-susceptibility. Studying the frequency dependence of the *ac*-susceptibility we have found that for all models the peak of its imaginary part shifts towards *lower* frequency with *increasing* particle concentration (dipolar interaction strength), but the shift amount strongly depends on the model applied. Again, for most practically relevant ferrofluids correct results can be obtained only using the ‘flexible dipoles’ model. Detailed discussion of these results will be given by the presentation.

Particle aggregation in ferrofluids. Using our fast methods for calculating magnetodipolar interaction field, we have simulated the formation of particle aggregates in an external field for systems with up to $2 \cdot 10^4$ particles. Within reasonable simulation times (corresponding to real physical times $\sim 10^{-3}$ sec) we could not achieve the system equilibration, which would manifest itself in the saturation of the spatial correlation function of particle positions. We also could not observe the formation of aggregates more complex than single chains (e.g., droplets), predicted by some mean-field based theories. We conclude that further increase of the system size and accessible simulation times are necessary to study these phenomena.

Hydrodynamic interparticle interaction. In the last part of our contribution we present analytical formulae which allow to study the influence of hydrodynamic interaction on the magnetization dynamics of ferrofluids (including the coupling between translational and rotational particle degrees of freedom) and show some preliminary results of these studies.

Pattern Formation in Isotropic Ferrogels – Nonlinear Analysis Using the Energy Method

S. Bohlius¹, H. Pleiner¹ and H. R. Brand²

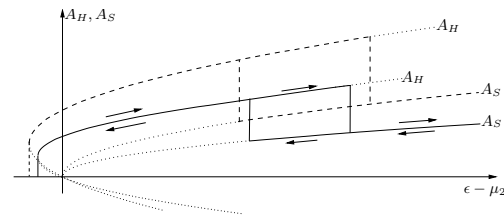
¹Max Planck Institute for Polymer Research, 55021 Mainz, Germany

²Theoretische Physik III, Universität Bayreuth, 95440 Bayreuth, Germany

Ferrogels are chemically cross-linked polymer networks that are generated using a ferrofluid as a solvent. Just as ferrofluids [1], ferrogels undergo an instability from an initially flat surface to a stationary spike structure, if an external magnetic field applied perpendicular to the surface exceeds a certain critical value. In the case of isotropic ferrogels this critical magnetic field is enhanced by the shear modulus of the network. The wavelength of the critical mode, however, does not change with respect to usual ferrofluids at the onset of the instability [2]. For a nonlinear discussion of this instability, we extend the previous discussions for magnetic fluids of Gailitis [3] and Friedrichs and Engel [4], who used an energy minimizing method, to media with elastic degrees of freedom. In addition to the known surface energy density of ferrofluids we add the contribution due to elasticity. We discuss the stability of three regular surface patterns: stripes, squares and hexagons.

Stripes turn out to be never stable with respect to one of the other two regular patterns. At the linear threshold hexagons are energetically more favorable than squares. The transition from the flat surface to the hexagonal pattern for increasing magnetic fields takes place at a higher threshold than the back transformation to the flat surface in case of decreasing magnetic fields. This hysteretic region shrinks with increasing shear modulus. For higher magnetic fields the hexagonal pattern becomes unstable in favor of squares. Also this transition shows a hysteresis for the back transformation to hexagons. With increasing shear modulus

this hysteretic region shrinks.



The figure shows qualitatively (not to scale) the behavior of the amplitudes of the surface spikes arising beyond the linear threshold $\epsilon - \mu_2 = 0$. The amplitudes of the spike patterns are smaller for ferrogels (solid lines) than for ferrofluids (dashed lines).

References

- [1] R. E. Rosensweig, *Ferrohydrodynamics* (Cambridge University Press, Cambridge, England 1985)
- [2] S. Bohlius, H. R. Brand and H. Pleiner, *Z. Phys. Chem.* **220**, 97 (2006)
- [3] A. Gailitis, *J. Fluid Mech.* **82**, 401 (1977)
- [4] R. Friedrichs and A. Engel, *Phys. Rev. E* **64**, 021406 (2001)

Microstructure of ferrofluid monolayers: theory and computer simulations

J. Cerda¹, C. Holm^{1,2}, S. Kantorovich^{1,3}

¹*Frankfurt Institute for Advanced Studies, Frankfurt, Germany*

²*Max-Planck Institute for Polymer Research, Mainz, Germany*

³*Department of Mathematical Physics, Urals State University, Ekaterinburg, Russia*

The ferrofluid microstructure is not only a tasty morsel for theoreticians, but also is important for the applications. The particle size and the optical properties of carrier liquids make the natural studies of the aggregation processes in 3D samples difficult, but it is possible to use cryo-TEM in 2D (in monolayers) [1]. There it has been found in that 2D ferrofluid layers inherit a lot of properties from the bulk samples. In order to investigate the peculiarities brought by the 2D geometry into the aggregation processes in ferrofluids we use here a combination of theoretical density functional and molecular dynamic computer simulation approaches. Long-range dipolar interactions in model ferrofluid monolayers are computed using a modified P3M algorithm in combination with a dipolar layer correction. In comparison to the traditional Ewald sum methods, this approach allows to handle with larger systems. The new theoretical approach for 2D systems describes the coexistence of chain- and ring-like structures.

Code	d_m, nm	l, nm	ϕ	λ, kT
A	16	2	0.05	2
B	20	2	0.05	4
C	9	2	0 – 0.04	0.1

Table 1: System parameters: d_m – the magnetic core diameter, l – the particle nonmagnetic layer thickness, ϕ – the surface fraction of particles, λ – the coupling constant.

In figures 1 – 4 typical equilibrium snapshots are presented for different mixtures of systems A – C (Table 1) . First we study the the behavior of the pure system A (Fig. 1), and pure system B (Fig. 2). In the system A the interparticle attraction is too weak to lead to aggregation, but in the system B chains and ring-like structures are visible. The appearance of rings is the consequence of the entropy in monolayers. Due to the same reason the average number of particles per chain (N) in 2D ($N \sim 1.6$, system B) is larger than in 3D (see, Ref. [2]) ($N \sim 1.2$). To understand the influence of small particles we add system C to systems A and B increasing the concentration of system C from $\phi = 0$ to 0.04. In Fig. 3 one can see aggregates in the A C mixture (surface fraction of small particles – 0.04). Fig. 4 illustrates the equilibrium conformation in B C mixture (for small particles $\phi = 0.04$). The calculation of the average number of large particles per chain showed no dependence on the small particle concentration for the mixtures A C, these systems remain almost nonaggregated. But N decreases for the B C mixture with the increase of the system C portion in the system.

The qualitative behavior obtained in theory and simulations is similar to the one predicted by experiments in Ref. [1]. An extensive quantitative comparison of the experimental results to the theoretical predictions and computer simulations will be presented.

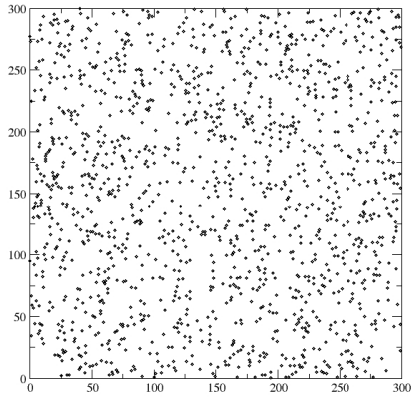


Figure 1: Simulation snapshot. System A (see Table 1).

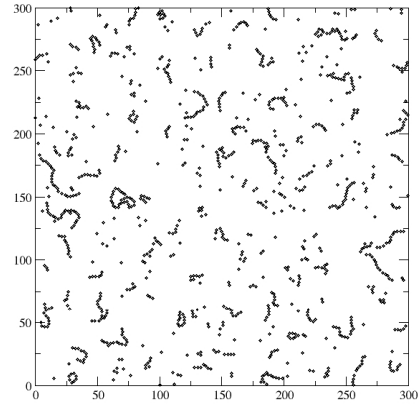


Figure 2: Simulation snapshot. System B (see Table 1).

Acknowledgments

The research was carried out with the financial support of INTAS Grant No. 03-51-6064, RFBR Grant No. 04-02-16078, CRDF Award No. REC-005, DFG Grant No. HO 1108/8-4, President RF Grant MK-4836.2006.2, CRDF Grant Y3-P-05-11, and the Dynasty Foundation.

References

- [1] M. Klokkenburg, R. Dullens, W. Kegel, B. Ern e, and A. Philipse *Phys. Rev. Lett.* **96**, 037203, (2006).
- [2] Z. Wang, Ch. Holm, and W. M ller *Phys. Rev. B.* **66**, 021405, (2002).

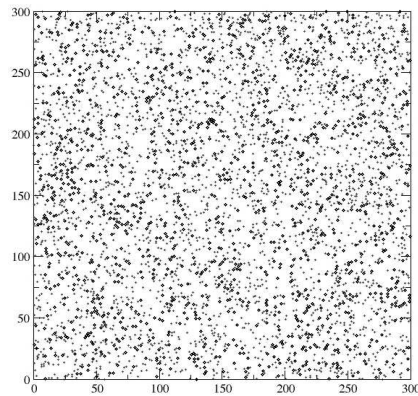


Figure 3: Simulation snapshot. A C mixture (see Table 1, small particle surface fraction is 0.04).

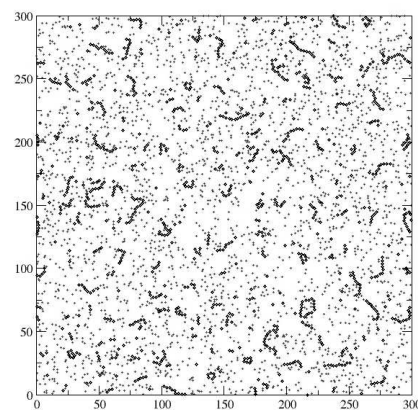


Figure 4: Simulation snapshot. B C mixture (see Table 1, small particle surface fraction is 0.04).

Parametric modulation of thermal and thermomagnetic convection in magnetic fluids

Harald Engler¹, Stefan Odenbach¹

¹ *Lehrstuhl für Magnetoﬂuidodynamik, Technische Universität Dresden, 01062 Dresden*

Motivation

The possibility to control the flow properties of ferroﬂuids by means of a magnetic field opens numerous possibilities in ﬂuid mechanics research. Heat and mass transfer phenomena in ﬂuids in general and convection phenomena in particular have been a topic in ﬂuid mechanics at all times. Due to the additional magnetic force in ferroﬂuids it is possible to control the convection, especially the critical temperature difference when the transfer of heat changes from diffusion to convective ﬂow. This kind of convection which is dependent on temperature difference and magnetic force is called thermomagnetic convection. It can be described by the magnetic Rayleigh-Number. First experiments in this ﬁeld were made by L. Schwab [1].

Previous investigations have shown [2] that the critical temperature difference of thermal convection in a horizontal ﬂuid layer depends on the geometric and thermal boundary conditions of the systems. For such thermal convection systems the driving force is constant in time. However, the behaviour in such a system changes dramatically if the driving force is periodically modulated in time. Former investigations predicted that the critical temperature of thermal convection is dependent on the frequency of the driving force [3].

In the case of pure thermal convection the driving force results from density differences in the ﬂuid forced by the temperature gradient. The inﬂuence of a temporal periodically modulated driving force on thermal convection was theoretical investigated in the end of the 60's [4, 5, 6]. The experimental realisation of a situation

where thermal convection is subjected to a time variable driving force fails due to immense technical problems risen by the fact that either the temperature gradient or gravitational acceleration would have to be modulated with frequencies in the order of 1Hz.

In contrast thermomagnetic convection is driven by the mentioned magnetic force which is created by an external magnetic ﬁeld. This ﬁeld can easily be modulated in time leading to the required time dependent driving force.

Experimental setup

The experimental set up is designed to measure the heat ﬂux through a horizontal ferroﬂuid layer and to modulate the generated magnetic ﬁeld.

An advanced Helmholtz coil arrangement is used to generate the magnetic ﬁeld (fig.1). Two additional coils are ﬁxed to the common Helmholtz arrangement extending the area of homogeneous ﬁeld in the center of the coils. The area which is useable for experiments has a diameter of 350 mm and a height of 100 mm. The homogeneity in this region is in horizontal direction better than 0.5 % and in vertical direction on a height of 10 mm better than 0.1 %. In the homogeneous area it is possible to generate a magnetic ﬁeld with a strength of up to 25 kA/m. For the temporal variation of the ﬁeld strength a frequency synthesiser is connected to the coil arrangement. The synthesiser is designed for frequencies between 0 and 10 Hz.



fig. 1: Fanselau arrangement to generate a magnetic field strength up to 25 kA/m

The measuring cell for detecting the heat flux in the horizontal layer consists of an upper and a lower temperature chamber which applies a global heat flux (fig.2).

The temperature chambers have been flown through by tempered water. It is possible to generate a temperature difference up to 65 K.

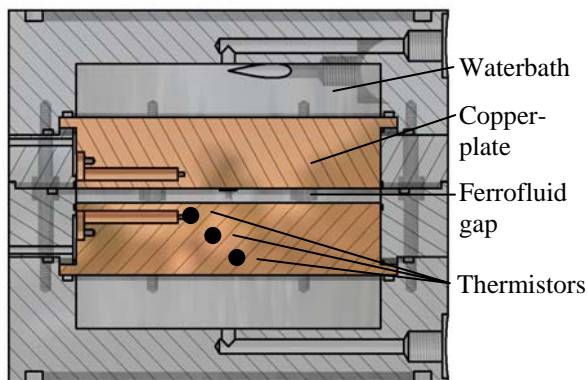


fig. 2: Measuring cell to determine the heat flux by using thermistors for temperature measuring.

Between the two temperature chambers a horizontal gap filled with ferrofluid is located. The gap is 4 mm high and the diameter is 88 mm, leading to an aspect ratio of 22. If the aspect ratio is larger than 15 the influence of the vertical gap boundaries are insignificant. The gap is bounded by two copper plates. The copper has a heat conductivity of 378 W/Km.

For the measurement of the temperature differences between the plates it is important to determine their average temperature. Temperature differences in the fluid

influenced by the convection flow are equalized in the surface zone of the copper plates due to the high heat conductivity of copper. The temperature distribution in the plates is thus homogenous in the region where the measuring sites are located. Thermistors with a temperature resolution of 0.01 K are used to measure the temperature in three vertically spaced positions in the copper plates (fig.2). The temperature difference of two points is used to calculate a temperature gradient. By extrapolation using the gradient and the temperature on one point one can obtain the surface temperature.

Finally the heat flux through the horizontal ferrofluid layer influenced by the modulated magnetic field can be calculated by using the measured temperature difference and the fluid properties.

References

- [1] L. Schwab, Konvektion in Ferrofluiden, Dissertation, Universität München, München (1989)
- [2] S. Chandrasekhar, Hydrodynamic and Hydromagnetic Stability, New York, Dover (1961)
- [3] G. Ahlers, P. C. Hohenberg, M. Lücke, Thermal convection under external modulation of driving force, *Phys. Rev. A*, 32 (1985), 3493-3518
- [4] g. J. Venezian, Effect of modulation on the onset of thermal convection, *J. Fluid. Mech.*, 35 (1969) 234-254
- [5] P. M. Gresho, R. L. Sani, The effect of gravity modulation on the stability of a heated fluid layer, *J. Fluid. Mech.*, 40 (1969) 783-806
- [6] S. Rosenblatt, G. A. Tanaka, Modulation of thermal convection instability, *Phys. Fluids*, 14 (1971) 1319-1322

Magnetic kicks to a ferrogel ball

How a ferrogel sphere elongates in a uniform pulsed magnetic field

Christian Gollwitzer¹, Alexander Turanov², Marina Krekhova³ and Reinhard Richter¹

¹Experimentalphysik V, Universität Bayreuth, 95440 Bayreuth, Germany

²Zavoisky Physical-Technical Institute, KSC, RAS, 420029 Kazan, Russia

³Makromolekulare Chemie I, Universität Bayreuth, 95440 Bayreuth, Germany

Introduction

Ferrogels are an interesting class of new intelligent materials that arise as a combination of soft matter and ferrofluids [1]. In contrast to merely combining the properties of both materials, they also exhibit new qualitative behaviour: because of the coupling of the magnetic particles to the gel network, they can convert a magnetic stress into a mechanical force. Macroscopic deformations have only been observed in gradient magnetic fields so far [2], because this effect is much larger than in uniform fields [3]. However, theoretical estimates of the elongation of a magnetizable, elastic sphere in a homogeneous magnetic field date back to 1960 [4].

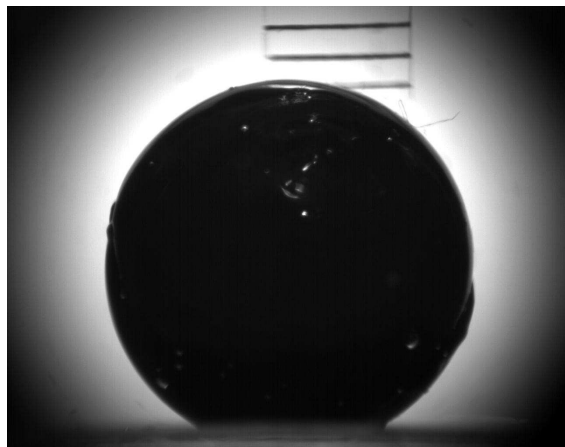


Figure 1: *Sphere made of a thermoreversible ferrogel and suspended in water.*

Experimental Methods

We produce a spherical sample of a thermoreversible ferrogel [5] by casting the gel

into an aluminium mould. The ferrogel has a density of $\rho = 1.006 \text{ g/cm}^3$ and is superparamagnetic (see figure 2). To minimize

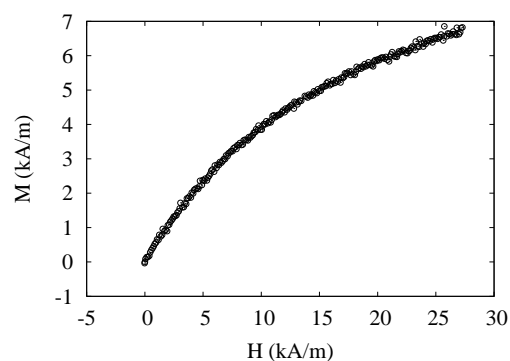


Figure 2: *Magnetization curve of the thermoreversible ferrogel sample.*

the influence of gravity on the shape, the ferrogel ball is immersed into water and observed laterally by a CCD camera. The contour of the sample is locally fitted with a circular arc to determine its position. The sample reveals elastic, anelastic and plastic deformation typical for gels. A pulse technique is utilized to measure only the truly elastic contribution to the elongation, where the ball is given subsequent magnetic “kicks” of increasing strength. To measure the Young modulus of this truly elastic deformation, a cylinder of ferrogel is deformed mechanically with different velocities, and the pure elastic contribution is extrapolated from the force exerted by the gel.

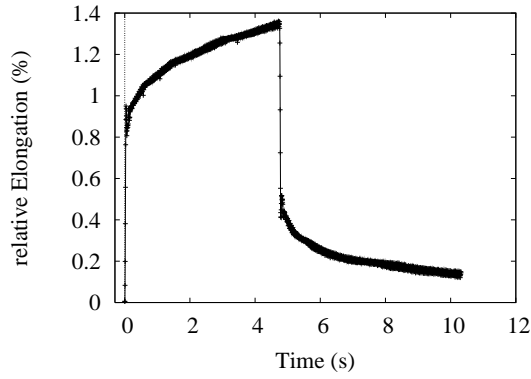


Figure 3: *Elongation of a ferrogel ball in response to a pulse of a spatially uniform magnetic field.*

Results

The response of the ball to a magnetic kick is shown in figure 3. The relative elongation is defined by $\varepsilon = (D(B) - D_0)/D_0$, where $D(B)$ is the diameter of the sample in the direction of the magnetic field and D_0 its undistorted size. The elongation as a function of the magnetization is then compared to the models by Raikher [6] and Landau [4]. Both predict the dependence of the relative elongation ε on the magnetization M to be

$$\varepsilon = \kappa \frac{\mu_0 M^2}{E}, \quad (1)$$

where $\kappa = \frac{1}{15}(\frac{5}{57})$ for Landau's (Raikher's) model, respectively. We find in fact a linear relation between ε and M^2 (see figure 4), but with a different constant κ .

In summary, we propose a simple testbed for the magnetoelastic response of ferrogels. Preliminary results indicate, that the complex elasticity of this new kind of smart material has to be taken into account for a proper theoretical description.

Acknowledgement

We are grateful for helpful advice by Günter Lattermann, Yuriy Raikher and Ingo Rehberg. Financial support by *Deutsche Forschungsgemeinschaft* under grant Ri 1054/2-1 is gratefully acknowledged.

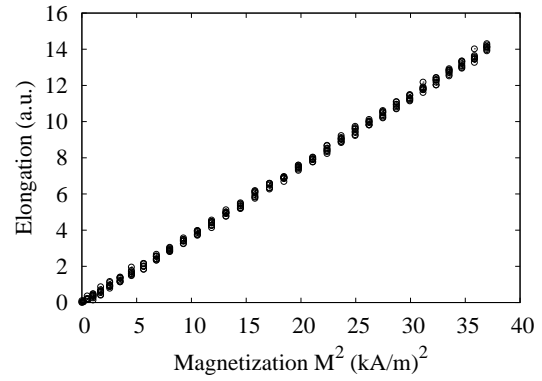


Figure 4: *Dependence of the elongation on the magnetization of the ball*

References

- [1] M. Zrinyi, L. Barsi, and A. Buki, *The Journal of Chemical Physics* **104**, 8750 (1996).
- [2] M. Zrinyi, L. Barsi, D. Szabo, and H.-G. Kilian, *The Journal of Chemical Physics* **106**, 5685 (1997).
- [3] L. Nikitin, G. Stepanov, L. Mironova, and A. Gorbunov, *Journal of Magnetism and Magnetic Materials* **272**, 2072 (2004).
- [4] L. D. Landau and E. M. Lifschitz, *Electrodynamics of Continuous Media*, 3. ed. (Pergamon, Oxford, 1960), Vol. 8.
- [5] G. Lattermann and M. Krekhova, to appear in *Macromol. Rapid. Commun.* (2006).
- [6] Y. Raikher and O. Stolbov, *Journal of Applied Mechanics and Technical Physics* **46**, 434 (2005).

Flip of hexagonal surface pattern under broken symmetry

Christopher Groh¹, Friedrich Busse², Ingo Rehberg¹ and Reinhard Richter¹

¹Experimentalphysik V, Universität Bayreuth, 95440 Bayreuth, Germany

²Theoretische Physik, Universität Bayreuth, 95440 Bayreuth, Germany

Introduction

One of the hallmarks of isotropic systems is the possibility to bifurcate subcritically to hexagons from an unstructured ground state, which is due to the interaction of three degenerate wave numbers [1]. The situation is *structurally unstable*, however: The smallest perturbation of this symmetry acts as a singular perturbation and will lead to a qualitatively different instability, namely, a primary bifurcation to stripe like pattern. As a specific example, an asymmetric realisation of the Rosensweig instability [2] has recently been investigated in theory [3] and experiment [4]. Different surface patterns were observed, comprising regular hexagons (see Fig.1a), anisotropic hexagons and ridges (b).

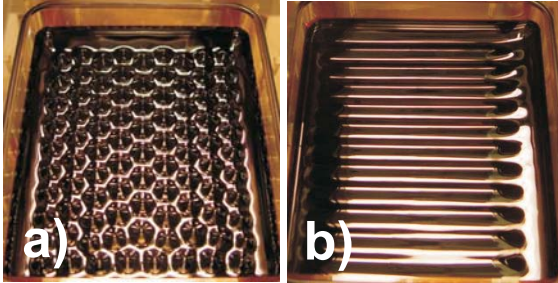


Figure 1: Hexagons (a) and ridges (b) on the surface of a ferrofluid.

Here we investigate transitions between these patterns under variation of the field components. The surface topography is quantitatively characterized via help of a radiosopic technique. This enables us to present the proper phase diagram for the tilted field instability. Moreover, we report a *new effect*: the reorientation of the hexagonal pattern under an increasing tangential field component.

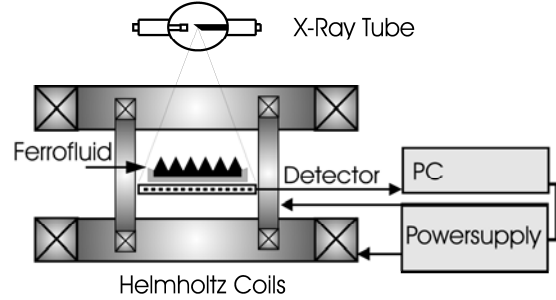


Figure 2: Scheme of the experimental setup with the two Helmholtz pair of coils for B_z and B_x .

Experimental setup

By means of two pairs of orthogonal Helmholtz coils we are able to apply a vertical and a horizontal magnetic induction, denoted by B_z and B_x , respectively. A rectangular vessel is brimful filled with magnetic fluid, and is placed in the centre of the coils. An x-ray tube is mounted above the center of the vessel at a distance of 1606 mm, in order to provide an almost parallel beam. The radiation transmitted through the fluid layer and the bottom of the vessel is recorded by an x-ray sensitive photo diode array detector with a resolution of 16 bit. The full surface relief can then be reconstructed with a resolution of 1 μm from the calibrated radiosopic images. For more details of this technique see [5].

Experimental results

Varying B_z for certain B_x we have mapped the stability regions of (stretched) hexagons and ridges in the full parameter plane. The outcome is in agreement with the theoretical predictions [3]. However, unpredicted behaviour was found, by setting B_z to an overcritical value and increasing B_x from zero. Figure 3 shows a

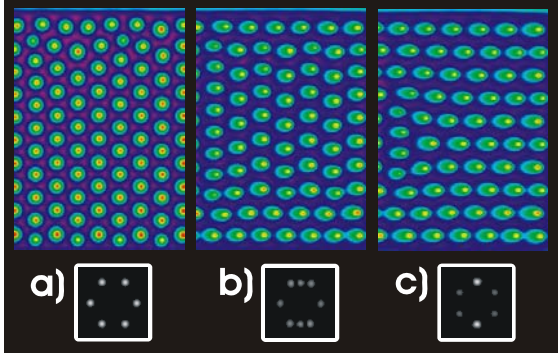


Figure 3: Series of surface reliefs taken via radioscopy and the corresponding 2D Fourier transforms. B_x increases from 1.3 mT (a) via 3.8 mT (b) to 5.3 mT (c).

sequence of three radioscopic surface reliefs unveiling a new type of transition. Starting at regular hexagons (Fig.3 a) the pattern rearranges under increase of B_x (b) until the hexagons are eventually “flipped” to a new orientation (c), as seen as well in Fourier space. Figure 4 gives the nomenclature of the different modes before and after the transition.

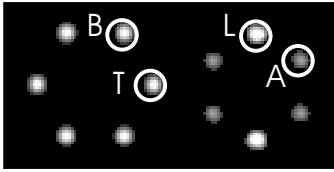


Figure 4: The hexagonal mode before (B) and after (A) the transition, and the transversal (T) and longitudinal (L) modes.

Obviously the primary orientation of the hexagonal mode (B) is not in accordance with the finally dominating longitudinal mode (L), which gives rise to the transition. The evolution of the amplitudes of the four different modes is plotted in Fig. 5. The modes B (dashed) and T (dashed-dotted) are decaying under increase of B_x whereas L (solid) is increasing. After a sudden collapse of B and T at $B_x = 5.5$ mT we observe a short flare of A (dotted), until only the mode L remains. This final state consists of plain ridges, as shown in Fig.1b).

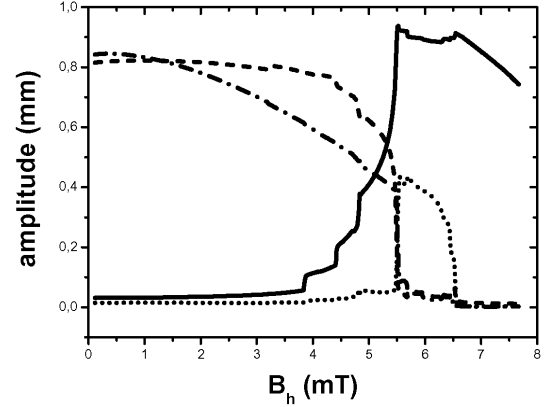


Figure 5: The evolution of the amplitudes B (dashed), T (dashed-dotted) L (solid) and A (dotted) under increase of B_x .

The competition between the different pattern can well be characterized by a weakly nonlinear analysis, based on a system of four coupled amplitude equations, describing the evolution of the modes B , T , L , and A , which will be presented in detail.

Acknowledgements

We thank R. Friedrich and W. Pesch for stimulating discussions. The experiments have been financially supported by *Deutsche Forschungsgemeinschaft* under grant Ri 1054/1-4.

References

- [1] M.C. Cross and P.C. Hohenberg, *Rev. Mod. Phys.* **65**, 851 (1993).
- [2] M.D. Cowley and R.E. Rosensweig, *J. Fluid Mech.* **30**, 671 (1967).
- [3] R. Friedrichs, *Phys. Rev. E*, **66**, 066215 (2002).
- [4] B. Reimann, R. Richter, I. Rehberg and R. Friedrichs, *Phys. Rev. E*. **71**, 055202 (2005).
- [5] R. Richter, J. Bläsing, *Rev. Sci. Instrum.* **72**, 1729 (2001).

Magnetic and optical properties of some Ferrofluids and of paramagnetic Metallomesogens doped with Ferrofluids

W. Haase¹ and Y. Galaymetdinov^{1,2}

¹*Eduard-Zintl-Institute of Inorganic and Physical Chemistry, Darmstadt University of Technology, Darmstadt, Germany*

²*Kazan Physical Institute, Russian Academy of Sciences, Kazan, Russia*

By doping nematic Liquid Crystals, which mainly behave diamagnetic, with Ferrofluids the so called Ferronematics will be obtained. Ferronematics showing special magnetic and optical properties which are well described.

Paramagnetic Metallomesogens usually don't show a nematic phase rather a smectic A phase. By doping such paramagnetic Metallomesogens with Ferrofluids a rather strong increase of the magnetic anisotropy appeared which can be stored below the liquid crystalline state, e.g. at room temperature. The external magnetic field strength needed to align the doped system is rather weak compared to the non doped system. The strong increase of the magnetic anisotropy is a consequence of the coupling of the magnetic properties of the host with them of the guest. The coupling depends on the orientation of the major axes of the paramagnetic Metallomesogen with respect to the external magnetic field. Several examples will be presented both with the paramagnetic anisotropy parallel or perpendicular to the long axes of the paramagnetic Metallomesogen.

To study such effects the magnetic behavior of the used Ferrofluids above room temperature must be investigated. By doing so we found an increase of the magnetic moment with increasing temperature for the Ferrofluids. This behavior will be explained.

Furthermore first results on the study of the Magnetic Circular Dichroism (MCD) of Ferrofluids will be presented. The experiments were done by using a CD spectrome-

ter in the wavelength range between 250 nm and 800 nm for different Ferrofluids dispersed in hexane or water. By doing so, the concentration of the dispersions and the external field strength has been changed.

Acknowledgments

We thank V.V. Sokolov and V. Yatseev for their help by the MCD experiments. The studies on paramagnetic Metallomesogens doped with Ferrofluids were supported by the Deutsche Forschungsgemeinschaft (Ha 782/70-1/3).

Dynamics of clustering in ionic ferrofluid from Raman scattering

D.Heinrich¹, A.R. Goñi², C.Thomsen¹

¹*Institut für Festkörperphysik, Technische Universität Berlin, Hardenbergstr. 36, 10623 Berlin, Germany*

²*ICREA Research Professor, Institut de Ciència de Materials de Barcelona, Campus de la UAB, 08193 Bellaterra, Spain*

Ferrofluids are colloidal suspensions of nanoparticles with permanent magnetic moments. In recent years groups investigated in theory [1–3] and experiments [4–6] the clustering and formation in ferrofluid under the influence of external magnetic fields. In our first measurements [5,6] we studied the behavior of a surfacted ferrofluid in magnetic fields up to 250 mT with Raman spectroscopy.

In our recent experiments we investigated the aggregation/disaggregation of magnetic nanoparticles in an ionic ferrofluid, especially with a volume fraction of 1 vol%. Evidence for changes in concentration and the size of the clusters in the fluid we obtained from the variation of the Raman intensity. The main Raman signal is obtained from the carrier medium water. In a time window from 20 s to 10 min we observed the change of the Raman signal of the carrier liquid at various temperatures from 7 to 60 °C and magnetic fields up to 350 mT.

We observed the static behavior of the ferrofluid in external fields. In this case we measured the Raman signal of the fluid after 5 min in an increasing magnetic field. Here we obtained a different behavior for fluids having been exposed to an external magnetic field or not having been exposed. Another effect is the increasing Raman signal for fields ≥ 50 mT after decreasing for fields up to 50 mT. The reason for the increase is the building of bigger structures and the change in scattering volume (Mie Scattering [7]).

In the second part of our experiment we in-

vestigated the intensity changes in steps of 20 s upon the field turning on or off. Here we observe a multi exponential dependence, representing the sum of the individual processes in the fluid after changing the field. The fastest and dominant part is the local density change in the light focus. The other parts are the aggregation and disaggregation of clusters in the ferrofluid. The behavior of the ferrofluid Raman signal has critical points at room temperature and an external field of 50 mT.

References

- [1] A.O. Ivanov, Z. Wang, and C. Holm, *Phys. Rev. E* **69**, 031206 (2004).
- [2] H. Morimoto, T. Maekawa, and Y. Matsumoto, *Phys. Rev. E* **68**, 061505 (2003).
- [3] Z. Wang, C. Holm, and H.W. Müller, *Phys. Rev. E* **66**, 021405 (2002).
- [4] A. Wiedenmann, *J. Magn. Magn. Mat.* **272-276**, 1487 (2004).
- [5] J.E. Weber, A.R. Goñi, D.J. Pusiol, and C. Thomsen, *Phys. Rev. E* **66**, 021407 (2002)
- [6] J.E. Weber, A.R. Goñi, and C. Thomsen, *J. Magn. Magn. Mat.* **277**, 96 (2004).
- [7] M. Born and E. Wolf, *Principles of Optics* (Pergamon, Oxford, 1964).

Magnetic properties of polydisperse ferrocolloid suspensions: A critical comparison between experiment, theory, and computer simulation

A. O. Ivanov¹, S. S. Kantorovich^{1,2,3}, E. N. Reznikov^{1,2}, C. Holm^{2,3}, A. F. Pshenichnikov⁴,
A. V. Lebedev⁴, A. Chremos⁵, and P. J. Camp⁵.

¹*Department of Mathematical Physics, Urals State University, Ekaterinburg, Russia*

²*Max Planck Institute for Polymer Research, Mainz, Germany*

³*Frankfurt Institute for Advanced Studies, Frankfurt, Germany*

⁴*Institute of Continuous Media Mechanics, Perm, Russia*

⁵*School of Chemistry, University of Edinburgh, United Kingdom*

The magnetic properties of polydisperse ferrocolloid suspensions determined from experiments [1] have been used to assess critically the predictions of analytical theories and computer simulations.

Various analytical theories have been used to extract the parameters of the particle-size distribution

$$p(x) = \frac{x^\alpha \exp(-x/x_0)}{x_0^{\alpha+1} \Gamma(\alpha + 1)} \quad (1)$$

from experimental measurements of the magnetization curve $M(H)$, where M is the fluid magnetization and H is the applied magnetic field. A key requirement of a successful and consistent theory is that the fitted parameters of $p(x)$ are independent of the ferrofluid concentration; it is shown that of all the available theories to date, only the second-order modified mean-field theory (MMF2) put forward by Ivanov and Kuznetsova [2] satisfies that criterion. From data for a kerosene-dispersed magnetite ferrofluid [1] we find that $x_0 = 1.2266$ nm and $\alpha = 4.95176$.

To confirm the validity of the MMF2 approach, comparisons are made with new results from canonical (NVT) Monte Carlo simulations [3] of polydisperse hard spheres and NVT Langevin molecular dynamics simulations [4] of polydisperse soft spheres. Careful attention has been paid to the discretiza-

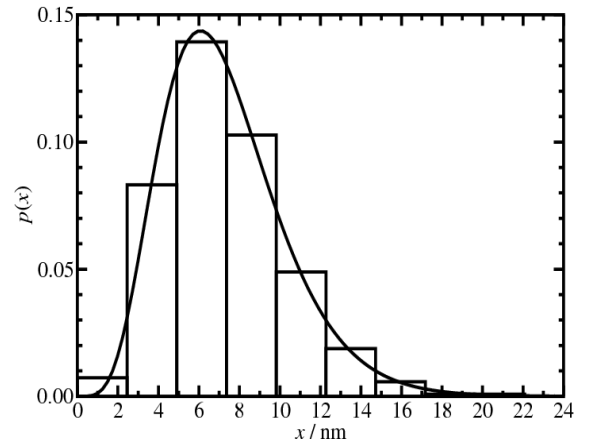


Figure 1: Discretized particle-diameter distribution for $N = 500$ particles (bars), corresponding to $p(x)$ with $x_0 = 1.2266$ nm and $\alpha = 4.95176$ (solid line).

tion of the particle-diameter distribution, so as to preserve the moments of the ‘exact’ distribution (1) within an error of less than 1%. An example of a discretized distribution containing $N = 500$ particles in nine fractions is shown in Fig. 1.

The simulation results provides a stringent and direct test of the theory for a well-defined interaction potential and a specific distribution of particle sizes, while the comparison with experiment should emphasize the reliability of the simulation model (dipolar soft

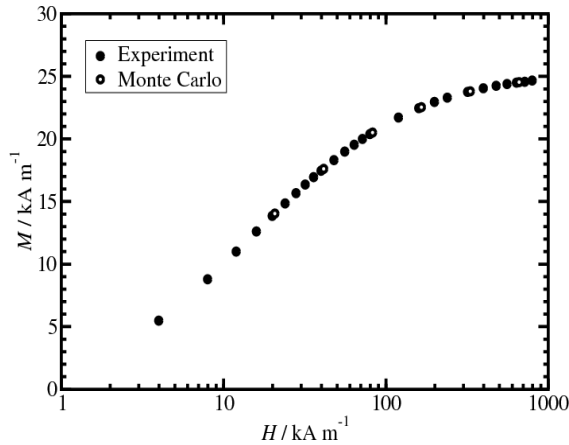


Figure 2: Magnetization curve – $M(H)$ – for a kerosene-based magnetite ferrofluid with saturation magnetization equal to 25.3 kA m^{-1} : experiment [1] (solid points); Monte Carlo simulation (open points).

spheres or hard spheres). Essentially perfect agreement between experiment, theory, and computer simulation is demonstrated, fully validating the MMF2 approach and the simulation models. An example of the agreement between simulation and experiment is shown in Figure 2.

Theory and simulation can also be used to investigate the microscopic characteristics of ferrofluids [3,5], yielding unique insights on the origins of the bulk properties. A snapshot from simulations of a polydisperse ferrocolloid is shown in Figure 3.

References

- [1] A. F. Pshenichnikov, V. V. Mekhonoshin, and A. V. Lebedev, *J. Mag. Magn. Mater.* **161**, 94 (1996).
- [2] A. O. Ivanov and O. B. Kuznetsova, *Phys. Rev. E* **64**, 041405 (2001).
- [3] P. J. Camp and G. N. Patey, *Phys. Rev. E* **62**, 5403 (2000).

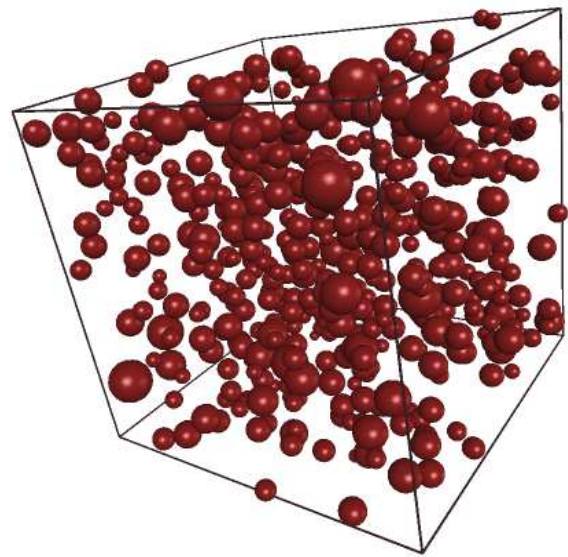


Figure 3: Simulation snapshot of $N = 500$ particles with applied magnetic field $H = 344 \text{ A m}^{-1}$ and saturation magnetization 7.8 kA m^{-1} .

- [4] Z. W. Wang, C. Holm, and H. W. Müller, *Phys. Rev. E* **66**, 021405 (2002); Z. W. Wang and C. Holm, *Phys. Rev. E* **68**, 041401 (2003).
- [5] J. P. Huang, Z. W. Wang, and C. Holm, *Phys. Rev. E* **71**, 061203 (2005).

Growth behaviour of solitary spikes on the surface of magnetic fluids

H. Knieling¹ and R. Richter¹

¹ *Experimentalphysik V, University of Bayreuth, 95440 Bayreuth, Germany*

Introduction

The Rosensweig or normal-field instability on the surface of a ferrofluid is well known. A hexagonal pattern of liquid spikes emerges in a normal magnetic field when a certain threshold of the magnetic induction is surpassed [1]. Recently a stable solitary spike was found in the hysteretic regime of this instability [2]. It can easily be generated by a local perturbation of the surface or the magnetic induction. Due to its solitary nature a lateral observation of its growth dynamics is not hindered by surrounding spikes. We perform time resolved measurements of its amplitude and compare them with the predictions of the growth rate of the standard Rosensweig instability.

Experimental Setup

A circular Teflon dish of diameter of 120 mm and depth of 2 mm is brimful filled with the magnetic fluid EMG 901 from Ferrotec. The dish is placed on the common axis midway between two Helmholtz coils. For a controllable perturbation of the magnetic induction, a small air coil with inner diameter of 6 mm was positioned under the center of the vessel. This allows to increase the magnetic induction locally. At first the magnetic field of the Helmholtz coils B_H is switched on to a subcritical induction, which lies inside the hysteretic regime of the Rosensweig instability, ranging from 8.62 mT to 9.47 mT. Then a local magnetic pulse B_L of the air coil, added at time $t = 0$ ms to the uniform field, produces a single stationary spike of fluid. Its growth is recorded with a high-speed camera with a time resolution of 1 ms (see figure 1), from which time resolved amplitude curves are extracted. Several series with different

magnitudes of the local perturbation B_L for various fields of the Helmholtz coils B_H were performed. Figure 2 shows an example of such a series.

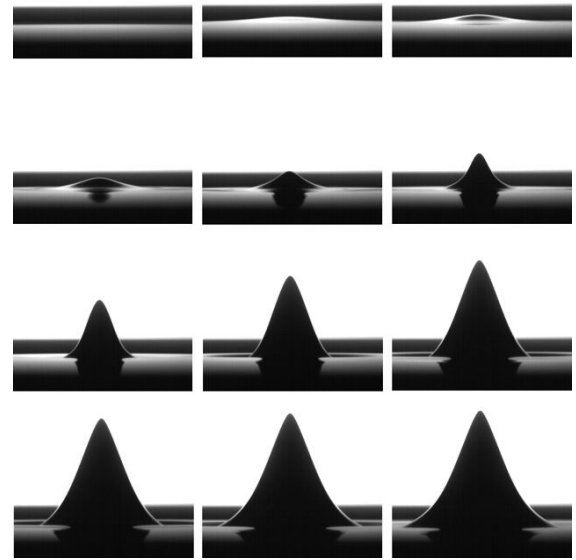


Figure 1: *Growth of a solitary spike on a ferrofluid surface. The time interval between consecutive pictures is 25 ms.*

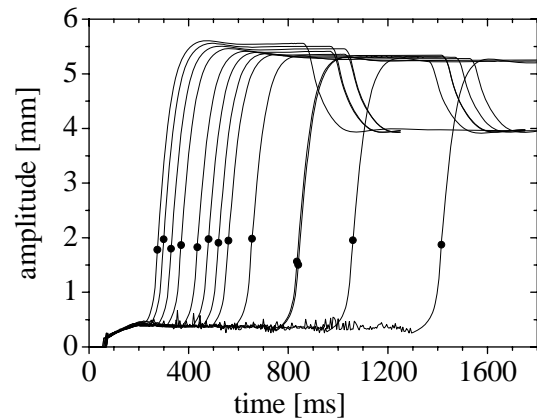


Figure 2: *Temporal evolution of the amplitude of solitary spikes for a magnetic field of the Helmholtz coils of $B_H = 8.93$ mT and*

local perturbations from $B_L = 1.06$ to 1.40 mT, increasing from right to left curves. The inflection points of the curves are marked by filled circles.

Results

For a quantitative description of the growth behaviour of the spikes we have a look at the inverse time of the inflection point t^{-1} of their amplitude curves (figure 3a) and the slope s at that point (b), as extracted from figure 2.

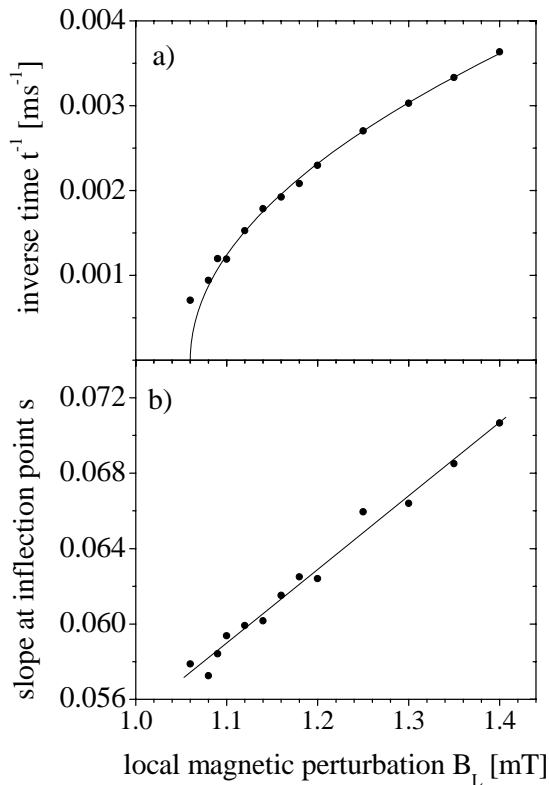


Figure 3: a) Inverse time and b) slope of the inflection points of the amplitude curves in figure 2. The solid lines are fits to the data (see text).

The data points for the inverse time in figure 3a are monotonously increasing and can well be fitted with

$$t^{-1} = a \cdot \sqrt{B_L - B_{L,c}} + b \cdot (B_L - B_{L,c}) \quad (1)$$

which leads to the critical magnetic induction $B_{L,c}$ of the local field for the applied induction of the Helmholtz coils B_H . The parameters a and b give information on the shift of the inflection point in dependence

of the applied local perturbation B_L , where b is nearly zero for all fields of the Helmholtz coils B_H and a is slightly linear decreasing for higher fields B_H . Note that (1) is in accordance with the scaling law for the growth rate of the standard Rosensweig instability [3].

The slope at the inflection point, as shown in figure 3b, can be described by a linear function $s = s_0 + m \cdot B_L$. The offset s_0 shows the maximal slope during the growth of the spike when no additional field is applied and therefore the growth is unforced. This maximal slope raises linear with the magnetic induction of the Helmholtz coils B_H and is negative for magnetic fields smaller than the lower threshold of the hysteretic regime of the Rosensweig instability. That means that a deformation of the surface is not growing but decaying. The parameter m is nearly constant for different magnetic inductions B_H .

Moreover we will present a phase diagram (B_L versus B_H) for the existence of solitary spikes, which can be obtained from the fitted parameter $B_{L,c}$ in (1).

To conclude we have quantitatively described the growth dynamics of solitary spikes. Recently solitary spikes have been found as well in numerical computations [4]. It remains to be investigated whether the scaling law (1) can also be reproduced there.

Acknowledgments

The experiments have been financially supported by *Deutsche Forschungsgemeinschaft* under grant Ri 1054/1-4.

References

- [1] M.D. Cowley and R.E. Rosensweig, J. Fluid Mech. **30**, 671 (1967).
- [2] R. Richter and I.V. Barashenkov, Phys. Rev. Lett. **94**, 184503 (2005).
- [3] A. Lange, Europhys. Lett. **55**, 327 (2001).
- [4] O. Lavrova and G. Matthies and L. Tobiska, J. Phys.: Condens. Matter, submitted (2006).

Maximal growth rate at the Rosensweig instability: theory, experiment, and numerics

A. Lange¹, H. Knieling², G. Matthies³, I. Rehberg², and R. Richter²

¹Fraunhofer-IWS, Winterbergstraße 28, D-01277 Dresden

²Experimentalphysik V, Universität Bayreuth, D-95440 Bayreuth

³Ruhr-Universität Bonn, Universitätsstraße 150, D-44780 Bochum

Instabilities in magnetic fluids (MFs) have had a long history with the most eye-catching phenomenon being the normal field or Rosensweig instability [1]. When a critical value B_c of the vertical magnetic induction is surpassed, static liquid peaks arranged in a hexagonal pattern are rising on the free surface of the fluid.

A linear description of the Rosensweig instability is amenable in theory, but restricted to small amplitudes. In experiments they can be observed only for a very short time during the increase of the pattern of ridges, which bifurcate supercritically. Thus a new pulse technique has been developed and applied [2, 3].

The ground state of a pattern forming system is subjected to small disturbances in order to study its stability. Generally it is assumed that in the linear stage of the pattern forming process the wave number with the largest growth rate will prevail. The growth rate of that mode is the last remaining quantity which has not been measured and compared to the theoretical results. This work is devoted to fill this gap and presents theoretical, experimental and numerical results for the maximal growth rate.

Theory

A horizontally unbounded layer of an incompressible, nonconducting, and viscous magnetic fluid of thickness h and constant density ρ is considered. It is assumed that the magnetisation \vec{M} of the magnetic fluid de-

pends linearly on the applied magnetic field \vec{H} , $\vec{M} = (\mu_r - 1)\vec{H}$, where μ_r is the relative permeability of the fluid.

All small disturbances from the basic state are decomposed into normal modes, i.e., into the form $\exp[-i(\omega t - \vec{q}\vec{r})]$, where $\vec{r} = (x, y)$ and the wave number is the absolute value of the wave vector, $q = |\vec{q}|$. With $\omega = \omega_1 + i\omega_2$, the real part of $-i\omega$, ω_2 , is called the growth rate and defines whether the disturbances will grow ($\omega_2 > 0$) or decay ($\omega_2 < 0$). Carrying out the linear stability analysis leads to the dispersion relation, $\omega = \omega(q)$, whose maximum $\omega_{2,m}$ denotes the maximal growth rate.

For a more appropriate comparison with the experiment, the maximal growth rate is also calculated if a nonlinear law of magnetisation is taken into account.

Experiment

The experimental setup is shown in figure 1. A cylindrical vessel with an edge machined from Teflon is brimful filled with the MF and situated in the center of a Helmholtz pair of coils. A camera is positioned above the vessel for optical observation. For measuring the temporal evolution of the surface amplitude we take advantage of the local variation of the magnetic field, which is increased immediately beneath a magnetic spike and reduced beneath the inter-spike area. In order to measure these local variations a linear array of 32 Hall sensors was mounted below the bottom of the dish. In this way line scans

with a frequency up to 7 kHz are possible. This time resolution makes the method suitable to measure the growth rate of the pattern evolution.

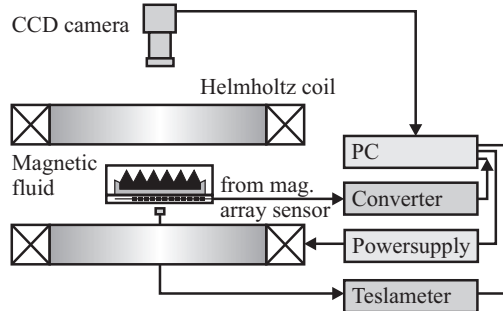


Figure 1: Sketch of the experimental setup.

Numerics

The numerical simulations of the Rosensweig instability is based on the coupled system of the Maxwell equations, the Navier-Stokes equation, and the Young-Laplace equation which describes the force balance at the unknown free surface. In an extension to earlier calculations a nonlinear magnetisation curve is taken into account [4]. For the simulations a bounded domain in the form of a hexagon is chosen in such a way that it contains just one peak. The bounds in vertical direction are assumed to be far away from the free surface.

Primarily Results

The maximal growth rate obtained via the different approaches is plotted in Fig. 2. The open squares give the experimental values. The best fit for those data using the approximation $c_1\sqrt{\hat{B}} + c_2\hat{B}$ yields $c_{1,\text{exp}} = 1.55$ and $c_{2,\text{exp}} = -1.07$ (thick solid line). Using a linear law of magnetisation and an infinite thickness of the layer, the dashed line shows the theoretical result with $c_1 \simeq 1.35$ and $c_2 \simeq 2.93$. The results with a nonlinear law of magnetisation and a finite thickness of $h = 5$ mm are indicated by the long-dashed line. From numerical simulations the result-

ing growth rate is given by the filled triangles with the thin solid line as guide for the eye. The reasons for the remaining deviations are discussed.

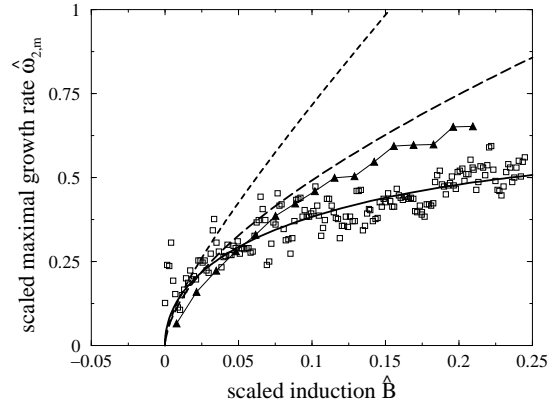


Figure 2: Plot of the scaled maximal growth rate $\hat{\omega}_{2,m}$ versus the scaled induction \hat{B} for the magnetic fluid EMG 909. For details see text.

Acknowledgments

The authors would like to thank L. Tobiska for discussion, C. Gollwitzer for measuring the magnetisation curve and B. Reimann for building the experimental setup. The work was supported by the *Deutsche Forschungsgemeinschaft* under Grants Nos. Ri 1054/1 and La 1182/2.

References

- [1] M. D. Cowley and R. E. Rosensweig, *J. Fluid Mech.* **30**, 671 (1967).
- [2] A. Lange, B. Reimann, and R. Richter, *Phys. Rev. E* **61**, 5528 (2000).
- [3] B. Reimann, R. Richter, I. Rehberg, and A. Lange, *Phys. Rev. E* **68**, 036220 (2003).
- [4] G. Matthies and L. Tobiska, *J. Magn. Mater.* **289**, 346 (2005).

Numerically resolved solitary pattern of the Rosensweig instability

O. Lavrova¹, G. Matthies², L. Tobiska¹

¹*Otto-von-Guericke University Magdeburg, Faculty of Mathematics, PF 4120, D-39016 Magdeburg*

²*Ruhr-University Bochum, Faculty of Mathematics, Universitätsstraße 150, D-44780 Bochum*

The Rosensweig instability is a well-known phenomenon shown by ferrofluids in uniform magnetic fields. The instability organises the fluid-air interface into spatially periodic patterns in the plane, taking the form of parallel ridges, squares or hexagons. Recently, a new equilibrated surface state in the form of a solitary pattern was discovered experimentally, [1]. A soliton-like surface configuration was generated on the ferrofluid layer in the hysteretic regime of the Rosensweig instability. This surface configuration can be interpreted as an additional stable state beside the flat surface and the fully developed pattern.

Modeling

We consider a semi-infinite ferrofluid layer in a uniform magnetic field of intensity H_0 , directed perpendicular to the flat surface.

In a uniform magnetic field the ferrofluid surface develops into a stationary state of a finite amplitude which has no sustained fluid motion. This allows to describe the Rosensweig phenomenon as a ferrohydrostatic problem with unknown free surfaces, see [2]. The equilibrium of forces is given by the coupled system of Maxwell's equations and the magnetically-augmented Young-Laplace equation. The constitutive law in the Langevin form is applied.

In the case of a fully developed pattern, we restrict the computational domain to a single cell of the hexagonal pattern [3,4] or to a circular cell approximation [5]. Periodicity boundary conditions are specified at the cell boundaries. In our calculations the wavelength acts as an input parameter which we

fix to its values λ_c from the onset of the instability, defined by the linear stability analysis in [2].

To resolve numerically a solitary pattern we consider an enlarged computational domain such that it covers a multiple of the pattern wavelength. Since the domain extends far from the peak region, boundary conditions corresponding to a flat surface are used. The wavelength is no more an input parameter of the model but can be estimated from numerical results.

Numerical treatment

Different numerical algorithms were elaborated to model the Rosensweig instability both in two-dimensional axisymmetric and fully three-dimensional cases [3–6]. The coupled problem is iteratively splitted into two subproblems, one for calculating magnetic field with a given interface position and the other for determining the interface location for a given field configuration. We combine finite element and finite difference methods to discretise the governing equations. Fixed-point iterations for linearisation are performed while the linearised systems are solved iteratively. It is worth to mention that the result of the outer iterations, starting from a given interface position, calculating the magnetic field, and determining a new position of the interface, depends strongly on the initial surface deformation. As a result, the coupled problem can have several solutions.

The initial local field perturbation applied in the experiment for a soliton generation is replaced in numerical simulations by an initial

surface deformation.

Results

Numerical simulations of the fully developed pattern for the ferrofluid EMG 901 give a hysteretic range $8.6 \leq H_0 \leq 9.1$ kA/m, see figure 1. After getting a soliton as an equilibrium surface shape for $H_0 = 9.0$ kA/m, we resolve a whole family of solitary configurations by increasing and decreasing the strength of the applied field with a step size of 0.01 kA/m, see figure 1.

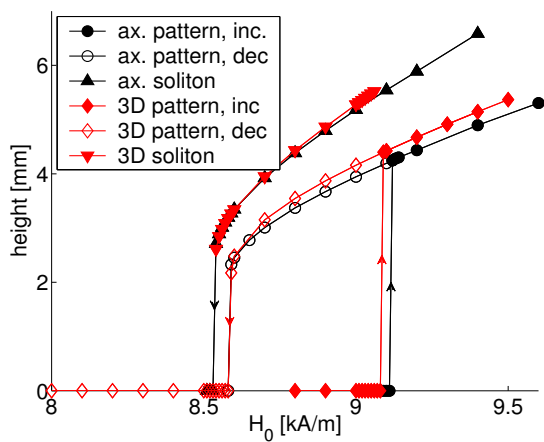


Figure 1: Dependence of the peak height upon the applied field.

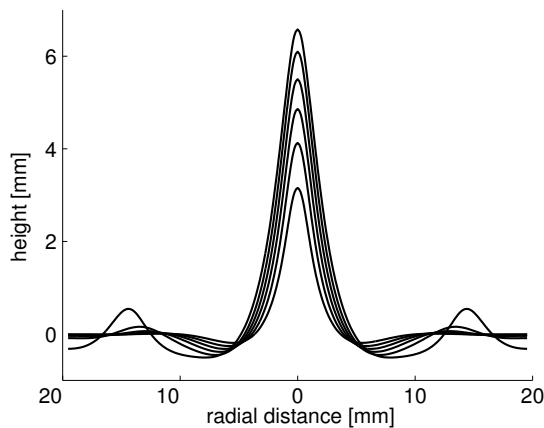


Figure 2: Soliton shapes for $H_0 = \{8.6, 8.8, 9, 9.2, 9.4, 9.6\}$ kA/m, axisymmetric model.

The numerical results shown in figure 1 agree qualitatively with experimental results, see [1, Fig. 3]. At the same field

strength, a soliton has a higher amplitude than a peak in the pattern. An increase of the field strength results in an increasing height of a soliton, while for the decreasing field the peak amplitude decreases. Figure 2 displays soliton shapes for different values of the applied magnetic field. We see that a stronger intensity of the magnetic field results in a higher peak amplitude and a deeper circular hollow around the soliton. Soliton configurations are experimentally observed within the bistability interval with a sudden transition to the fully developed Rosensweig pattern for the field $H_0 \approx H_c + 0.02$ kA/m, slightly stronger than the critical one. Results of numerical calculations predict an existence of soliton configurations in a wider range of field intensities, see figure 1. This numerical finding should be further studied.

Acknowledgments

This work is partially supported by DFG (SPP 1104).

References

- [1] R. Richter, I.V. Barashenkov, Phys. Rev. Lett. **94** (2005) 184503.
- [2] R.E. Rosensweig, Ferrohydrodynamics. Dover Pubns, 1998.
- [3] G. Matthies, L. Tobiska, JMMM **289** (2005) 346.
- [4] C. Gollwitzer, G. Matthies, R. Richter, I. Rehberg, L. Tobiska, J. Fluid Mech. (2006).
- [5] V.G. Bashtovoi, O.A. Lavrova, V.K. Polevikov, L. Tobiska, JMMM **252** (2002) 299.
- [6] O. Lavrova, G. Matthies, T. Mitkova, V. Polevikov, L. Tobiska, Lect. Notes Comput. Sci. Eng. **35** (2003) 160.

Magnetization of rotating ferrofluids: the effect of polydispersity

A. Leschhorn, J. P. Embs, M. Lücke

Institut für Theoretische Physik, Universität des Saarlandes, D-66041 Saarbrücken, Germany

The influence of polydispersity on the magnetization is analyzed in a nonequilibrium situation where a cylindrical ferrofluid column is enforced to rotate with constant frequency like a rigid body in a homogeneous magnetic field that is applied perpendicular to the cylinder axis. Then, the magnetization and the internal magnetic field are not longer parallel to each other and their directions differ from that of the applied magnetic field. Experimental results on the transverse magnetization component perpendicular to the applied field are compared and analyzed as functions of rotation frequency and field strength with different polydisperse Debye models that take into account the polydispersity in different ways and to a varying degree.

Charakterisierung magnetischer Nanoteilchen durch Analyse der Magnetisierungs- und Relaxationsdynamik mit Fluxgate-Magnetometern

F. Ludwig, E. Heim, M. Schilling

Institut für Elektrische Messtechnik und Grundlagen der Elektrotechnik, TU Braunschweig, Hans-Sommer-Str. 66, D-38106 Braunschweig

Magnetische Nanopartikel (MNP) finden eine breite Anwendung in verschiedenen Bereichen der Medizin und Bioanalytik. Dabei unterscheiden sich die Anforderungen an die MNPs von Anwendung zu Anwendung stark: Für die Kernspintomografie werden beispielsweise eher kleine Partikel benötigt, während beim „magnetic drug targeting“ und der magnetischen Separation größere Teilchen erforderlich sind. Bei der magnetischen Hyperthermie und beim Magnetrelaxations-Immunoassay (MARIA) sind MNPs mit einer schmalen Größenverteilung um einen optimalen Wert erforderlich.

Wie Eberbeck et al. [1] als auch Ludwig et al. [2] demonstriert haben, ist die Magnetrelaxometrie ein Verfahren, das eine schnelle und zuverlässige Charakterisierung von MNPs erlaubt. Darüber hinaus ermöglicht die Magnetrelaxometrie auch eine Quantifizierung des Aggregationsverhaltens der MNPs [3]. Die Aggregation kann insbesondere für in-vivo Anwendungen ein ernsthaftes Problem darstellen.

Die Analyse von Magnetrelaxationskurven und die Extraktion von Parametern der MNP-Probe erfolgt dabei im Rahmen des so genannten Momentensuperpositionsmodells (MSM), das wechselwirkungsfreie Partikel mit i.a. kugelförmigen Kernen betrachtet. Für die Größenverteilung der Kerne wird von einer logarithmischen Normalverteilung $f(\mu, \sigma)$ ausgegangen, wobei μ der geometrische Mittelwert und σ die geometrische Standardabweichung sind.

Die Verwendung von Fluxgates im Vergleich zu SQUIDs als Magnetfeldsensoren bietet dabei den Vorteil, dass Absolutwerte des Magnetfeldes und nicht Feldänderun-

gen gemessen werden und dass der gesamte Magnetisierungs- und Relaxationszyklus gemessen und analysiert werden kann.

Es wurden Messungen des Magnetisierungs-Relaxations-Zyklus an verschiedenen verdünnten, gefriergetrockneten Magnetit-MNP-Proben durchgeführt und im Rahmen des MSM analysiert. Die Messungen wurden mit einem differentiellen Fluxgate-Aufbau durchgeführt, der auch Messungen ohne jegliche magnetische Schirmung zulässt [4].

Abb. 1 zeigt das zeitliche Verhalten des Aufmagnetisierungsprozesses für verschiedene Werte der Magnetisierungsfeldstärke. Um die Unterschiede der einzelnen Kurven hervorzuheben, wurden die einzelnen Kurven auf den jeweiligen Wert bei 20 s normiert. Das „Auffächern“ der einzelnen Kurven reflektiert die Abhängigkeit der Néel-Zeitkonstante τ_N vom Magnetfeld und von der Anisotropiekonstante K . In Abb. 2 ist der beste mit dem MSM berechnete Fit dargestellt.

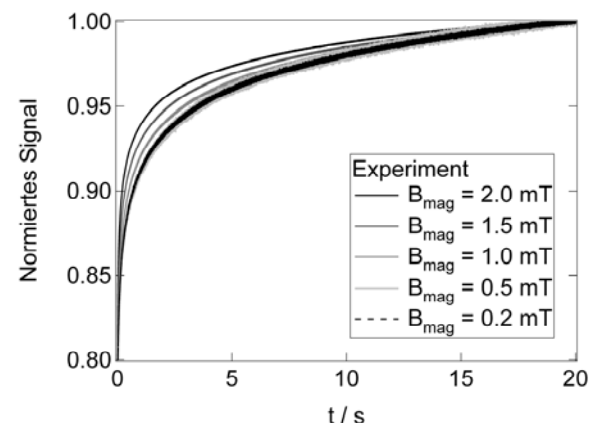


Abb. 1: Normierte Zeitabhängigkeit des Probensignals für den Magnetisierungsprozess aufgenommen für verschiedene Magnetisierungsfeldstärken.

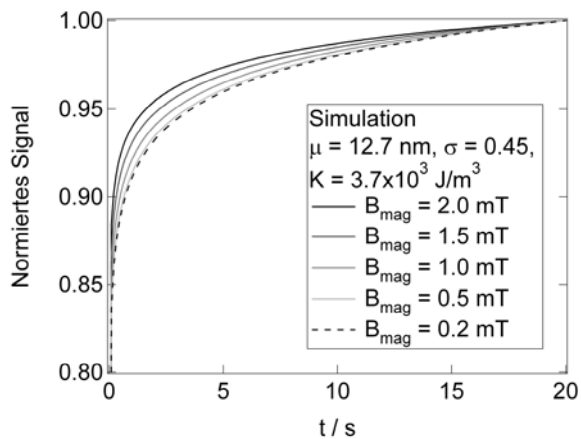


Abb. 2: Mit dem MSM berechnete Zeitabhängigkeit der normierten Magnetisierungskurven.

In Abb. 3 sind die für verschiedene Magnetisierungsfeldstärken gemessenen, auf den jeweiligen Wert vor dem Abschalten des Magnetisierungsfeldes normierten Relaxationskurven gezeigt. Das beobachtete Kreuzen der einzelnen normierten Kurven kann durch das MSM durch geeignete Wahl der Parameter μ , σ und K erklärt werden und ist ein Ergebnis der Abhängigkeit der Néel-Relaxationszeiten τ_N der einzelnen MNPs vom Magnetfeld und vom Winkel zwischen deren magnetischen Momenten m und dem angelegten Magnetfeld H [2]. Es zeigt sich, dass – über die Analyse einer einzelnen Relaxationskurve hinausgehend – die Abhängigkeit der Magnetisierungs- und Relaxationskurven von der Magnetisierungszeit und der Magnetisierungsfeldstärke wertvolle Information zur eindeutigen Bestimmung der Größenverteilung der MNP-Kerne als auch der Anisotropiekonstante enthält.

Die aus den Magnetisierungs- und Relaxationskurven erhaltenen Probenparameter werden mit den aus statischen Magnetisierungs-, ac-Suszeptibilitäts-, rasterelektronenmikroskopischen und PCS-Messungen erhaltenen Werten verglichen. Unterschiede der Parameter sollen zur weiteren Verfeinerung des MSM, insbesondere der Abhängigkeit der Néel-Zeitkonstante τ_N vom Magnetfeld und der Anisotropieenergie $K \cdot V$, verwendet werden. Kombiniert mit einer Verfeinerung des MSM bietet ein

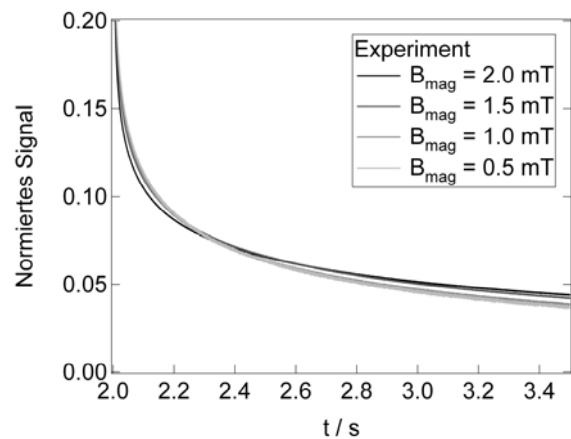


Abb. 3: Normierte Relaxationskurven aufgenommen für verschiedene Magnetisierungsfeldstärken nach 2 s Magnetisierungszeit.

fluxgate-basiertes System zur Messung der Magnetisierungs- und Relaxationsdynamik von MNPs eine effektive, kostengünstige und schnelle Methode zur Charakterisierung von magnetischen Nanoteilchen, insbesondere hinsichtlich deren Einsatz für biomedizinische Anwendungen.

Gefördert durch die DFG über SFB 578.

References

- [1] D. Eberbeck, S. Hartwig, U. Steinhoff, and L. Trahms, *Magneto-hydrodynamics* 39, 77 (2003)
- [2] F. Ludwig, E. Heim, D. Menzel, and M. Schilling, *J. Appl. Phys.* 99, 08P106 (2006)
- [3] D. Eberbeck; Ch. Bergemann; F. Wiekhorst, and G. Glöckl, *Magneto-hydrodynamics* 41, 305 (2005)
- [4] F. Ludwig, S. Mäuselein, E. Heim, and M. Schilling, *Rev. Sci. Instrum.* 76, 106102 (2005)

Rodlike Magnetic Core Shell Particles as Model System for Lyotropic Liquid Crystals

C. Märkert, J. Wagner, R. Hempelmann

Physical Chemistry, Saarland University, D-66123 Saarbrücken

Silica coated colloidal particles bearing a magnetic moment are interesting model systems for the investigation of the structural and dynamic response of mesoscale structured colloidal suspensions to weak magnetic interactions [1, 2]. Such particles can be prepared with a polydispersity significantly smaller than the one of conventional ferrofluids. Due to the silica shell with negative surface groups, in addition, a predominant repelling electrostatic repulsion prevents the formation of agglomerates. Compared to spherical core-shell particles, the complexity of the system can be increased by the preparation of rodlike particles with tunable aspect ratio.

Rodlike particles are accessible by addition of substances selectively covering one crystal surface and thus enabling growth in a different direction. As consequence, anisotropic crystal growth can only be achieved with a combination of a crystal structure with a singular preferred direction and suitable surface active agents. In presence of dihydrogenphosphate, nanoscale rods of rhombohedral maghemite $\alpha\text{-Fe}_2\text{O}_3$ can be prepared (Fig. 1) with an aspect ratio depending on the concentration of NaH_2PO_4 [3] (Fig. 3). The size distribution of the resulting nanorods is with typical geometric standard deviations of $\sigma_D \approx 1.10 - 1.15$ for the diameter and $\sigma_L \approx 1.05 - 1.08$ for the length considerably narrow (Fig. 2). The saturation magnetization of $\alpha\text{-Fe}_2\text{O}_3$ is with $M_S = 2.11 \times 10^3 \text{ A m}^{-1}$ rather low. Due to the form anisotropy with a large aspect ratio, however, even weakly magnetic particles can be aligned in strong external

fields [4]. Electrostatic stabilization of the nanorods can be achieved via coating by a silica shell using a Stoeber process (Fig. 4).

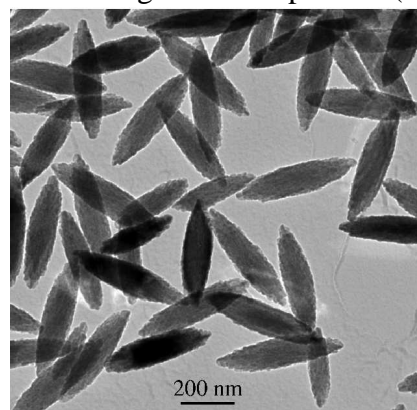


Fig. 1 TEMicrograph of $\alpha\text{-Fe}_2\text{O}_3$ nanorods prepared by precipitation of FeCl_3 in presence of NaH_2PO_4 . The concentration of NaH_2PO_4 controls the aspect ratio of the resulting nanorods.

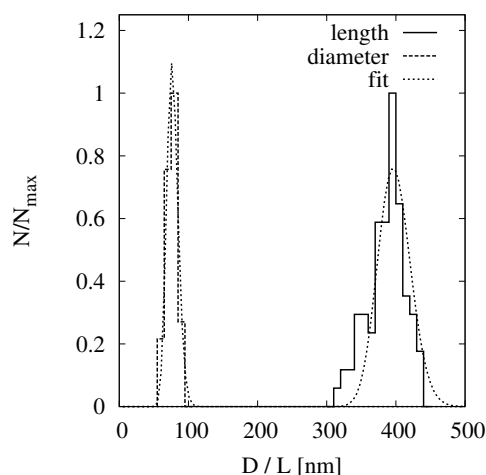


Fig. 2 Size distribution of rodlike particles from TEM. For the length of the rods, a median of $L_0 = 397 \pm 3 \text{ nm}$ and a geometric standard deviation of $\sigma_w = 1.06 \pm 0.01$ are obtained. For the diameter of the rods, a median of $D_0 = 77 \pm 1 \text{ nm}$ with $\sigma_D = 1.11 \pm 0.01$ are obtained. The aspect ratio of these particles is $r = 5 \pm 1$.

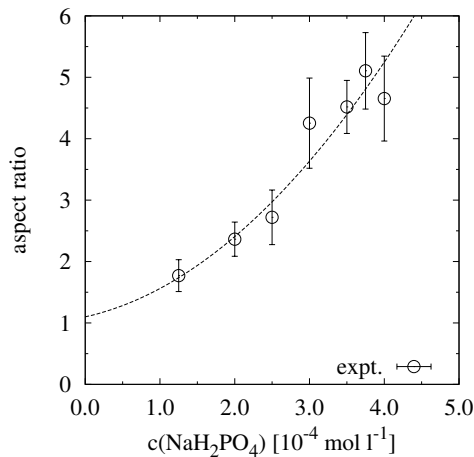


Fig. 3 Aspect ratio of $\alpha\text{-Fe}_2\text{O}_3$ rods in dependence on the concentration of NaH_2PO_4 . With increasing concentration of NaH_2PO_4 more elongated particles are obtained.

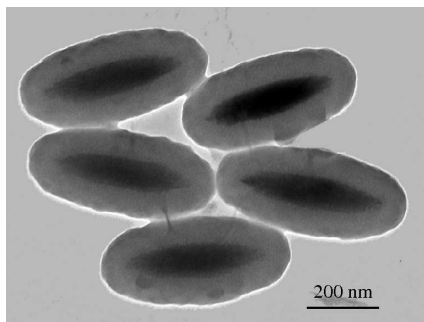


Fig. 4 TEMicrograph of rodlike core-shell particles consisting of $\alpha\text{-Fe}_2\text{O}_3$ rods coated by silica. Negative charges of the silica shell prevent agglomeration without contamination by surfactants.

A significant increase of the saturation magnetization can be achieved by reduction of maghemite ($\alpha\text{-Fe}_2\text{O}_3$) to magnetite (Fe_3O_4) in hydrogen atmosphere at 350°C .

The availability of defined anisotropic core-shell particles will enable the investigation of lyotropic liquid crystalline phases [5] that can be influenced by external magnetic fields. Due to the large aspect ratio, significant effects on the diffusion of aligned rods can be expected, i.e. $D_{\parallel} \gg D_{\perp}$. Due to an anisotropic polarisation tensor, the rotational diffusion in highly dilute suspensions is accessible via depolarized light scattering experiments.

Acknowledgments

The present work is supported by the Deutsche Forschungsgemeinschaft in the priority program SPP1104.

References

- [1] A. Robert, J. Wagner, T. Autenrieth, W. Härtl, and G. Grübel. *J. Chem. Phys.* **122**, 084701 (2005)
- [2] J. Wagner, B. Fischer, and T. Autenrieth. *J. Chem. Phys.* **124**, 114901 (2006)
- [3] M. Ozaki, S. Kratochvil, and E. Matijevic *Journal of Colloid and Interface Science*, **102**,146 (1984)
- [4] B. J. Lemaire, P. Davidson, J. Ferr, J. P. Jamet, P. Panine, I. Dozov, and J. P. Jolivet, *Phys. Rev. Lett.*, **88**, 125507, (2002)
- [5] G. J. Vroege and H. N. W. Lekkerkerker, *Reports on Progress in Physics*, **55**, 1241 (1992)

Faraday instability on a ferrofluid in a vertical magnetic field: non-linear planform selection

V. Mekhonoshin^{1,2}

¹*Institut für Theoretische Physik, Universität des Saarlandes, 66123, Saarbrücken*

²*Institute of Continuous Media Mechanics, Urals Branch of RAS, 1, Korolev st., 614013, Perm, Russia*

The Faraday instability (known since 1831) is the parametrical generation of standing waves on the free surface of a liquid by vertical vibrations. Numerous studies of the Faraday instability revealed a large variety of the patterns, what makes the instability interesting as symmetry braking phenomenon. Unique properties of ferrofluids, namely the combination of their fluidity with strong interaction with magnetic field provides one more way to control the stability of the free surface and/or the symmetry of the wave pattern.

In the present work, a horizontally unbounded layer of a incompressible, non-conductive viscous ferrofluid with a finite depth d is studied. The layer is subjected to vertical vibrations with the acceleration $a \cos \omega t$ and the vertical magnetic field. If either the mechanical vibrations or the magnetic field is strong enough, each of them can alone generate the Faraday or the Rosensweig instability respectively. In the present work, the Faraday instability is studied at the fields below the critical one for the Rosensweig instability B_R . In the fields close to B_R , the surface waves are governed by a non-monotonic dispersion relation. The anomalous dispersion was predicted and observed in the case of a low-viscous ferrofluid [1]. Another consequence of the extremes in the dispersion relation consist in the significant deformation of the tongues, representing the neutral stability curve.

In order to study the pattern formation theoretically, weakly non-linear analysis is performed using the standard perturbation the-

ory [2]. Solution of the linear problem at the first order of the perturbation theory gives us the critical acceleration amplitude a_c , the critical wave number k_c , and the coefficients of the Floquet ansatz, for instance, for the surface deformation one gets

$$\zeta_j(x, y) = \sin(\mathbf{k}_j \mathbf{r}) e^{i\alpha \omega t} \sum_{n=-\infty}^{\infty} \zeta_n e^{I(2n-1)\omega t}, \quad (1)$$

where j denotes degenerate modes and α distinguishes between subharmonic ($\alpha = 1/2$) and harmonic ($\alpha = 0$) response. Each spatial harmonic of the surface profile (reffloquet) is determined at the first order up to **real** constant A_j . Interaction of the spatial modes (1) at the higher orders leads to the amplitude equation, which allows one to determine the amplitudes A_j and to predict the resulting pattern.

At the second order of the perturbation theory, the problem is simplified, when the primary response is subharmonic. In this case, no temporal resonance is possible because of harmonic type of the quadratic terms. The solvability condition at the third order gives the amplitude equation

$$\partial_t A_1 = s A_1 - g_0 A_1^3 - \sum_{j \neq 1} g(\vartheta_{j1}) A_j^2 A_1, \quad (2)$$

where s (times subcriticality) is the linear growth rate and ϑ is the angle between the 1st and j th modes. The equations for all other modes are obtained by permutaion of indexes.

Figure 1 shows two dependencies of $g(\vartheta)$ calculated at different magnetic fields. It is

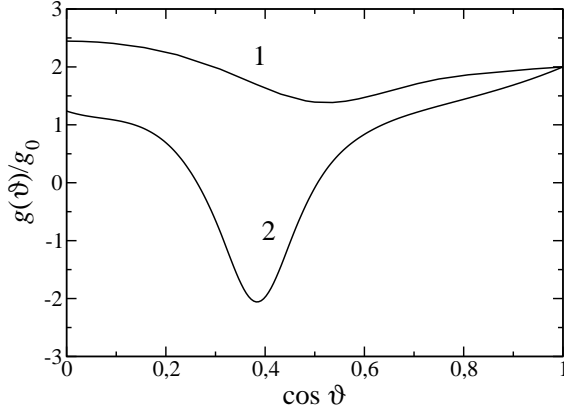


Figure 1: Dependencies of the mutual coupling coefficient on the angle between the interacting modes at $B = 0.05B_r$ (curve 1) and $B = 0.98B_R$ (curve 2) $f = \omega/2\pi = 100$ Hz.

seen that the vertical magnetic field makes the dependence much more pronounced. Using the criterion suggested in [2], the number of the interacting modes N of the selected regular pattern has to minimize the quantity

$$-\frac{N}{g_0 + \sum_{m=2}^N g(\vartheta_{m,1})}. \quad (3)$$

At $B = 0.05B_r$, the predicted pattern is rolls, and at $B = 0.98B_R$ the amplitude equation predicts hexagons.

Unfortunately, there are large regions of the parameters, where the back bifurcation is predicted. Though there was no hysteresis detected in the experiment, the latter can be hindered by the the perturbation caused by the the meniscuses and the field inhomogeneity. This issue has to be clarified additionally, as well as some numerical difficulties, which arise at moderate frequencies, as ϑ tends to zero.

Acknowledgments

This work was supported by the Deutsche Forschungsgemeinschaft under Grant No ME 2677/1-1

References

- [1] H.-W. Müller, Phys. Rev. E **58**, 6199 (1998)
- [2] P. Chen and J. Viñals Phys. Rev. E **60**, 599 (1999)

Magnetic Field Driven Sedimentation Instability in Ferrofluids

A. Ryskin, H. Pleiner

Max-Planck-Institut für Polymerforschung, 55021 Mainz, Germany

Introduction

Despite the fact that the concentration dynamics of the magnetic nanoparticles in a ferrofluid is extremely slow, it cannot be neglected when one deals with thermal instabilities [1, 2, 3]. Instead, one has to consider the ferrofluid as a binary mixture. Compared to usual molecular binary mixtures, however, ferrofluids are atypical, because the two constituents (magnetic particles and the carrier liquid) have very different densities and show very different mobilities due to the large size of the magnetic particles on the molecular lengthscale. In earth's gravity field, the density difference is responsible for rather strong sedimentation effects in ferrofluids which are generally negligible in molecular binary mixtures. For thermal instabilities, with a temperature gradient along gravity, sedimentation is a stabilizing effect on the system, since the heavier constituent accumulates at the bottom, thus counteracting thermal buoyancy. In this communication we will show, however, that even without a temperature gradient a sedimenting ferrofluid can become unstable, if a strong enough external magnetic field is applied. This novel type of sedimentation instability is due to the Kelvin force acting on the magnetic particles.

Setting up the problem

Let us consider a horizontal layer of ferrofluid between two rigid impermeable plates and subject to a gravitational field $\vec{g} = g\vec{e}_g$ along the negative z direction. If one waits long enough, the concentration distri-

bution of the magnetic particles becomes exponential in vertical direction [4]

$$c(z) = c_0 \exp(-z/h_s). \quad (1)$$

In the dilute limit this is essentially a Boltzmann distribution with the sedimentation length $h_s = k_B T / (m_p g)$, where m_p is the mass of the magnetic particles. If h_s is much larger than the distance between the two plates, h , which is usually the case in experiments, we can approximate this exponential distribution by $c(z) = c_0(1 - z/h_s)$ and get a linear concentration profile.

The general system of dynamic equations to describe ferrofluids with concentration variations has been derived in [2]. In order to include sedimentation effects one needs to add the appropriate mass flux to the concentration dynamics [5]

$$\vec{j}_s = \frac{D_c}{h_s} c(1 - c) \vec{e}_g, \quad (2)$$

where D_c is the concentration diffusion coefficient. After the concentration distribution is equilibrated, a magnetic field in horizontal direction is switched on. We study the stability of this steady and flow-free system by introducing time- and space-periodic perturbations from the equilibrium values for all relevant variables (concentration, velocities, magnetic potentials).

There are two important parameters in the problem. The first is the Barometric number [6] describing the relative importance of gravity and viscosity effects (using the viscous diffusion time as unit time)

$$B = \frac{\beta g \bar{c}_0 h^4}{\nu^2 h_s}, \quad (3)$$

where \bar{c}_0 is the mean volume fraction of magnetic particles, $\beta = \rho^{-1}(\partial\rho/\partial c)$ is the coefficient of solutal expansion, and ν is the kinematic viscosity.

The second parameter, which we call the magnetic Barometric number, is due to the presence of the magnetic field (Kelvin force) and describes the relative importance of gravity and magnetic effects

$$B_m = \frac{\chi_c^2 \bar{c}_0^2 H_0^2 h^4}{\rho_0 (1 + \chi) \nu^2 h_s^2} \quad (4)$$

where $\chi_c = \partial\chi/\partial c$ describes the concentration dependence of the magnetic susceptibility χ of the ferrofluid. This number depends quadratically on the strength of the magnetic field and shows that the magnetic field is always destabilizing despite its orientation with respect to gravity.

Linear stability

The system becomes linearly unstable with respect to stationary, spatially periodic disturbances when $B_m > B$. At the very onset, $B_m^c = B$, the most unstable mode has a very large wave number k (small wavelength) proportional to the reciprocal diffusion length of the magnetic particles. However, as was shown in [1], just above the threshold the growth rate of the unstable modes is extremely small, since there the time scale is set by the slow dynamics of the concentration field. If one is interested in a finite growth rate, which can be measured experimentally, one has to operate somewhat above the threshold. For very large B_m the wavenumber asymptotically reaches $k \lesssim 2\pi/h$.

Nonlinear behavior

To investigate amplitudes and patterns of the variables in the unstable regime, one has to use a nonlinear theory. We employ a numerical method described in detail in [2]. We start from the stationary, flow-free state (with linear concentration and magnetic

potential profiles) and allow for a finite velocity. In the case $B_m > B$, the linear regime with an exponential growth of the velocity is seen at the beginning. Then, the amplitude of the velocity reaches a maximum and decreases to a very small value in the final stationary state. This is due to the (partial) remixing effect of the convective flow. This state is almost motionless, since the amplitude of the velocity is extremely small. On the other hand, the (lateral) periodic variations of the concentration and the magnetic field are not small and it should be possible to experimentally discriminate this state from the laterally homogeneous one below the threshold.

References

- [1] A. Ryskin, H.-W. Müller, H. Pleiner, *Phys. Rev. E* **67**, 046302 (2003)
- [2] A. Ryskin, H. Pleiner, *Phys. Rev. E* **69**, 046301 (2004)
- [3] A. Ryskin, H. Pleiner, *Phys. Rev. E* **71**, 056303 (2005)
- [4] T. Biben, J.-P. Hansen, and J.-L. Barrat, *J. Chem. Phys.* **98**, 7330 (1993)
- [5] E. Blums, *J. Magn. Magn. Mat.* **252**, 189 (2002)
- [6] M. I. Shliomis and B. L. Smorodin, *Phys. Rev. E* **71**, 036312 (2005)

Effects of Sedimentation in the Thermal Convection of Ferrofluids

A. Ryskin, H. Pleiner

Max-Planck-Institut für Polymerforschung, 55021 Mainz, Germany

Introduction

The effects of the concentration dynamics on the thermal convection in ferrofluids have been considered in [1, 2, 3]. Despite the fact that the concentration dynamics of the magnetic nanoparticles in a ferrofluid is extremely slow, it leads to very pronounced effects and cannot be neglected when dealing with thermal instabilities. Instead, one has to consider the ferrofluid as a binary mixture. Compared to usual molecular binary mixtures, however, ferrofluids are atypical, because the two constituents (magnetic particles and the carrier liquid) have very different densities and show very different mobilities due to the large size of the magnetic particles on the molecular lengthscale. Thus, applying an external temperature gradient to a slab of ferrofluid the concentration distribution takes a much longer time to adjust (Soret effect) than the temperature (thermal diffusion). Therefore, thermal instability experiments are done mostly in a state where the temperature has reached the linear spatial profile, while the concentration is still homogeneous (apart from small boundary layers). Here we study, how and under what circumstances, the results obtained earlier are modified, when we take into account sedimentation of the magnetic particles. Recent experiments [6] indicate that there are new effects due to sedimentation.

The problem

Let us consider a horizontal layer of ferrofluid between two rigid impermeable plates subject to a gravitational field $\vec{g} =$

$g \vec{e}_g$ along the negative z direction. There are two, essentially different ways to perform experiments - 1) one can wait long enough such that the magnetic particle distribution equilibrates in the gravitational field, and only then start to heat the lower plate, or 2) one can start heating immediately the still homogenous ferrofluid. In the first case the distribution of the magnetic particles in the gravitational field becomes exponential in the vertical direction [4]

$$c(z) = c_0 \exp(-z/h_s), \quad (1)$$

In the dilute limit this is essentially a Boltzmann distribution with the sedimentation length $h_s = k_B T / (m_p g)$, where m_p is the mass of the magnetic particles. If h_s is much larger than the distance between the two plates, h , which is usually the case in experiments, we can approximate this exponential distribution by $c(z) = c_0(1 - z/h_s)$ and get a linear concentration profile.

In order to include sedimentation effects one has to add the appropriate mass flux [5] into the binary-mixture model [2].

$$\vec{j}_s = \frac{D_c}{h_s} c(1 - c) \vec{e}_g \quad (2)$$

where D_c is the concentration diffusion coefficient. The parameter, which measures the importance of sedimentation relative to viscosity and thermal diffusion is the Barometric number [7]

$$B = \frac{\beta g \bar{c}_0 h^4}{\kappa \nu h_s} \quad (3)$$

where \bar{c}_0 is the mean volume fraction of the magnetic particles, $\beta = \rho^{-1}(\partial \rho / \partial c)$ is the coefficient of solutal expansion, h is the

distance between the plates, ν is kinematic viscosity, and κ is the thermal diffusion coefficient. B can vary considerably, typically from 1 to 10^5 , due to the strong h -dependence.

Linear stability

Starting with a homogenous ferrofluid no effects of sedimentation are expected to happen within the typical (thermal diffusion) time scale and the previous linear descriptions [1, 2, 3] apply. The situation is different, if we start with a linear concentration profile. First, in this situation the ferrofluid is much more stable due to the additional stabilizing buoyancy force compared to the homogeneous concentration case. That results in a shift of the threshold to a higher Rayleigh number. Second, at the onset, the instability is not stationary but rather oscillatory. This is due to antagonistic interplay of thermal and solutal buoyancy. However, if we go to higher values of the Rayleigh number, the instability again becomes stationary, i.e. the frequency vanishes and the linear (positive) growth rate becomes real, since then the thermal buoyancy dominates completely. This behavior is also typical for the case of a ferrofluid with negative separation ratio (and heated in the homogeneous concentration state), while here we get it in a system with a positive separation ratio.

Nonlinear behavior

We use the same numerical method as in [3] to investigate the time evolution of the system in the non-linear regime. We find that the system always ends up at long times in a stationary state regardless, whether the linear transition to this state contains oscillations (when starting from a linear concentration profile), or whether the linear transition is purely exponential (when starting from a homogeneous ferrofluid). We also find that there is a certain range of param-

eters, where there are two quasi-stable possible stationary solution – one of them is the fully motionless state (with a linear concentration profile) and the other one is a state with convection. That means, depending on the strength of the perturbation, the system can either return to a quiescent state or, if the perturbation is strong enough, the convective motion sets in. This is called 'hard excitation of the convection' and has been observed in experiments [6].

References

- [1] A. Ryskin, H.-W. Müller, H. Pleiner, *Phys. Rev. E* **67**, 046302 (2003)
- [2] A. Ryskin, H. Pleiner, *Phys. Rev. E* **69**, 046301 (2004)
- [3] A. Ryskin, H. Pleiner, *Phys. Rev. E* **71**, 056303 (2005)
- [4] T. Biben, J.-P. Hansen, and J.-L. Barrat, *J. Chem. Phys.* **98**, 7330 (1993)
- [5] E. Blums, *J. Magn. Mat.*, **252**, 189 (2002)
- [6] A. Bozhko, G. Putin, *Magnetohydrodynamics* **30**, 147 (2003)
- [7] M. I. Shliomis and B. L. Smorodin, *Phys. Rev. E* **71**, 036312 (2005)

Effect of Hydrodynamic Interaction on the Short-Time Dynamics of Ferrofluids

R. Schmitz¹

¹*Institut für Theoretische Physik C, RWTH Aachen, 52056 Aachen, Germany*

The dynamical properties of ferrofluids are not only controlled by magnetic and possibly other direct interactions between the ferroparticles, but also by the hydrodynamic interaction which is mediated by the carrier liquid. We have analyzed the effect of this interaction on the structural and magnetic relaxation.

Starting point of our investigation is a generalized Smoluchowski equation that governs the Brownian dynamics of the correlated ferroparticles. Hydrodynamic interaction is taken into account by a diffusion matrix which depends on the instantaneous configuration of the many-body system. Applying the Mori-Zwanzig projection method one obtains formally exact microscopic expressions for the relaxation kernels which we evaluate in the short-time limit.

The diffusion tensor has translational and rotational sectors which are strongly coupled. Its computation is a somewhat intricate mathematical problem which we shall outline in some detail for particles in an unbounded fluid and for systems with periodic boundary conditions. Various approximations are discussed and compared.

Mikrosecond dynamics of field-induced ordering in magnetic colloids studied by new time-resolved Small Angle Neutron Scattering techniques

A. Wiedenmann,^{1*} U. Keiderling,¹ K. Habicht,¹ M. Russina,¹ and R. Gähler²

1 Hahn-Meitner-Institut, Structure Research, Glienicker Str. 100, D-14109 Berlin, Germany

2 Institut Laue-Langevin, BP. 85X, F-38042 Grenoble Cedex, France

Dynamical studies of nanosized inhomogeneities by means of Small Angle Neutron Scattering (SANS) usually are limited to slow processes where the system remains in a quasi-steady state during data acquisition time. A breakthrough to time resolution of microsecond range was achieved by new SANS techniques, allowing the dynamics of fast ordering processes in Co-ferrofluids to be analysed.

In concentrated surfactant stabilised Cobalt ferrofluids samples above 1 vol.% Co a pseudo-crystalline hexagonal ordering of the core-shell nanoparticles was found to be induced by an external magnetic field (\mathbf{H}), where magnetic particle moments are aligned along \mathbf{H} [1-8]. The dynamics of the reversal of magnetic moments of nanoparticles in concentrated Co-ferrofluids corresponding to ordering and relaxation processes was studied by a new stroboscopic SANSPOL techniques [9]. In first experiments a Co-FF sample was placed in a homogenous magnetic field the strength of which was cycled between zero and 0.5 T. Time-frame histogram data acquisition has been performed in time slices between 200 and 500 ms synchronised with the cycles of the magnetic field. A second type of experiments were performed in an oscillating magnetic field with a strength of up to 30 mT and oscillation frequencies up to 600 Hz by analysing the time-resolved SANS response using a continuous monochromatic beam. In a third type of experiments (TISANE) a pulsed polychromatic beam has

been used to monitor the oscillating response in an external field with frequencies up to 3000 Hz.

The analysis of the time-resolved 2D SANS patterns allowed reliably to extract magnetic and nuclear correlations. The overall dynamics of the relaxation processes in the first experiments is characterised by an exponential decay of the correlation peaks [6] corresponding to a gradual transformation from local hexagonal order to segments of particle chains (Fig. 1). In the experiments with oscillating magnetic fields a modulation of the magnetic contrast has been found as a function of time with a periode twice that of the applied field (Fig.2). Time resolution in the μs range was achieved by using a pulsed beam technique, TISANE, while in continuous mode resolution was limited by the wavelength spread to about 1ms.

The frequency dependence of anisotropic scattering patterns has been modeled using Langevin dynamics. The dynamics follows a two step mechanism (Fig.3): Field induced ordering is governed by fast Brownian rotation of nanoparticles with a characteristic time of about 160 μs . Magnetic relaxation of locally ordered domains of about 100 nm in size takes place within a few seconds by Brownian rotation or by Néel type rotation of magnetic moments.[11]

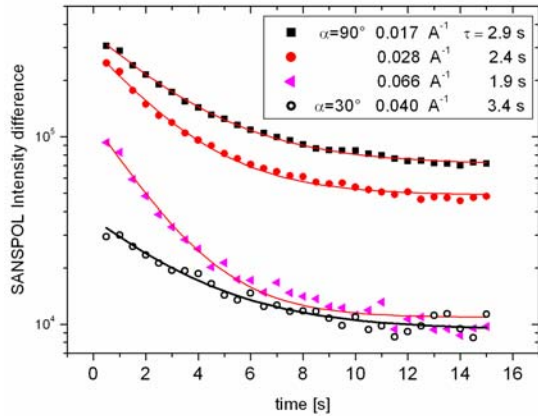


Fig.1: Time decay of the SANS POL intensity differences as measured in a continuous stroboscopic technique Intensities in sectors perpendicular to H ($\alpha=90^\circ$) and in the sector 30° at different values of Q (solid symbols) after switching off the magnetic field. The solid lines correspond to fits of an exponential decay with the time constants τ which depend on Q. [9]

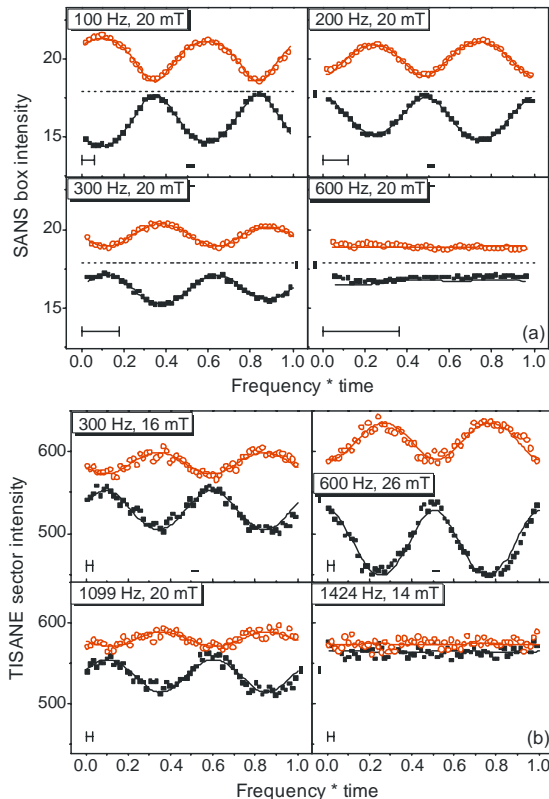


FIG. 2. Frequency dependence of scattering intensities in oscillating magnetic fields. Bars indicate the experimental resolution. (a) Stroboscopic SANS mode at Q_B . (b) TISANE mode. Symbols: 0° (closed),

90° (open). Solid lines: fits to Langevin statistics. Dashed lines: static SANS mode $B=0$.

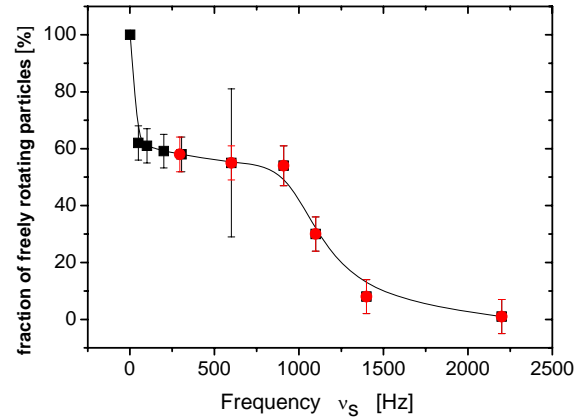


Fig.3. Fraction of freely rotating moments in an oscillating external magnetic field [10]

Acknowledgments

Project granted partially by DFG SPP1104 Project No Wi 1151/2.

References

- [1] A. Wiedenmann, J. Appl. Cryst. **33** (2000)428-432
- [2] A. Wiedenmann, Physica B 297(2001)226-233
- [3] A. Wiedenmann, in Lecture Notes in Physics vol 594:, Springer, S. Odenbach (2002), S. 33-61
- [4] K. Butter, A. Hoell, A. Wiedenmann, G.J. Vroege, J.Appl. Cryst. 37(2004)847-856
- [5] A. Wiedenmann, A. Hoell, M. Kammel, P. Boesecke, Phys Rev. E 68 (2003) 031203, 1-10
- [6] A. Heinemann, A. Wiedenmann J. Appl. Cryst. 36 (2003), 845-849
- [7] A. Wiedenmann, A. Heinemann, JMMM 289(2005)58-61
- [8] A. Wiedenmann, Physica B 356(2005)246-253
- [9] A. Wiedenmann¹, U. Keiderling¹, R. P. May², C. Dewhurst² Physica B (2006)
- [10] A. Wiedenmann, U. Keiderling, K. Habicht, M. Russina, R. Gähler Phys.Rev. Lett.(2006) in print

Synthesis and rheological characterization of Magnetorheological fluids in a varying external magnetic field

A. Fahmi, C.Mendoza, V. Kancharla, T. Pietsch and N. Gindy

School of Mechanical, Materials and Manufacturing Engineering, University of Nottingham, United Kingdom.

Abstract

Magnetorheological (MR) fluids are regarded as a class of smart materials that have the unique ability to undergo rapid (within a few μs) changes in their viscosity upon the application of an external magnetic field.[1-2]. In this study, a series of a novel magneto-rheological fluids (MRF) are prepared with blends of nano sized (20-30nm) and micro sized (1-8 μm) iron particles dispersed in a polymeric matrix.

A systematic rheological characterization was carried out to evaluate the effect of particle content on material viscosity under steady state flow in a custom made Couette geometry, exposed to varying external magnetic field. [3]

On increasing intensity of the applied magnetic field, the apparent viscosity rheograms shows an up shift decades higher compared to those obtained in the absence of magnetic field, also showing typical shear-thinning behaviour.

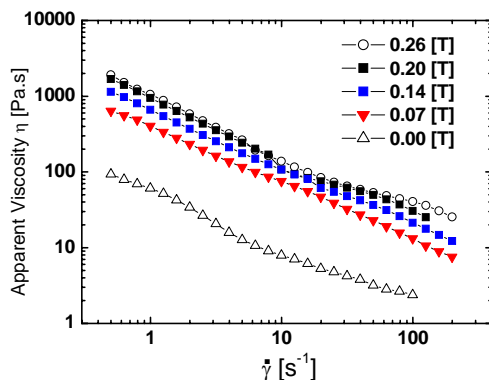


Figure 1. Apparent viscosity rheograms showing the influence on varying the intensity of the magnetic field (in Tesla).

Scanning electron microscope of a sample of the MR fluid was taken to relate material structure with properties. Particle alignment is observed forming a chain-like structure, parallel to the magnetic field due to magnetic dipole interactions.

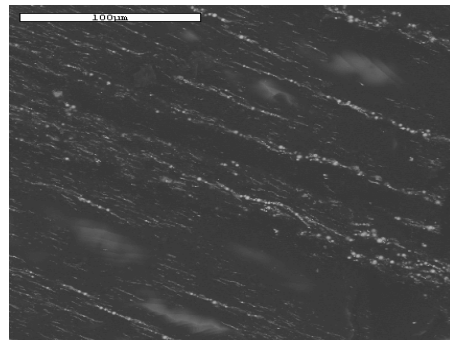


Figure 2. Scanning electron micrograph of aligned particles in MR fluid.

It was found that the mixture of micron and nano-sized particles provides a synergistic effect on the magneto rheological response under low magnetic fields. This has the potential of enhancing the performance of MR fluids in applications requiring high viscosity and may open the scope of their utilization in new applications such as re-configurable fixturing systems.

References

- [1] H. J. Choi, I. B. Jang, J. Y. Lee, A. Pich, S. Bhattacharya, and H. J. Adler, *Ieee Transactions on Magnetism*, 41, 3448-3450, 2005.
- [2] L. Pop, S. Odenbach, A. Wiedenmann, N. Matoussevitch, H. Bönnemann (2005). *Journal of Magnetism and Magnetic Materials*. Vol. 289, 303-306.
- [3] V. Kancharla, A. Fahmi, Q. Liu and N. Gindy. *Nanotech* 2006. Vol. 1., 362-364.

Structural, dynamical, and viscous properties of ferrofluids from computer simulations

Patrick Ilg^{1,2}, Eric Coquelle¹, and Siegfried Hess¹

¹*Institut für Theoretische Physik, TU Berlin, Hardenbergstr. 36, D-10623 Berlin*

²*Polymer Physics, Departement of Materials, ETH Zürich, CH-8093 Zürich*

Introduction

Recent experiments on newly synthesized ferrofluids show huge magnetoviscous effects and significant structural changes under shear flow [1]. These results challenge our theoretical understanding, in particular since the ferrofluids used in these experiments are rather well characterized.

The experimental observations can be described, at least semi-quantitatively within recent extensions of the chain model [2]. Within the chain model, the ferromagnetic particles are assumed to form rigid, chain-like aggregates that can be distorted in a shear flow. For sufficiently strong shear flows, a phenomenological rupture criterion is adopted. Computer simulations provide an alternative approach that allows to test several assumptions underlying the chain model. In the last years, computer simulations played a major role in order to improve the understanding of the equilibrium structure and magnetization of ferrofluids [3].

Here, we summarize recent simulation results for dynamical and viscous properties of ferrofluids and discuss their relationship with nonequilibrium structural properties as found in the simulations. Furthermore, the simulations are compared to experimental results on rheological and structural properties for suitable choices of the model parameters.

Model system

Present day computer simulations study highly idealized model systems consisting of spherical particles with embedded magnetic point dipoles. Besides dipolar interactions, steric interactions due to the stabilizing shell of the particles are taken into account. Usually, monodisperse or bidisperse systems are considered.

The solvent molecules are not resolved explicitly. Instead, their effect is approximately accounted for by friction and Brownian forces as well as hydrodynamic interactions.

The equations of motion are integrated until a stationary state is reached. Having access to the positions of every magnetic particles simulated allows in principle to extract all desired structural and dynamical quantities.

Anisotropic diffusion

We have studied the short and long time equilibrium dynamics in terms of the self (or tracer) diffusion as well as the collective (or mass) diffusion. In the presence of a magnetic field, both, self and collective diffusion become anisotropic. Comparison with a simplified mean-field model show satisfactory agreement for the self-diffusion coefficients of monodisperse systems [4].

In more recent simulations, we extended these studies to investigate the effect of polydispersity and hydrodynamic interactions on diffusion coefficients [5]. It is found that hydrodynamic interactions modify the values of the diffusion coefficients. However, polydispersity effects appear to have a much stronger

influence on diffusion coefficients, at least within the parameter ranges investigated.

Magnetoviscous effect

Building upon earlier work [6], we study the influence of polydispersity and hydrodynamic interactions on the magnetoviscous effect in ferrofluids [5]. Nonequilibrium Brownian dynamics simulations in the presence of a magnetic field and planar shear flow were performed.

Again, the effect of hydrodynamic interactions was found to be relatively weak within the parameter range studied. Therefore, it seems reasonable to neglect these interactions in the following, allowing to study much larger system sizes. Polydispersity effects, on the other hand, can lead to drastic changes in the nonequilibrium structure and viscosities, similar to the findings for equilibrium properties [7].

Shear thinning

The shear thinning phenomenon, i.e. the decrease of the viscosity with increasing shear rate, is observed experimentally and reproduced in the simulations. The simulations show that strong shear thinning behavior is intimately related to a reduced cluster size distribution. These findings therefore support the phenomenological rupture criterion assumed in the extended chain model. These results also help to interpret the strong structural changes that have been observed in small angle neutron scattering experiments under shear flow [1]. Similar results for the nonequilibrium structure factor are also obtained in the simulations.

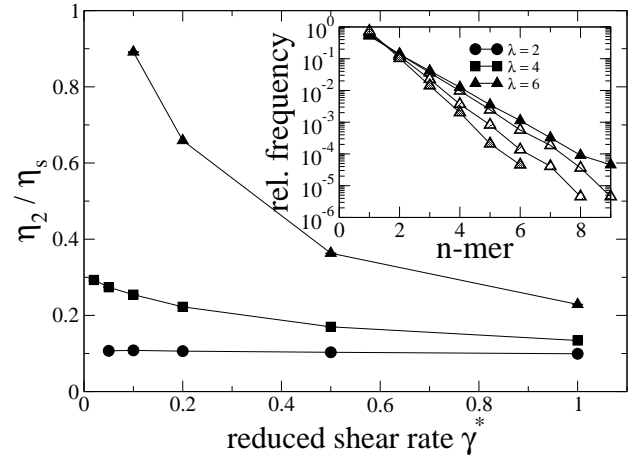


Figure 1: Shear viscosity as a function of shear rate for different dipolar interaction strengths λ . The inset shows the corresponding change of the cluster size distribution for $\lambda = 6$.

References

- [1] L.M. Pop, S. Odenbach, A. Wiedemann, N. Matoussevitch, and H. Bönnemann, *J. Magnetism Magn. Mater.* **289** (2005) 303.
- [2] A. Yu. Zubarev, J. Fleischer, and S. Odenbach, *Physica A* **358** (2005) 475.
- [3] C. Holm and J.-J. Weis, *Curr. Opinion Coll. Interf. Sci.* **10** (2005) 133.
- [4] P. Ilg and M. Kröger, *Phys. Rev. E* **72** (2005) 031504.
- [5] E. Coquelle, P. Ilg, and S. Hess, preprint 2006.
- [6] P. Ilg, M. Kröger, and S. Hess, *Phys. Rev. E* **71** (2005) 031205. *Phys. Rev. E* **71** (2005) 051201.
- [7] Z. Wang and C. Holm, *Phys. Rev. E* **68** (2003) 041401.

Rheological properties of magnetic suspensions with chain-like aggregates

L.Iskakova, A.Zubarev

Ural State University

The work deals with theoretical study of rheological properties of magnetic suspensions under the action of external magnetic field. There are known two approaches for explanation of the observed strong magnetorheological effects in these systems. The first approach is based on the assumption that linear chain-like aggregates appear in the suspensions due to the dipole-dipole interactions between the particles and create the macroscopical rheological phenomena (see, for example, [1],[2]). The second approach uses the hypothesis that these phenomena are created by the bulk dense ellipsoidal aggregates (microdrops), consisting of tremendous number of the particles [3]. Both of these models deal with identical chains (drops) which size is determined by the balance between the magnetic forces, attracting the particles to each other, and the hydrodynamical shear forces, tending destroy these aggregates. Both of the models lead to the power relation

$$\eta(H)/\eta(0) - 1 = Mn^{-\Delta} \quad (1)$$

between the suspension effective viscosity η and the applied magnetic field H , parallel to the gradient of the suspension flow. Here $Mn \sim \dot{\gamma}/H^2$ is the so-called Mason number which is equal to the ratio of the destructive hydrodynamical shear force to the magnetic attractive force acting between two particles. In the known models of chains $\Delta=1$, in the models of the drops $\Delta=2/3$. In the both models the magnitudes of the exponent Δ are fixed, this parameter depends neither on the field H nor on the particle volume concentration φ . The power dependence of the viscosity η on the shear rate $\dot{\gamma}$ has been observed in many

experiments, but the measured magnitudes of Δ have never been either 1 or 2/3. They always have been between these limit magnitudes (see overview in [4]). Moreover, in experiments [3] and [5], carried out with quite different suspensions, it was detected an increase of Δ with the field H from (approximately) 2/3 to (approximately) 1 and its slow increase with the particle concentration φ . These dependencies of Δ on H and φ are look curiously because they qualitatively contradict to the known theories, where Δ is fixed. Analysis shows that the variations of Δ with H and φ from the “drop” magnitude 2/3 to the “chain” magnitude 1 can not be explained by the transformation of the internal heterogeneous structures from the drops to the chains.

Very often in experiments the Mason number Mn is much less or much greater than unity. That is why even small errors in the theoretical determination of the exponent Δ lead to large errors in the prediction of the effective viscosity η . It is more important that the magnitude of Δ reflects a type of the internal structure in the suspension. Therefore misunderstanding of Δ magnitude and its dependencies on H and φ means lack of even qualitative knowledge about microscopical physical nature of the observed macroscopical rheological effects in these systems.

From our point of view, the field and concentration dependencies of Δ can be explained by polydispersity of ensemble of the chains in the suspensions. Indeed, unlike the assumptions of [1,2,5], these chains, been specific heterogeneous fluctuations of density, can not be identical. There must be some statistical distribution

over number of particles in the chains. The relatively short chains react on the shear flow weaker than the long chains. Therefore the viscosity of the suspension with the long chains must stronger depend on the shear rate than the viscosity of the suspension with the short chains. On the other hand, when the applied field or/and the particle concentration increases, the percentage of the long chains also increases, therefore the reaction of the suspension on the shear flow becomes stronger. Mathematically it leads to increase of the exponent Δ with H and φ .

In order to check this hypothesis, we have considered a system of identical non Brownian particles, typical for the magnetorheological fluids and inverse ferrofluids, submitted into shear flow and magnetic field parallel to gradient of the flow velocity. We supposed that magnetic moment of each particle is proportional to the applied field H .

Balancing the hydrodynamical and magnetic torques, acting on the chain, we have estimated the angle of each chain deviation from the field. Balancing the radial components of the hydrodynamical destructive and magnetic attractive forces, we estimated the maximal, for a given field and shear rate, number of particles in the chain. Then, by using developed methods of statistical physics, we determined the distribution over number of particles in the chains. Neglecting any interactions between the chains and using the known results of hydromechanics of suspensions, we estimated the suspension macroscopical viscosity η and came to the power form (1) with Δ dependent on the field H and particle volume concentration φ . The dependencies of Δ on H and φ as well as the calculated magnitudes of η are quite close to those observed ones in [3],[5].

Some results of calculations of the exponent Δ are shown in Fig. 1.

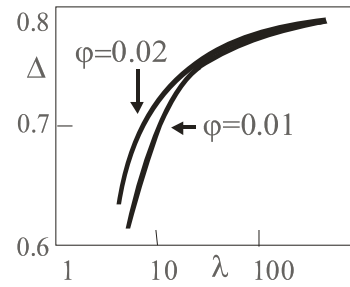


Fig.1. The exponent Δ vs. dimensionless parameter $\lambda = \mu_0 m^2 / (4\pi d^3 kT)$ of magnetic interaction between particles, where m and d are magnetic moment and diameter of the particle

Like in the experiments of [3],[5] the exponent slowly increases with the dipole moment m of the particle, i.e. with the the applied field H .

Thus, our analysis shows that the observed rheological effects in magnetic suspensions can be produced by polydispersity of ensemble of the chains. The chain size distribution is a result of competition between magnetic interaction of the particles, shear hydrodynamical forces and the thermal effects. The factor of the chain polydispersity is crucially important for formation of the macroscopical properties and magnetorheological effects in magnetic suspensions and must not be ignored in the theoretical investigations of these phenomena.

1. J.E.Martin, R.A.Anderson, J.Chem.Phys. 76, 635 (1996)
2. O.Volkova, G.Bossis et al., J.Rheology, 44, 91 (2000).
3. T.Halsey, J.E.Martin, D.Adolf, Phys.Rev.Lett., 68, 1519 (1992); B.J. de Gans, H.Hoekstra, J.Mellema, Faraday, Discuss. 112, 209, (1999).
4. G.Bossis, O.Volkova, S.Lacis, A.Meunier, in Ferrofluids. Magnetically Controllable Fluids and their Applications. Ed. S.Odenbach, Springer, 2002, P. 202.
5. B.J. de Gans, H.Hoekstra, J.Mellema, Faraday, Discuss. 112, 209, (1999).

Optical birefringence in ferrofluids

L.Iskakova, A.Zubarev

Ural State University

Being subjected into magnetic field, ferrofluids become optically anisotropic - light with electric polarization parallel to the magnetic field experiences a higher refraction index (positive birefringence) than the light polarized perpendicular to the field. Usually this optical anisotropy is explained either by the existence of particles with anisotropic shape (for example, so called primary agglomerates, which appear on the stage of the ferrofluid preparation due to colloidal interaction between fine magnetic particles) or by appearance of the anisotropic chain-like aggregates due to the magnetic interaction between the particles. Both of these mechanisms of the ferrofluid optical anisotropy undoubtedly can take place in the real systems. However, one needs to take into account that appearance of the primary agglomerates can be considered as, possibly inevitable, defect of the ferrofluid preparation. Concentration of these agglomerate in the well prepared systems must be very small. The chains can consist only of the particles which magnetic interaction is strong, i.e. the particle volume is large enough. However in the modern ferrofluids, as a rule, absolute majority of the particles are relatively small and energy of magnetic interaction between them is about kT or less. These particles can not form any aggregates. Concentration of the particles large enough to form the chains usually is very small. From the point of view of the technological usage of ferrofluids any heterogeneous structures, as a rule, are undesirable. That is why the presence of the large particles, able to formation of the chains and other heterogeneous structures, also can be considered as a defect of the ferrofluid preparation and the producers often try to

remove the large particles from the ferrofluid.

At the same time there is a mechanism of the optical anisotropy of ferrofluids, which takes place even in the homogeneous systems without any heterogeneous structures and the primary anisotropic agglomerates. Indeed, if the energy of the magnetodipole interaction between the particles is about kT , this interaction can not lead to formation of any heterogeneous structures, however it influence on the mutual disposition of the particles, i.e. on their binary long range correlations. In the presence of external magnetic field these correlations are anisotropic with the axis of symmetry parallel to the field. This anisotropy of the binary correlations induces anisotropy of the effective dielectrical permeability of the ferrofluid and, therefore, anisotropy of the optical properties of the fluid. Of course, the influence of a couple of the large particles, united into a dense doublet, on the anisotropy of the effective permeability is stronger than the influence of a couple of the homogeneously correlated small particles. However, since the concentration of the small particles in the real ferrofluids usually is significantly higher than concentration of the large particles, the total effect of the weakly correlated small particles can be stronger than the effect of the large particles, united into the chains.

In the presented work we study theoretically the optical anisotropy of a ferrofluid created by the long range homogeneous correlations between the small particles. We consider the ferrofluid as homogeneous system of identical spherical magnetic particles.

For maximal simplification of the calculations we take into account only the pair correlations of the particles, neglecting any interaction of a "third" particle on the mutual disposition of two particles. In this case the binary correlation function of the particles obeys to the Boltzman law. In the presence of the applied magnetic field this function depends on the angle between the field and radius-vector connecting the particles. We take into account that the wave length of the visible light is much more than size of the particles in ferrofluid. Thus the effective optical properties of the ferrofluid are determined by the tensor ϵ of the stationary effective permeability of the fluid.

We have estimated the components of this tensor by using the strict results of the theory of effective properties of composites taking into account anisotropy of the binary interparticle correlations. Then we calculated the birefringence index Δn by using the standard formula

$$\Delta n = \sqrt{\epsilon_{\parallel} - \epsilon_{\perp}}$$

Here \parallel and \perp mark the tensor components parallel and perpendicular to the field. Some results of calculations of the index Δn in the model of the non spherical primary agglomerates, in the model of chains and in the presented model of the homogeneous anisotropic correlations of small particles are shown in Fig.1. We suppose that all particles and agglomerates are magnetite, diameter of the small particles is about 10-12 nm, their magnetic volume concentration is 5%. Diameter of the large particle is 17 nm, magnetic volume concentration of these particles is 0.7%. The major axis of the primary agglomerate is twice as long as the minor axis, volume concentration of these agglomerates is about 0.1%. The chosen parameters of the system correspond to the typical magnetite ferrofluids.

The results presented in Fig.1 show that, for the considered system, effect of the chains dominates over the effect of the homogeneous long range correlations when the applied magnetic field is weak. The effect

of these correlations between the small particles dominates in the region of moderate and strong magnetic field. The calculated effect of the long range correlations for all magnitudes of the field is greater than the effect of the primary agglomerates. Of course, the calculated ratio between the birefringence indexes depends strongly on the volume concentrations of the small particles, primary agglomerates, large particles, as well on their sizes and magnetic properties of the particles.

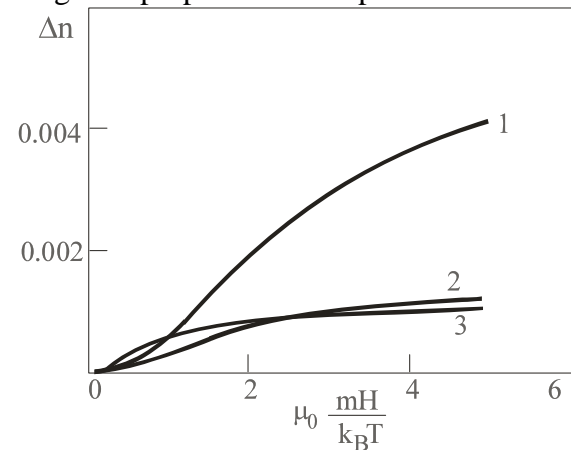


Fig.1. The birefringence indexes Δn vs. applied magnetic field H , calculated in the presented model of the long range correlations between small particles (1), in the model of chains consisting of the large particles (2) and in the model of anisotropic primary agglomerates (3); m is magnetic moment of the small particle. Parameters of the system are given in the text.

In conclusion we would like to note that the results of the optical birefringence experiments are used in order to study the internal structures in ferrofluids; the effect of the optical anisotropy very often is considered as a sign of existence of the anisotropic agglomerates and/or heterogeneous chains. Our results demonstrate that the optical anisotropy can be produced by the homogeneous correlations between the relatively small particles. We think that this result must be taken into account when interpreting of the optical experiments.

Kinetics of internal structure formation in magnetic suspensions

L.Iskakova, A.Ivanov, S.Kantorovich, A.Zubarev,

Ural State University

Experiments, both numerical and laboratory, demonstrate two types of internal structures in magnetic suspensions – linear chain-like and bulk dense drop-like (column-like) aggregates. There are known many theoretical investigations of equilibrium states and properties of suspensions with these structures. The problem of kinetics of the structure formation, important both from the general scientific point of view and viewpoint of these suspensions application, is studied weakly. We present results of theoretical study of kinetics of evolution of ensembles of the chains and the drops (columns). Since study of these different structures requires quite different approaches, the chains and drops are considered here separately.

Chains. The first model of kinetics of the chain formation has been developed by M.Doï with collaborator in ref. [1]. In this model irreversible cluster-cluster aggregation has been considered, the Brownian motion of the particles has been ignored. The rate of the aggregation, following from this model, is several orders of magnitude greater than the rate, detected experimentally (see Fig.1).

In our model we take into account that the numerical concentration of the clusters (their number in a unit volume of the system) usually is significantly less than the concentration of the single particles; the hydrodynamical mobility of the cluster is less than the mobility of the particle. That is why we consider the cluster-particle type of aggregation. Then, unlike the Doï model, we take into account the Brownian diffusion of the single particles as well as disintegration of the aggregates due to evaporation of the particles from them.

Mathematically our model consists of a chain of the governing equation for the functions $g_n(t)$ – time depended number of the n -particle chains in a unit volume of the system. These equations take into account the joining of the single particle to the chains and evaporation of the particles from this clusters. The coefficients of the particle aggregation and evaporation have been determined from the detailed analysis of the particle diffusion and dipole attraction to the chain.

Some results of our calculations of the mean number $\langle n \rangle$ of the particles in the chain and the results of experiments of G.Bossis et al. (University Nice –Sophia Antipolis) are shown in Fig.1. These experiments have been carried out with an electrorheological fluid, because technically organization of those experiments was much easier than experiments with magnetic suspensions. However, theoretical description both of these systems is identical. First of all one can see that the Doï model predicts the rate of the aggregation much greater than that in the experiments. Second, our model is in reasonable agreement with the experiments. It should be noted that no free fitted parameters have been used in our calculations.

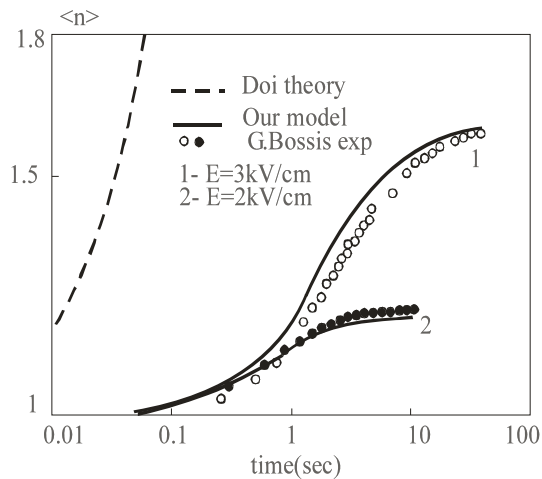


Fig.1. Theoretical and experimental results for the kinetics of the chain growth for water based electrorheological fluid with dielectrical particles $0.4\mu\text{m}$ in diameter, 3% of volume concentration.

Drops. The bulk drop-like structures, aligned along applied magnetic field, have been detected in many experiments with various ferrofluids and other magnetic suspensions. Very often they were observed in thin layers of the systems placed into normal magnetic field. In these layers the drops look like cylindrical domains spanning the chamber with the suspension. The typical diameter of the domains, observed in ferrofluids, is about several microns. The bulk domains, spanning the chamber, are responsible for the quasielastic, yield-stress and other rheological effects in the magnetic suspensions. Analysis [2] shows that the equilibrium structure of these drops (domains) is determined by the competition between the demagnetizing effects in the domain bulks and the capillary effects on the domain boundaries.

In the presented work we have considered evolution of the domain in a thin (about 1 mm of thickness) flat gap, filling by a magnetic suspension. Analysis shows that the domain evolution starts after switching on the field and consists of two stages. The first, fast, stage corresponds to appearance and formation of the cylindrical domain overlapping the gap. The typical duration of this stage is about second or less. On the second, slow, stage the domain tends to its equilibrium state. In order to study this slow period of the evolution, we have written down equations of the single

particle diffusion in the space between the domains. The distribution of local magnetic field around the domain has been taken into account in these equations. The equation for the domain diameter growth includes the terms, corresponding to the particle flux onto the domain surface and flux of the particles, evaporated from the domain. Some results of our calculations of the ratio of the domain radius R to its equilibrium (final) magnitude R_0 for the water based suspension with the particles about $1\mu\text{m}$ in diameter is presented in Fig.2. The ratio of the energy of the particle interaction with the applied to kT is 5.

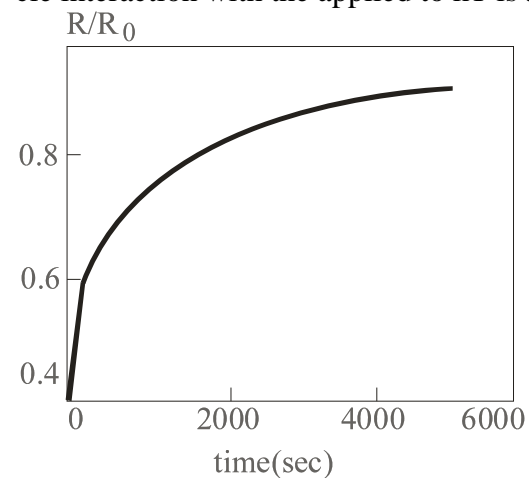


Fig.2. Dimensionless domain radii R vs. time. Explanations are in the text.

The results indicate fast domain growth in the onset of the process and then its slow tendency to the equilibrium state. It should be noted that the micron size of the particles is typical for magnetorheological suspensions and inverse ferrofluids. For ferrofluids with nanoparticles the rate of the domain growth is much higher. The long (during hours) evolution of the domains in magnetic suspensions must induce long drift of macroscopical (for example, rheological) properties of these systems, which can be detected in experiments.

References

- [1] H. See, M. Doi, J. Phys. Soc. Japan, **60**, 2778 (1991)
- [2] A. Zubarev, L. Iskakova, Physica A, **367**, 55 (2006)

Giant relaxation times in novel type of magneto-rheological fluid

Robert Krauss¹, Birgit Fischer^{1,2}, Youyong Xu², Axel H. E. Müller², and Reinhard Richter¹

¹*Experimentalphysik V, Universität Bayreuth, D-95440 Bayreuth, Germany*

²*Lehrstuhl für Makromolekulare Chemie I, Universität Bayreuth, D-95440 Bayreuth, Germany*

Introduction

By dispersing non-permeable particles in a common ferrofluid one obtains a so-called inverse ferrofluid, as first investigated by Skjeltorp [1]. These particles create a hole in the ferrofluid, which appears to possess a magnetic moment corresponding to the amount and susceptibility of the displaced fluid. Due to dipolar interactions chain formation sets in, as shown in Fig. 1.

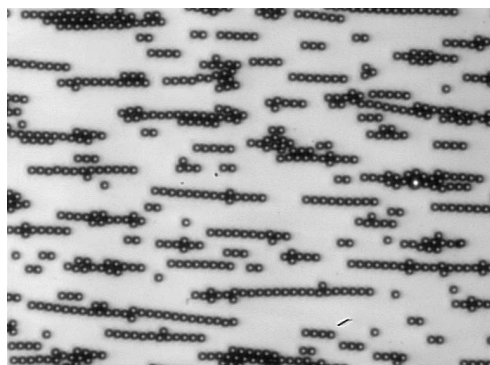


Figure 1: *Chain formation of PS particles (diameter $10\mu\text{m}$) dispersed in a ferrofluid. The field is oriented horizontally.*

In recent studies monodisperse polystyrene spheres were used to investigate magneto-rheological phenomena occurring in these inverse ferrofluids such as yield stress or viscoelasticity [2, 3]. In our contribution we present the temporal evolution of the complex shear modulus after a jump-like increase of the magnetic induction. We compare the stretched exponential relaxation of an inverse ferrofluid made from PMMA spheres with the one of a novel inverse fluid made from polymer brushes.

Experimental

A Physica MCR301 rheometer (Anton Paar) with the commercial magnetorheological cell PP 20/MR was used to measure the magnetorheological properties of the different samples. The field was oriented perpendicular to the plates of the rheometer, and thus, perpendicular to the direction of the shear. The distance between the plates was adjusted to $500\mu\text{m}$. Two different kinds of inverse ferrofluid have been prepared: The first one by dispersing spherical PMMA particles with a diameter of $3\mu\text{m}$ in the commercial ferrofluid APG512A from Ferrotec, Co. The other one is the first example of an inverse ferrofluid made from semi-flexible cylindrical polymer brushes. To get the novel samples polymeric macromolecules were prepared by atom transfer radical polymerization (ATRP) of monomer lauryl methacrylate from a macroinitiator. These brushes are then soluted in paraffin oil and thus can be easily dispersed in a ferrofluid that also uses paraffin oil as carrier liquid. AFM pictures display a nearly cylindrical shape of the lauryl methacrylate brushes and one can estimate the size to about 150 nm length and 30 nm diameter.

Results

Figure 2 shows the temporal evolution of the loss and storage modulus of the dispersed spheres following a jump of the induction from zero to $B = 384\text{mT}$. The slow increase of G' and G'' is indicating that the field induced formation of a network of chains takes place on a rather large time scale. The

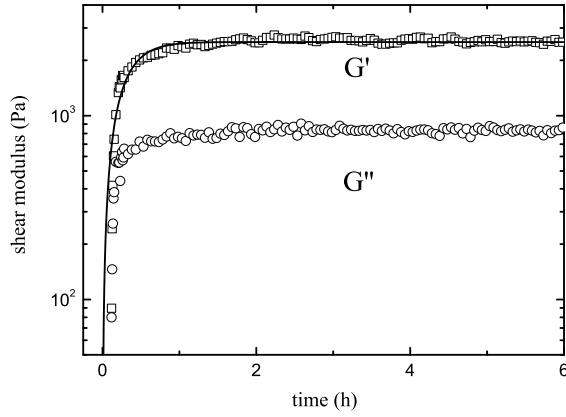


Figure 2: Time evolution of the loss and storage modulus of the PMMA-ferrofluid-suspension.

solid line displays a fit using Eq. (1),

$$G'(t) = G_{\infty} - (G_{\infty} + G_o) e^{-\left(\frac{t}{\tau}\right)^{\beta}} \quad (1)$$

describing a stretched exponential behaviour, as first proposed by Kohlrausch [4]. Here G_o and G_{∞} denote the starting and saturation values of the shear modulus, τ the characteristic relaxation time and β the fractional Kohlrausch exponent. For the fit, where G_o was fixed to the value at zero field, we obtained $\beta = 1.17$ and $\tau = 18.8$ minutes. Next we investigate the same relaxation process for G' for the magneto-rheological fluid made from the polymer brushes, as shown in Fig. 3. The fit according to Eq. (1) marked by the solid line yields now values of $\beta = 0.96$ and $\tau = 18.3$ hours. This giant relaxation time originates from the small and flexible polymer brushes. They experience much smaller forces in the magnetic field. Moreover their orientation can be hindered by mutual entanglements. Similar relaxation processes are known from the gel like networks of clay and quicksand [5, 6].

Acknowledgments

The authors would like to thank Marina Krekhova and Ingo Rehberg for helpful advice, and the *Deutsche Forschungsgemeinschaft* for financial support under grant SFB 481, project B9.

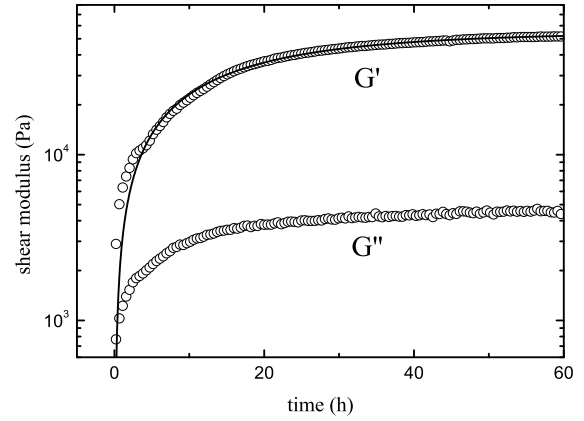


Figure 3: Time evolution of the loss and storage modulus of the polymer-ferrofluid-system.

References

- [1] A.T. Skjeltorp, Phys. Rev. Lett., **51**, 2306 (1983).
- [2] R. Saldivar-Guerrero et al., Magneto-hydrodynamics, **41**, 4, 385 - 390 (2005).
- [3] R. Saldivar-Guerrero et al., accepted by J. Chem. Phys.(2006).
- [4] F. Kohlrausch, Pogg. Ann. Phys., **119**, 337 (1863).
- [5] H. Van Olphen, An Introduction to Clay Colloid Chemistry., (Wiley, New York, 1977).
- [6] A. Khaldoun et al., Nature, **437**, 635 (2005).

Viscous Properties of a Magnetite-based Ferrofluid From Capillary Wave Spectroscopy

Jens Patzke, Bernd Rathke, and Stefan Will

Universität Bremen, Technische Thermodynamik, Badgasteiner Str. 1, D-28359 Bremen

The viscous properties of ferrofluids under the influence of magnetic fields are investigated by two complementary techniques of Dynamic Light Scattering (DLS). One technique, DLS from the bulk phase, provides information on particle sizes and geometries of dispersed particles, the second, Capillary Wave Spectroscopy (CWS), yields information on the viscous properties of a ferrofluid without application of external shear.

Thermally excited waves on a liquid surface can be represented by a superposition of different modes of surface waves with amplitudes $\zeta_{\mathbf{q}}$ and wave vectors \mathbf{q} . Depending on the viscosity η , surface tension σ , and density ρ of the fluid and the modulus q of the wave vector via

$$y = \frac{\sigma\rho}{4\eta^2q}$$

a surface mode can propagate ($y > 0.145$) or is overdamped ($y < 0.145$). By choice of a particular wave vector through the scattering vector of the optical arrangement a CWS experiment probes a particular surface mode. The characteristics of this mode are reflected in the autocorrelation function of the scattered light.

CWS is used to investigate the viscous properties of magnetite-based ferrofluids with different concentrations of particles varying the strength and orientation of an externally applied magnetic field relative to the scattering vector \mathbf{q} .

For the provision of an homogeneous magnetic field two symmetric pairs of coils are used, which can produce fields up to 250kA/m with an inhomogeneity of about 5% in a region of 1000cm³. Another impor-

tant prerequisite for successful CWS-experiments on ferrofluids is the reduction of surface deformations of the fluid that arise because of the difference in magnetic susceptibility between the fluid and its container. To that end various susceptibility-matched sample cells of epoxy-raisin containing magnetite particles with volume concentrations up to 0.1 were produced and employed.

We have performed a series of CWS-experiments on a commercial iso-octane based ferrofluid (Buske, Berlin; $M_{\text{sat}}=47.5$ kA/m; $\phi = 0.105$) at various dilution steps. At low concentrations propagating waves are detected, at higher concentrations a change to over-damped waves is observed. Furthermore, results of experiments are shown in which the strength and the orientation of the applied magnetic field were varied.

From DLSmeasurements from the bulk it is demonstrated that upon application of a magnetic field larger particles appear in a ferrofluid that can be interpreted as particle aggregates.

In situ SANS investigations of microstructure changes of cobalt based ferrofluids under shear and magnetic field influence

L. M. Pop¹, S. Odenbach¹, M. Kammel², A. Wiedenmann²

¹ *Technische Universität Dresden, 01062 Dresden*

² *Hahn-Meitner Institute, 14109 Berlin*

Previous rheological experiments, performed for magnetite as well as for cobalt based ferrofluids, have evidenced strong magnetoviscous effects that could be correlated with structural changes within the fluid samples in shear flow and under the influence of a magnetic field.

In the last years, a lot of experimental and theoretical studies have been performed in order to explain the microscopic mechanisms of the magnetoviscous effect. As a result of these efforts a model, based on numerical and experimental data, has been established, which is able to explain the observed behavior [1]. Chain formation of magnetic particles with strong particle-particle interaction as well as structure destruction by means of shear influence are the essential processes for the understanding of the magnetoviscous phenomena.

Experimental setup

Since experimental data proving such a connection between the structure of ferrofluids and their viscous properties were missing the study of the microstructure of ferrofluids under shear – for different magnetic field strengths and shear rates – and its consequences on the magnetoviscous effect is in the focus of recent research. Using a specially designed rheometer [2], rheological as well as small angle neutron scattering investigations have been performed in the same experimental environment.

For the SANS experiments two configurations, one with the magnetic field oriented parallel to the neutron beam and the other with 10 degree between the magnetic field

direction and the neutron beam, have been used. Both, rheological and SANS investigations have been carried out for magnetic fields varied between 0 and 160 kA/m, applied perpendicular to the vorticity of the flow. The shear rates have been varied within the range from 0 up to 200 s⁻¹.

Experimental results

Scattering as well as rheological experiments were performed for four different cobalt based ferrofluids, manufactured by N. Matoussevitch and H. Bönemann (Forschungszentrum Karlsruhe) [3]. The concentration of the magnetic material was varied in the range from 0.35 vol.% up to 3.25 vol.% in order to observe its influence on the magnitude of the magnetoviscous effect. Additionally, the mean particle diameter as well as the viscosity of the carrier liquid have been changed.

Depending on the parameters of the investigated ferrofluids, strong dependency of the resulting scattering patterns on the magnetic field strength and shear rate were observed in the case of the fluids with large mean particle diameter (10 nm).

Depending on the applied shear rate and magnetic field strength an anisotropy of the scattering patterns could be observed. The anisotropy as well as its deviation from the vertical direction – corresponding to the static case in the 10° setup – indicates modification of the length and orientation of the chain-like structures with respect to the applied stress. In the case of the fluid with smaller mean particle diameter (8 nm), i.e. with a low content of particles which are able to form structures, no

changes of the microstructure due to the magnetic field influence or shear rate have been observed.

The obtained results show a strong connection between structure formation in ferrofluids and their rheological behaviour. The evidence for a formation of chains and their deviation in a shear flow validates therefore the model of chain formation as an explanation for the magnetoviscous effect. These results are in a good agreement with the rheological data and with the chain formation model developed to explain the mechanism of the magnetoviscous effect [1, 4].

Further on, the influence of the concentration of the cobalt particles on the structure formation within the ferrofluid samples, i.e. on the magnitude of the magnetoviscous effect, will be discussed. Thus, the SANS results will be compared with the rheological data obtained for the investigated ferrofluids. The experimental results will be compared with two different theoretical approaches, the chain formation theory [5] as well as molecular dynamic simulations [6]. Further information, concerning the local magnetisation of the sample in a shear flow relative to the direction of the chains, obtained from experiments using polarised neutrons, will be presented. Additionally, the possibility of combining X-Ray and neutron experiments will be discussed.

Establishing a connection between the changes of the microstructure of ferrofluids, under the influence of a magnetic field, and their consequences on the macroscopical behaviour of these systems could allow an optimisation of the fluids. Based on the knowledge gained from experimental and theoretical studies, new applications can be developed, making ferrofluids an attractive medium for potential further research.

Acknowledgments

The financial support by the Deutsche Forschungsgemeinschaft under grant number DFG OD 18/4 in SPP1104 is gratefully acknowledged.

References

- [1] S. Odenbach, Magnetoviscous effects in ferrofluids, LNPm71, Springer Verlag (2002)
- [2] L. M. Pop, J. Hilljegerdes, S. Odenbach, A. Wiedenmann, Applied Organometallic Chemistry, (2004), 18
- [3] H. B. Bönemann, et al., Magneto hydrodynamics, (2003)39
- [4] Pop, L. M., Investigation of the microstructure of ferrofluids under the influence of a magnetic field and shear flow, to be published
- [5] A. Zubarev, private communication
- [6] P. Ilg, M. Kröger, S. Hess, JMMM (2005) 289

Controlled shear stress rheological investigations of ferrofluids

Hamid Shahnazian¹, Stefan Odenbach¹

¹ *Technische Universität Dresden, 01062 Dresden*

Motivation

Recent rheological experiments, performed on ferrofluids, have shown strong magnetoviscous effects that can be described with chain and structure formation due to interparticle interaction in the presence of a magnetic field. Furthermore, with increasing shear rate the mechanical torque becomes dominant, the chain-like structures break up and the relative change of viscosity decreases. This effect is called shear thinning [1].

In the last years, a lot of theoretical studies for a description of the effects have been performed, which vary in the basic modeling of the ferrofluid and its phenomena. Some models try to explain the effects on the basis of microscopic assumptions [2, 3], some other models base on a mesoscale and even macroscopic descriptions abstaining from microscopic assumptions [4, 5]. The predictions of the models rely on experimental data concerning effects; one effect is the question of an appearance of a magnetic field dependent yield stress in ferrofluids. In the previous experiments on the magnetoviscous behaviour [1], a shear rate controlled rheometer has been used. With this rheometer the question whether a yield stress exists can not be answered directly. Extrapolating the measured flow curves to shear rate zero, an upper border for the yield stress of 0.1 Pa could be estimated for the fluid APG513A and a magnetic field strength of 30 kA/m [1].

Experimental setup

In order to prove the appearance of a magnetic field dependent yield stress for ferrofluids of different structural make up, a special shear stress controlled rheometer

has been designed. The magnetic field, which is perpendicular to the vorticity of the flow, is produced by a cylindrical coil (fig.1). The experiments have been carried out for magnetic fields varied between 0 and 80 kA/m with a homogeneity of 0.05 % in the region of the shear cell. The measuring cell is a cone-plate arrangement combined with a Couette region.



fig. 1: The shear stress controlled rheometer for the investigations of the yield stress in ferrofluids.

The cone is fixed via an air bearing with an optical encoder. With this device, which works contactless, the rotation frequency of the cone is measured with high precision. The encoder allows the detection of a minimum rotation frequency of 10^{-7} Hz corresponding to a shear rate resolution of about 10^{-5} s⁻¹. To apply shear stresses below the mentioned value of 0.1 Pa [1] a conventional electric motor is used in combination with a fluid coupling. The upper plate of the coupling is fixed to the

electric motor. The torque is transmitted by the liquid to the second plate, which is fixed to the cone of the cone-plate cell. With this system a minimum torque of 10^{-9} Nm can be realized, which corresponds to a shear stress of 10^{-5} Pa.

Experimental results

In the first experiments with the driving unit – electric motor combined with the fluid coupling – a magnetorheological fluid (MR) has been investigated. For such kind of fluids the dependence of yield stress on magnetic field strength is already observed. Using a MR-fluid will give information whether a direct measurement of yield stress as a function of an applied magnetic field can be carried out.

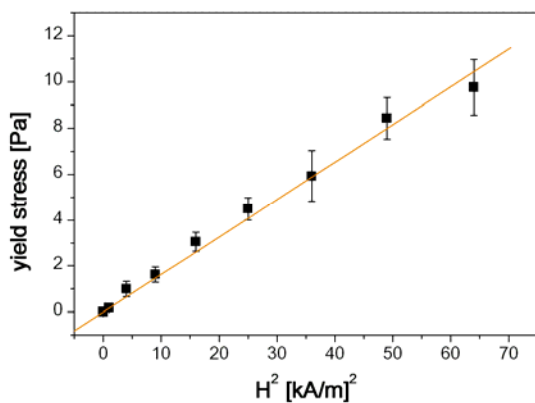


fig.3: The yield stress of the MR-fluid as a function of the square of the applied magnetic field

For the MR-fluid a clear dependence of the yield stress on the magnetic field strength is observed (fig.3). This effect depends quadratically on the strength of the applied magnetic field. These results confirm that the shear stress controlled rheometer enables a direct measurement of the yield stress and its dependence on magnetic field strength.

In order to perform the field dependent yield stress measurements for ferrofluids, one magnetite-based (APG513A) and one cobalt-based (Co91) ferrofluid have been investigated. For the APG513A and a magnetic field strength of 30 kA/m a yield stress of $\tau_y = 0,012$ Pa is measured, which is well below the estimated taken from the previous extrapolations of the flow curves

with the shear rate controlled rheometer [1].

The yield stress grows for both ferrofluids quadratically with the strength of the applied magnetic field (fig4). Further a significant higher value of yield stress for the fluid Co91 compared to APG513A is observed. The magnetic interparticle interaction has already been proven as the determining parameter for the appearance of magnetoviscous effects in ferrofluids. For cobalt-based fluids with 10 nm particles a modified interaction parameter of $\lambda^* = 5.26$ is obtained [1], which is about two times higher than for the 16 nm magnetite particle fraction in APG513A. It appears that the yield stress depends also strongly in the interparticle interaction.

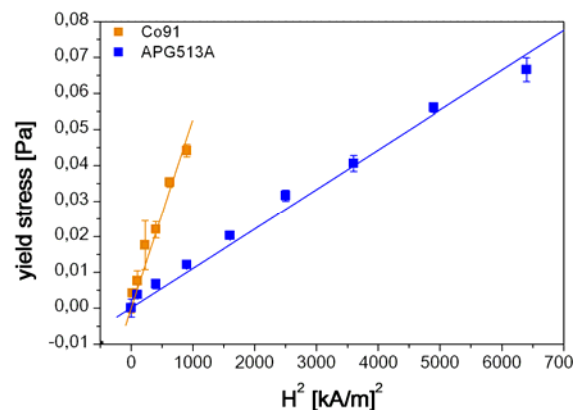


fig.4: The yield stress of the ferrofluid APG513A as a function of the square of the applied magnetic field.

References

- [1] S. Odenbach, Magnetoviscous effects in ferrofluids, LNPM71, Springer Verlag (2002)
- [2] S. Odenbach, H. Störk, Shear dependence of field induced contributions to the viscosity of magnetic fluids at low shear rates, JMMM, 183 (1998) 188-194
- [3] A.Yu. Zubarev, S. Odenbach and J.Fleischer, Rheological properties of dense ferrofluids, JMMM, 252 (2002) 241
- [4] P. Ilg, M. Kröger, S. Hess, Structure and rheology of model-ferrofluids under shear flow, JMMM, 289 (2005) 325-327
- [5] H. W. Müller, M. Liu, Structure of ferrofluid dynamics, Physical Review E, 64 061405 (2001)

Magnetorheological actuator for the control of primary mirror elements of extra-large telescope

D. Borin¹, V. Mikhailov²

¹ *Technical University Dresden, Institut für Strömungsmechanik, George-Bähr-Str.3, 01062, Dresden, Germany*

² *Bauman Moscow State Technical University, 2nd Baumanskaya st., MT-11, 105005, Moscow, Russia*

Magnetorheological fluids (MRF) are widely used in technical applications because of their ability to provide simple, quiet, rapid-response interfaces between electronic controls and mechanical systems.

For a long time it is proposed to use MRF as a working medium for semi-active dampers, fluid clutches etc [1]. Besides, MR fluids have been offered as a promising candidate for developing ultra precise hydraulic actuators for use in various technical systems, e.g.: X-ray lithography; tuning, adjusting and control of optical and laser systems; nanoscale surface analytical techniques, etc [2]. The magnetorheology control has advantages of nanometer scale accuracy of positioning at long-range travel, millisecond response time and high loading ability. On the basis of it, a number of MR actuators have been developed. Among them the 6-coordinate table for microlithography, long-range travel ultra-high vacuum manipulator etc [3]. The one of the recent project is developing of positioning actuator with MR control for the elemental mirrors of extra-large astronomical telescope AST-25.

The main feature of extra-large astronomical telescope AST-25 is a segmented primary mirror, which segments constitute the whole reflecting system. This design resolves the problem of the primary mirror manufacturing however it makes a problem of mirror segment positioning, since a mirror elements positions should be accurately and continuously adjusted during the telescope operation. The mirror segment actuators should ensure extremely high requirements on accuracy of positioning, on processing speed and loading ability, that is caused by necessity

of repeated motion and precise positioning during telescope operation. As a result of the lead works it is offered and realized actuator of hydraulic type with MR control which idea consist in use of the valves system based on Wheatstone bridge hydraulic power circuit.

It was demonstrated that this actuator have excellent features, i.e.: the error of positioning less than 0.1 μm which can be reduced potentially to about 10 nm by optimization of control laws and actuator design. The time of response of actuator is less than 50 milliseconds which depend on MR fluid behavior. The load capacity of MR actuators can be more than 1000 N.

References

- [1] M. R. Jolly, J.W. Bender and J. D. Carlson (1999) "Properties and Applications of Commercial Magnetorheological Fluids," *J. Intelligent Material Systems and Structures*, 10(1), 5.
- [2] Deulin E.A., Mikhailov V.P., Sytchev V.V., Borin D.Y., Variable rheology usage for precise drive// *Proc. of 4th International Symposium "Vacuum technology and equipment"*: Charkov, Ukraine, 2001. – pp.163-166.
- [3] V.V.Anisimov, E.A.Deulin, S.V.Khramtsov et al. (1996) "New manipulators of nanometer precision for surface analysis," *Vacuum*. - V.28, №10. - P.1163-1165.
- [4] A.A.Boyarchuk, N.V.Steshenko, N.D.Belkin et al. "Design project of large astronomical telescope AST-10", *Proc. of SPIE*. – 1994. - Vol. 2199. - P.76-79.

Development of a Linear Guide and a Foam Damper based on Magnetically Controllable Fluids

J.M. Guldbakke, J.Hesselbach

TU Braunschweig, Institute of Machine Tools and Production Technology, Langer Kamp 19b, 38106 Braunschweig, Germany. Contact information: j-m.guldbakke@tu-bs.de

Introduction

Semi-active devices have received significant attention in recent years because they offer the adaptability of active control devices without requiring the usually associated large power sources. Bearings and dampers based on magnetically controllable fluids are such semi-active devices. They change fluid properties to control load capacity and controllable damping forces respectively.

This paper presents a linear guide based on ferrofluids and a magnetically controllable foam damper. The ferrofluid based magnetohydrostatic linear guide uses the magnetic pressure inside a magnetically controllable fluid that arises from a magnetic field. The developed magnetorheological fluid damper consists of an open porous foam piston. This piston is directly placed inside the active volume of the damper. The fluid is pressed through the pores when the piston moves. By changing the magnetic field the fluid viscosity can be influenced and thus the flow rate can be controlled.

Ferrofluid based Linear Guide

Magnetohydrostatic linear guides get their load bearing capacity from the magnetohydrostatic pressure that is generated by the gradient of the magnetic field along a fluid surface [1].

In Fig. 1 the developed linear guide with a traverse path of 3.5 cm is shown. The



Figure 1: Magnetohydrostatic linear guide

device consists of three elements: a magnetic field source, a magnetically controllable fluid and a paramagnetic bearing area. A magnetostatic repulsive force acts on the bearing area submerged into the ferrofluid. When this force is stronger as the normal force on the bearing area, the set-up begins to float. The magnetic field can be controlled by change of an air gap. For the magnetic field generation NdFeB permanent magnets were used. As a magnetically controllable fluid a ferrite-based ferrofluid (TTR 656, particle size /sim 11 nm, carrier liquid = TR-30 oil) with a saturation magnetization of 60.3 mT was used.

Metallic Foam Damper

The basic idea of this new kind of damper is based on open porous metallic foams. The main advantage of these foams is a

high stability combined with a low weight. For magnetorheological applications especially the open porosity is important: The metallic foam can be directly placed into the active volume of the damper. For system modeling in a first approximation the foam may be considered as an additionally rheological resistance. Hence, the achievable damping forces can be shifted to higher values. Fig. 2 shows a magnetorheological fluid foam damper that was developed and built by the IWF [2]. The



Figure 2: Metallic foam damper

piston consists of an open porous metallic foam and is located inside a magnetic coil. Moving this foam piston presses the magnetic fluid through the pores of the foam. The flow in the pores can be controlled by changing the viscosity of the fluid by applying a magnetic field. Additionally, the damping force can be adjusted by the use of different open porous metallic foams. The used metallic foam consists of a bronze alloy with an open porosity of 10 ppi (pores per inch). As a filling for the damper a magnetorheological fluid from the company Lord (MRF-132AD, particle size $\approx 2\text{-}20\ \mu\text{m}$, carrier liquid = oil) was chosen.

To find basic damper properties repeated test sequences were carried out. Therefore currents from 0 A to 3 A were applied to the coil inside the damper. With a signal generator a sinusoidal oscillation was generated. The frequencies of this oscillation were between 3 Hz and 10 Hz. Fig.

3 shows experimental data which was obtained at an excitation frequency of 5 Hz. In this figure the displacement versus the

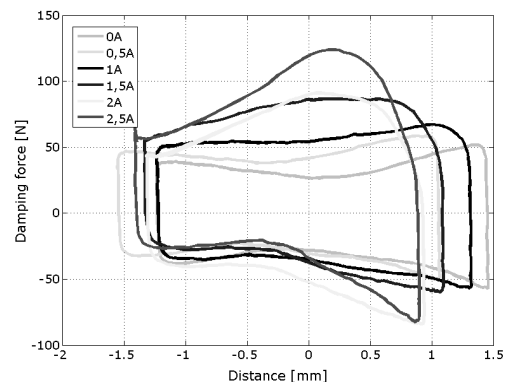


Figure 3: Damping force as a function of displacement

force is shown for currents between 0 A and 2.5 A. It can be seen that the area under the force-displacement curve is increasing with rising current. Further on the clockwise tilting of the graph is remarkable. The increase of the enclosed area at higher currents can be explained with the increase of the fluid viscosity. The tilting seems to be caused by the elastic properties of the fluid.

Conclusion

Concepts of a magnetohydrostatic linear guide and a damper based on open porous foams were developed. For both, demonstrators were set up and successfully tested.

References

- [1] B. M. Berkovsky et al.: Magnetic Fluids - Engineering Applications. Oxford University Press, 1993.
- [2] J. M. Guldbakke, J. Hesselbach: Development of a New Magnetorheological Damper based upon Open Porous Metallic Foams. 10th Int. Conf. on Actuators, 2006, pp. 845-847.

Multidimensional Magnetofluidic Positioning Systems

E. Uhlmann¹; N. Bayat¹; M. Hipper¹

¹ TU Berlin, Institute for Machine Tools and Factory Management (IWF), Pascalstrasse 8 – 9, 10587 Berlin

Introduction

The ability of ferrofluids to be controlled by applied magnetic fields allows their use as an active medium in positioning systems. Prototypes of ferrofluidic driven one-axis and multi-axis positioning systems have been developed at the Institute for Machine Tools and Factory Management (IWF). The load capacity, positioning accuracy and positioning velocity of the positioning systems were determined by experimental investigations. Their main disadvantages for applications turned out to be their dependence on the direction of the motion and their geometrical dimension. In this case a characteristic active and passive direction of the actor could be determined. Therefore, any optimization should aim at multidimensional positioning and miniaturization. The miniaturized prototype of multidimensional magnetofluidic positioning system was developed and investigated in this program.

Development of new prototypes

The new prototypes enable a precise adjustment on a plane reference platform. They are not affected by negative ambient conditions, the adjustment or the direction of the positioning. The main idea was to combine two coils that apply a controlled magnetic field to an actor which is embedded in a ferrofluid. Due to an existing gradient between the permeability of the ferrofluid and of the actor material a force was generated by the applied magnetic field. This force could be concentrated and amplified by field formers on both sides of the actor surface. A shaft with precise

guideways was used for the transmission of the motion to the object platform, **figure 1**.

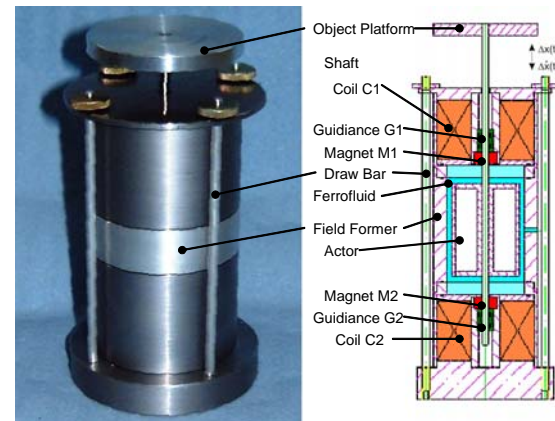


Figure 1: Principle (right) and a new prototype (left) of a multidimensional positioning system

Generally, each moved mechanical component which is embedded in a liquid medium had to be sealed against leakages. Permanent ring magnets were arranged on both sides of the moved shaft. A specific experimental set up was developed to investigate the sealing effect with magnets at given restrictions, **figure 2**.

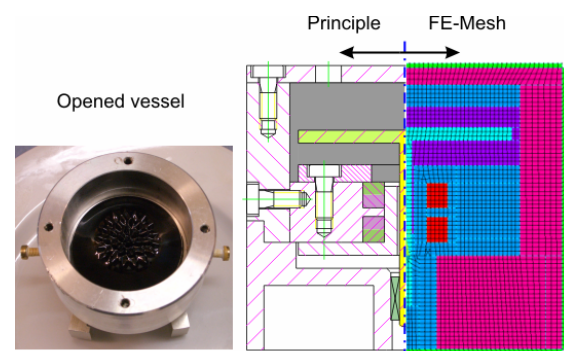


Figure 2: Principle (right) and prototype (left) of an experimental set up for magnetic sealing

Especially the sensitivity of miniaturized apparatus to existing friction coefficients and the resulting low forces require non-contact seals with permanent magnets. The

technical challenges had been to manufacture precise shafts with small tolerances regarding its diameter and cylindricity.

Experimental investigations

The investigated sealing parameters were the gap width, the used ferrofluid, the magnetic field strength, the shaft material and the pressure within the vessel. Thereby the curves of pressure loss measured with a sensor represent the sealing ability. In this context only gap widths lower than 0.1 mm were suitable to avoid leakages. The exemplary clear decrease of the pressure loss for the used ferrofluid “CO-MF” emphasizes its low sealing ability, **figure 3**.

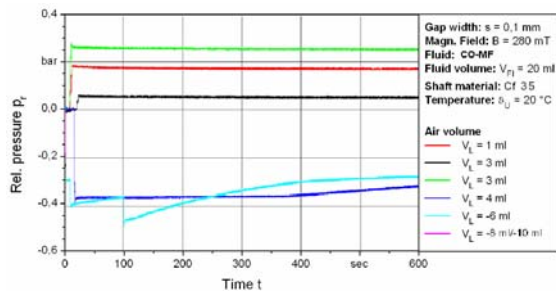


Figure 3: Curves of pressure loss for the cobalt ferrofluid “CO-MF” and Cf 35 shaft

Marginal deviations and differences in quality of the measured curves could not be determined for different parameters. The curves with a “negative pressure” characterize states of vacuum, in which the pressure in the ambient medium was lower than the pressure inside the encapsulated vessel. This represents a change of direction of the multidimensional positioning system.

Similar investigations have been carried out for the oil based ferrofluids “AP201 MF” and the new ferrofluid “Co-MF” with a relatively high magnetization. These fluids allowed a low pressure loss and were better suited for applications in multidimensional systems. This effect is shown exemplarily for “Co-MF”, **figure 4**.

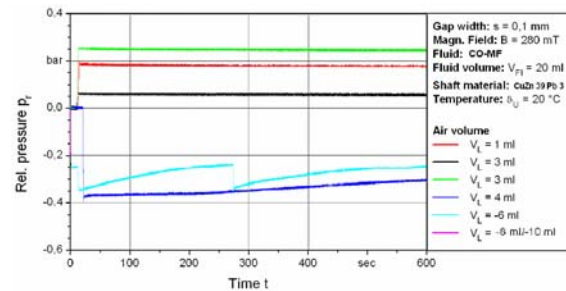


Figure 4: Curves of pressure loss for the cobalt ferrofluid and CuZn 39 Pb 3 shaft

Besides the ability of sealing, these fluids allowed principally a higher load capacity of the multidimensional system and required lower electrical power for the motion. The evaporation of the original kerosene based ferrofluid with cobalt particles was avoided by using the oil “AP201” as carrier liquid. Based on this assumption an additional parameter and negative influence could be excluded whereby the comparability of ferrofluids was ensured for the better. Due to the fact that coils are integrated into the positioning system to generate the magnetic field in the multidimensional system and that permanent magnets were used for sealing the moving shaft, a contradictory effect regarding acting force and sealing ability was existing. Thus, an additional adjustment of the sealing and of the required acting force for applications depended on the geometrical design of the actor.

Acknowledgements

We sincerely thank Dr. N. Buske and Dr. N. Matoussevitch for preparing the ferrofluids for the investigations.

References

- 1) Uhlmann, E.; Bayat, N.: Applications of Ferrofluids in Bearings and Positioning Systems. Production Engineering X (2003) 1, pp. 125-128.
- 2) Uhlmann, E.; Bayat, N.: Investigations on Ferrofluidic Positioning Systems. Production Engineering XI (2004) 2, pp. 195-198.

Locomotion of Mobile Robots based on Ferrofluid

K. Zimmermann¹, I. Zeidis¹, V.A. Naletova², V. Böhm¹, E. Kolev¹, J. Popp¹

¹ Faculty of Mechanical Engineering, Technische Universitaet Ilmenau, PF 100565, 98684, Ilmenau, Germany

² Department of Mechanics and Mathematics, M.V. Lomonosov Moscow State University, Moscow, Russia

The realization of a motion using the deformation of magnetizable materials (a magnetic fluid or a magnetizable polymer) in a magnetic field is an actual problem. The application mobile robots for industrial inspections and in the area of medical endoscopy is considered in [1] [2].

1. Locomotion using a magnetic fluid

We consider a plane flow of an incompressible viscous magnetic fluid layer along a horizontal surface in a nonuniform magnetic field (see figure 1).

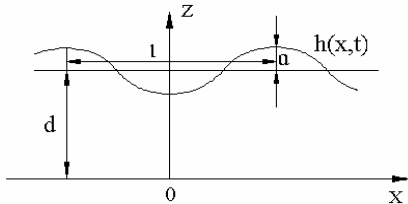


Figure 1. Magnetic fluid layer

The pressure on the free fluid surface is constant. In the case of a constant magnetic permeability the body magnetic force is absent and the magnetic field manifests itself in a surface force acting on the free surface. In this case the system of equations consists of the continuity and Navier-Stokes equations:

$$\operatorname{div} \mathbf{V} = 0, \\ \frac{\partial \mathbf{V}}{\partial t} + (\mathbf{V} \cdot \nabla) \mathbf{V} = -\frac{1}{\rho} \operatorname{grad} p + \frac{\eta}{\rho} \Delta \mathbf{V}.$$

Here, \mathbf{V} is the velocity vector (u and w are the horizontal, and vertical coordinates), p is the fluid pressure, η is the

dynamic fluid viscosity coefficient, ρ is the fluid density, and t is time. On the rigid substrate the no-slip condition is satisfied. On the free surface the kinematic and dynamic conditions should be satisfied (see [3]). The strength of the magnetic field creating a travelling sinusoidal finite-amplitude wave on the surface of the fluid is found and the average volume flow-rate is calculated. The magnetic field strength amplitude is found as a function of the wavelength and other parameters of the problem. The existence of the minimum magnetic field amplitude at a certain length of the surface wave is shown.

2. Magnetizable bodies in a magnetic field

The motions of a magnetizable body (magnetizable worm) in an alternate magnetic field are studied experimentally for a large diapason of the electromagnetic system frequency. The prolate bodies from the magnetizable composites (an elastic polymer and solid magnetizable particles) and a capsule with a magnetic fluid are used (see figure 2). The analytical estimation and numerical calculation of the deformation of the bodies in an applied magnetic field and the velocity of the bodies are done.

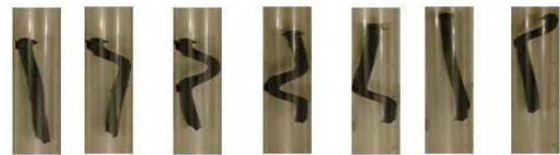


Figure 2. The magnetizable worm

The initiator of the motion in such a device is an alternate magnetic field, which forms to exterior sources (electromagnetic system

or motion permanent magnets). A micro-robot with individual cells corresponding to the earthworm's segment and sealed with water-based magnetic fluid is developed in [4]. In [5] the theoretical study of the behaviour of a locomotion system using periodic deformation of a magnetizable polymer is done, when an alternate uniform magnetic field operates. The average velocity of such locomotion systems is proportional to the difference of the friction coefficients between the system and the substrate, which depends on the directions of motion. It is found that there is an undulation of the magnetizable elastic body in a periodic traveling magnetic field of special structure and the body moves along the channel. It is proved, that the direction of its motion is opposite to the direction of the traveling magnetic field. It is shown that for $n < 50\text{s}^{-1}$ (n is the number of the switches of the coils per second) the theoretical results agree with the experiments. The optimum relation of the geometrical sizes of the body and the channel, the parameters of spatial periodicity of a magnetic field is explored. In experiments maximal body velocity has been 6.45cm/s . A calculation of the worm deformation using FE-method is shown in figure 3.



Figure 3. Numerical results

3. Interaction between a controlled magnetic field and a magnetic fluid

A moving magnetic field can generate a travelling wave on the surface of magnetic fluids. The figure 4 shows a travelling wave on a free surface of a ferrofluid in a controllable magnetic field during fundamental experiments for developing biologically inspired locomotion systems. This travelling wave can be useful as a drive for locomotion systems. Therefore, peristaltically moving active locomotion systems could be realized with an integrated elec-

tromagnetic drive. Also passive locomotion systems can be taken into account. Objects, which are on the surface of the fluid or are lying in the fluid, could be carried floating and/or shifting.

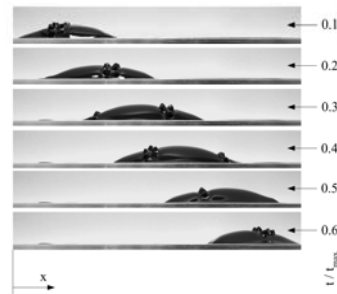


Figure 4. Wave fronts at different times

Acknowledgments

This work is supported by Deutsche Forschungsgemeinschaft (DFG, Zi 540/7-1) and the Russian Foundation for Basic Research (project 05-01-04001) and Grant Sci.Sc. 4474.2006.1.

References

- [1] Choi H.R., Ryew S.M., Jung K.M., Kim H.M., Jeon J.W., Nam J.D., Maeda R. and Tanie K. Microrobot actuated by soft actuators based on dielectric elastomer *Proc. of IEEE/RSJ International Conference on Intelligent Robots and System* **2**, 2002, 1730-35
- [2] Menciassi A. and Dario P. Bio-inspired solutions for locomotion in the gastrointestinal tract: background and perspectives *Phil. Trans. R. Soc. London A* **361**, 2003, 2287-98
- [3] Zimmermann K., Zeidis I., Naletova V.A. and Turkov V.A. Waves on the surface of a magnetic fluid layer in a travelling magnetic field *J. Magn. Magn. Mater.* **268**, 2004, 227-31
- [4] Saga N. and Nakamura T. Development of a peristaltic crawling robot using magnetic fluid on the basis of locomotion mechanism of the earthworm *Smart Mater. Struct.* **13**, 2004, 566-569
- [5] Zimmermann K., Zeidis I., Naletova V.A. and Turkov V.A. Travelling waves on a free surface of a magnetic fluid layer *J. Magn. Magn. Mater.* **272-276**, 2004, 2343-44

Superparamagnetische Nanoteilchen als Sonden für die Hydrogel-Charakterisierung mittels Fluxgate-Magnetrelaxometrie

E. Heim¹, S. Harling², A. Schwoerer³, F. Ludwig¹, H. Menzel², M. Schilling¹

¹Institut für Elektrische Messtechnik und Grundlagen der Elektrotechnik, TU Braunschweig, Hans-Sommer-Str. 66, D-38106 Braunschweig

²Institut für Technische Chemie, TU Braunschweig, Hans-Sommer-Str. 10, D-38106 Braunschweig

³Institut für Biochemie und Biotechnologie, TU Braunschweig, Spielmannstraße 7, D-38106 Braunschweig

Die Anwendung der Magnetrelaxometrie (MRX) beruht auf dem unterschiedlichen Relaxationsverhalten von frei beweglichen und gebundenen superparamagnetischen Nanopartikeln (MNPs). Mit Hilfe der MRX können magnetische Nanoteilchen charakterisiert [1,2] sowie Magnetrelaxations-Immunoassay (MARIA) durchgeführt werden [3]. Eine weitere neue Anwendung dieses Verfahrens zur Charakterisierung von Hydrogelen haben wir kürzlich vorgestellt [4].

Hydrogele sind in der Lage das Vielfache ihres eigenen Gewichtes an Wasser oder Puffer aufzunehmen, wodurch sie eine optimale Umgebung für medizinisch wirksame Proteine und Peptide schaffen. Deren Speicherung und kontrollierte Freigabe ist somit über einen längeren Zeitraum möglich. Die Bildung des Hydrogels findet bei unserem Verfahren in Gegenwart der Wirkstoffe statt, wodurch sie in dem Netzwerk eingeschlossen werden. Die Freisetzung der Medikamente erfolgt bei Hydrogelen durch Diffusion, die wiederum durch die Degradation des Netzwerkes beeinflusst wird. Bekannte Methoden, wie z.B. die Diffusionsmessung, um die Freisetzung aus Medikamentendepots zu analysieren, basieren darauf, den freigesetzten Stoff zu detektieren. Die Vorgänge im Inneren des Depots bleiben verborgen. Mit Hilfe der MRX ist es möglich, Vorgänge innerhalb des Hydrogels zu analysieren. Einerseits kann die Bildung des Gels beobachtet werden und zum anderen auch dessen Abbau. Hierzu werden anstatt Proteinen oder Peptiden magnetische Nanoteilchen in das Hydrogel eingebaut, die als Sonden dienen und somit eine Messung der Freisetzung und der Degradation des Netzwerkes ermög-

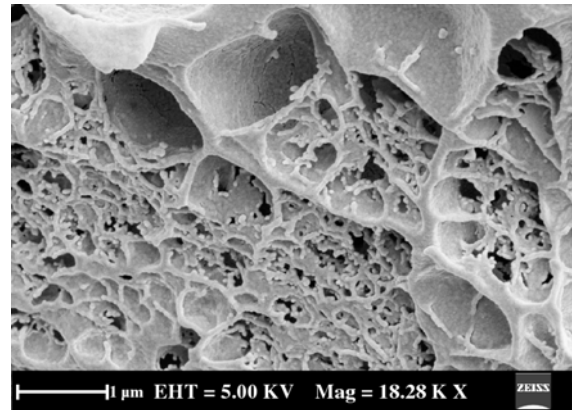


Abb. 1: REM-Aufnahme eines gefriergetrockneten Hydrogels mit eingebauten Nanoteilchen.

lichen. Abb. 1 zeigt eine REM-Aufnahme eines gefriergetrockneten Hydrogels mit MNPs. In REM-Aufnahmen ist eine Analyse nur im getrockneten Zustand möglich. Es ist nicht erkennbar, ob sichtbare MNPs frei beweglich sind. Wird jedoch an dem ursprünglichen Hydrogel das MRX-Verfahren angewendet, kann man freie von gebundenen MNPs trennen. Mit Hilfe der MNPs als Sonden kann man die Kinetik der Gelierung und des Gelabbaus beobachten. Bei beiden Prozessen werden die verschiedenen Relaxationszeiten sowie Relaxationsverläufe von freien als auch gebundenen MNPs ausgenutzt. In Abb. 2 sind die Relaxationskurven eines Vergelungsprozesses und Referenzproben von rein mobilen und rein immobilisierten MNPs der gleichen Konzentration und Art dargestellt. Die Vergelung findet durch Photopolymerisation einer mit vernetzbaren Substituenten variierten Hydroxyethylstärke in Lösung statt (Abb. 3). Die Relaxationskurven wurden nach jeweils fünf Minuten UV-Bestrahlung mit einem

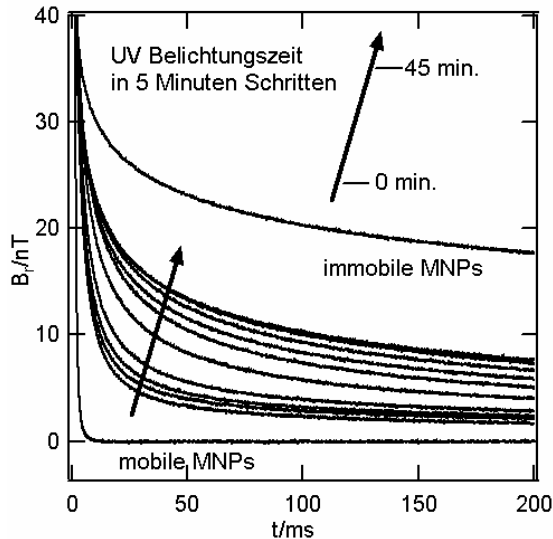


Abb. 2: Relaxationskurven eines Vergelungsprozesses und von Referenzproben.

fluxgate-basierten System aufgenommen. In Abb. 4 sind die relativen normierten Fitparameter, die man über eine phänomenologische Beschreibungsgleichung erhält [4], dargestellt. Man kann aus den Relaxationskurven und den Fitparametern auf die Vernetzungskinetik schließen. Das Einbetten der MNPs in das sich vernetzende Hydrogel ruft zwischen 15 und 30 min die stärksten Änderungen hervor. Die Diskrepanz zwischen der Relaxationskurve der vernetzten Probe und der vollständig immobilisierten Referenzprobe lässt darauf schließen, dass sich noch freie MNPs im Hydrogel befinden. Durch das Beobachten des Vergelungsprozesses erhält man somit

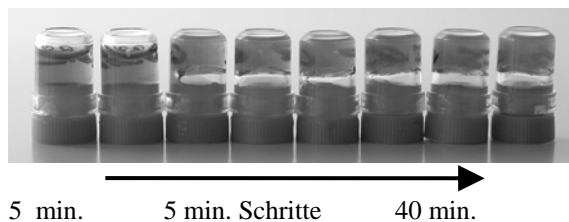


Abb. 3: Inversionstest der hergestellten Hydrogele in Abhängigkeit der Belichtungszeit.

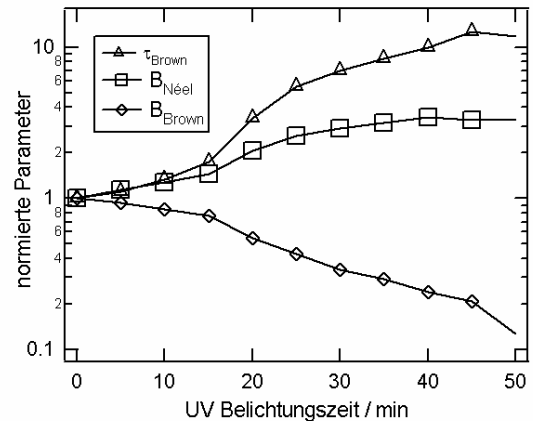


Abb. 4: Relative normierte Fitparameter der Relaxationskurven.

Informationen über das Abschließen des Vergelungsvorgangs sowie über die Aufnahmekapazitäten des Hydrogels. Die Anwendung der hier untersuchten Hydrogele als Medikamentendepot soll in Form von Mikrosphären erfolgen. Um das Freisetzungverhalten in dieser Form zu untersuchen, werden die MNPs in die bis zu $40\mu\text{m}$ großen Hydrogel-Mikrosphären eingebettet. Das hier vorgestellte Verfahren bietet eine interessante Ergänzung zu den bisherigen Methoden, da mit ihm zusätzlich die Vorgänge innerhalb von Hydrogelen erfasst werden können.

Gefördert durch die DFG über SFB 578.

Referenzen

- [1] D. Eberbeck, S. Hartwig, U. Steinhoff, and L. Trahms, *Magneto hydrodynamics* 39, 77 (2003)
- [2] F. Ludwig, E. Heim, D. Menzel, and M. Schilling, *J. Appl. Phys.* 99, 08P106 (2006)
- [3] R. Kötitz, L. Trahms, H. Koch, W. Weitschies, in: C. Baumgartner, L. Decke, S.J. Williamson (Eds.), *Bio magnetism: Fundamental research and clinical applications*, Elsevier Science, Amsterdam, (1995)
- [4] E. Heim, S. Harling, F. Ludwig, K. Pöhlig, H. Menzel, M. Schilling, *J. Magn. Mater.* (eingereicht)

Determination of binding parameters of antigen/antibody systems based on magneto-optical relaxation measurements

K. Aurich, E. Heister, S. Nagel, W. Weitschies

Institute of Pharmacy, University of Greifswald, 17487 Greifswald, Germany

Introduction

Homogeneous immunoassays require only the mixing of a sample and signal generating reagents followed by detection. Binding between the interacting partners produces a physically detectable signal that obviates the need to separate bound from free sample. Measurement of the magneto-optical relaxation of ferrofluids (MORFF) is a new principle for the performance of a homogeneous immunoassay enabling measurements by the use of magnetic nanoparticles as signal generators [1].

Various clinically relevant antigens and their polyclonal as well as monoclonal antibodies were evaluated by this method: Carcinoembryonic antigen (CEA) is an oncofetal antigen which is only detectable on tumors and the luminal surface of the gut. It is highly expressed in most gastrointestinal carcinomas and in a number of breast, lung and ovarian carcinomas [2]. Eotaxin is a cc-chemokine with diverse functions in inflammable processes [3]. A raised blood level of insulin-like growth factor (IGF) increases the risk of cancer through its anti-apoptotic activity and therefore it can act as a cancer indicator [4].

Methods

Magnetic nanoparticles (DDM128N, Meito Sangyo; MNP) were functionalized with the polyclonal or monoclonal antibody. Antigen was added to the antibody-MNP suspension in different amounts. Binding reactions resulting in an increase of the particles' diameter were detected by measuring the relaxation of the optical birefringence signal occurring when a pulsed magnetic field is applied to the ferrofluid.

Results and discussion

Assuming a simple exponential decay resulting from a monodisperse size distribution an increasing relaxation time is found with passing reaction time. For example the addition of CEA to monoclonal anti-CEA conjugated MNP in different amounts yields an enlargement in the particles' hydrodynamic diameter from 65 nm to 95 nm within 60 min (Fig. 1).

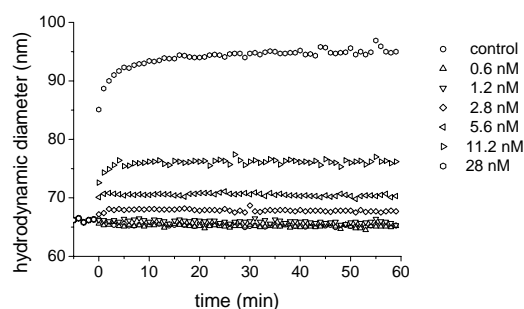


Figure 1. Mean hydrodynamic diameter obtained by the exponential fit from the incubation of CEA and monoclonal anti-CEA-MNP. Control=3 nM BSA

The effective hydrodynamic diameter obtained by the exponential fit of the relaxation signal represents the mean of the particle size distribution, including the MNP aggregates formed during a coupling reaction. Assuming the formation of linear chains of MNP which are linked to each other via antigen molecules, standard methods for the statistical description of stepwise polymerization can be utilized. Within this model, the mean of the size distribution can be expressed in terms of the conversion of antigen molecules.

For the conversion parameter α , defined by

$$\alpha = \frac{c_{AB}^2}{c_A^0 c_B^0}, \quad (1)$$

where c_{AB} is the concentration of bound antigen, and c^0 denotes the total concentra-

tion (bound or free) of the respective species, we obtained the expression

$$\alpha = (D - 1)/(D + 1). \quad (2)$$

Here, $D=d/d_0$ is the effective diameter normalized by the value found at the beginning of the reaction. An affinity analysis of the systems were performed considering the steady state achieved some minutes after the addition of a definite amount of antigen to the functionalized MNP. Under these conditions, the equilibrium constant K_D can be expressed by

$$K_D = \sqrt{\frac{c_A^0 c_B^0}{\alpha^{SS}}} - (c_A^0 + c_B^0) + \sqrt{c_A^0 c_B^0 \alpha^{SS}} \quad (3)$$

whereas c_A^0 denotes the total amount of antigen added to the system, and α^{SS} is the steady state conversion which can be obtained from measured D values via equation 2, the total concentration of antibody c_B^0 is so far unknown. The amount of antibodies coupled on MNP depends on the efficiency of the functionalization procedure. We assume that only a small fraction of the antibodies deployed for functionalization are coupled to the MNP. In analogy to scaled plots usually performed for the data of immunoassays we looked for a linear relation between terms containing α^{SS} and c_A^0 , which are the known quantities in our system. An equation of the form $y = Ax + B$ can be given with

$$x = c_A^0, \quad y = \sqrt{c_A^0} \cdot \frac{\alpha^{SS} + 1}{\sqrt{\alpha^{SS}}},$$

$$A = \frac{1}{\sqrt{c_B^0}}, \quad B = \frac{c_B^0 + K_D}{\sqrt{c_B^0}}.$$

After calculating x and y from experimental data, a regression analysis can be performed. The slope of the regression line is related to the total amount of antibody of the system, and K_D can be determined from the intersection with the x -axis.

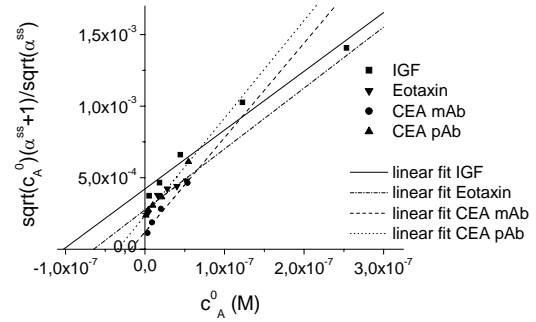


Figure 2. Linear plot for steady state conditions for different antigen/antibody systems. K_D =intersection of linear fit with x -axis.

The results were compared with those obtained from surface plasmon resonance biosensor analysis, a standard tool for biomolecular interaction analysis. For all investigated antigen/antibody systems similar K_D -values were determined.

These data may confirm the application of MORFF as a novel tool in *in-vitro* diagnostic.

Acknowledgement

This work is supported by the German Research Foundation under contract No. WE 2555/1-4.

Literature

- [1] E. Romanus, et al., *Magneto hydrodynamics* **2**, 328-33 (2000)
- [2] K. A. Chester, et al., *Cancer Chemother Pharmacol* **46 Suppl**, S8-12 (2000)
- [3] A. D. Luster and M. E. Rothenberg, *J Leukoc Biol* **62**, 620-33 (1997)
- [4] G. D. Smith, et al., *Bmj* **321**, 847-8 (2000)

Agglutination of functionalised MNP as a tool for quantification of biomolecules

D. Eberbeck¹, C. Bergemann², F. Wiekhorst, U. Steinhoff¹, L. Trahms¹

¹ PTB, Abbestraße 2-12, 10587 Berlin, dietmar.eberbeck@ptb.de

² chemicell GmbH, Wartburgstrasse 6, 10823 Berlin

Introduction

Magnetic nanoparticles (MNP) serve as markers for biomolecules in the Magnetic Relaxation Immunoassay (MARIA) [1]. MARIA is an homogeneous immunoassay, in which bound and unbound probes (conjugates of detection molecules and MNP) can be distinguished by their relaxation behavior. To make MARIA work, the binding of the probes to the analyte of interest should decrease the Brownian relaxation of the probes significantly. This can be achieved by attaching the analyte to a solid surface [2]. Alternatively, the molecules of interest can be parts of larger structures such as bacteria [3]. Further, the biomolecules can be linked to beads being large in comparison to the MNP-probes [4].

Another possibility for detecting comparatively small biomolecules in solution by MARIA is the aggregation assay [5]. Here, the agglutination of probes by the presence of the *free* analytes produces large aggregates and causes the reduction of the Brownian relaxation of the MNP-probes. In the present work we elucidate this agglutination phenomenon quantitatively.

Materials and Methods

In the present assay Biotin-BSA (biotinylated bovine serum albumin) is the analyte and streptavidin-MNP probes serves as the detection agent. The magnetic relaxation of the samples is measured by highly sensitive SQUID-based Magnetorelaxometry (MRX) system, and we use the decay time $t_{1/e}$ of the relaxation curves as a measure of the size of the aggregates, which are generated by the agglutination of the MNP. Two different types of MNP were used, namely fluidMagBC*SA (chemicell) with

an overall mean diameter of about 20 nm, and μ MACS*SA (Miltenyi Biotec) with a mean diameter of about 55 nm.

Results and Discussion

First we have checked the binding capacity of the probes by MRX. The incubation of μ MACS*SA with an excess of biotin, which is linked to agarose beads, leads to a nearly complete immobilisation of the probes at the beads (figure 1).

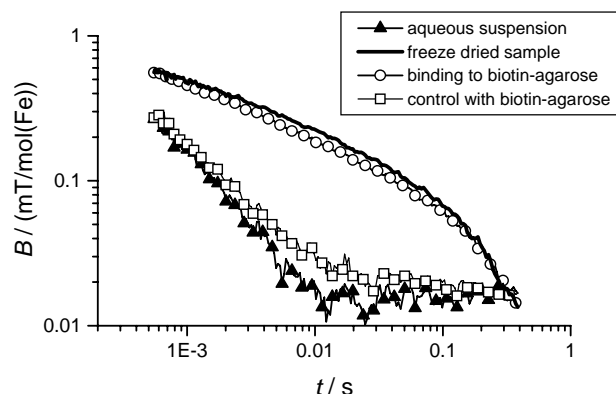


Figure 1: Relaxation curves of μ MACS*SA ($c(\text{MNP})=10^{-10}$ mol/l) in aqueous suspension with and without biotinylated agarose beads ($c(\text{Biotin})=10^{-4}$ mol/l). The incubation time was 5 h. The relaxation curve of freeze dried MNP is added as a reference for the fully immobilised MNP. The behavior of MNP, saturated with free biotin before coupling experiment (control experiment) reveals that the binding is predominantly specific.

The measurements of the MagBC*SA particles on the other hand revealed that only about 40% of the MNP are functionalised with streptavidin.

Solutions of various concentrations of the analyte Biotin-BSA were incubated with the streptavidin functionalized MNP MagBC*SA ($c(\text{MNP})=8.3 \cdot 10^{-8}$ mol/l) and μ MACS*SA ($c(\text{MNP})=4.2 \cdot 10^{-10}$ mol/l), respectively. The magnetic relaxation

curves yielded decay times $t_{1/e}$ that show pronounced maxima at distinct MNP-to-analyte concentration ratios of 3.5:1 for MagBC*SA, and of 1:150 for μ MACS*SA (fig. 2). We attribute the maxima to maximal aggregate size appearing at well-defined concentration ratios.

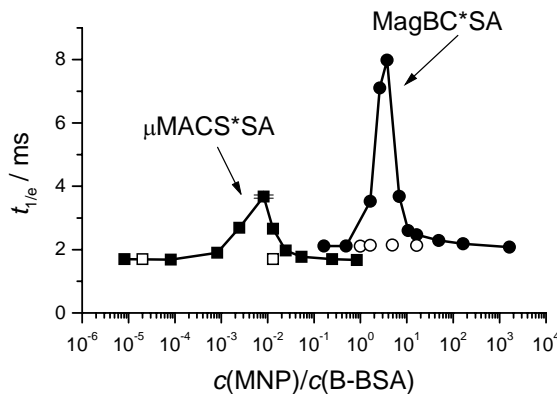


Figure 2: Decay times estimated from the relaxation curves for MagBC*SA (circles) and μ MACS*SA-probes (squares). The incubation time was 1 day. The control experiment (probes saturated with free biotin) reveals the specificity of the binding (open symbols).

The low binding efficiency (40%) of MagBC*SA may be the reason why in aggregates where all binding sites are saturated the MNP to Biotin-BSA ratio is higher than 1.

The MNP concentration of maximal agglutination of μ MACS*SA is about 500 times smaller. This cannot be explained by the higher binding capacity of the μ MACS*SA alone. Rather, the large size of the probes themselves may be the deciding factor. Only a small fraction of the small Biotin-BSA molecules on the surface of the large MNP may efficiently contribute to the agglutination by forming a bond between two MNP, while the majority of Biotin-BSA on the MNP remains idle.

Conclusion

We employed MRX for quantifying the agglutination of functionalized magnetic nanoparticles. The resulting aggregate size shows a clear maximum at a distinct concentration ratio of analytes to probes, enabling the sensitive estimation of the concentration of an analyte. We assume the

origin of the dramatic difference in the location of the agglutination maxima for the two investigated analyte-probe pairs to be the different size and binding valence of the probes.

Acknowledgments

This work was supported by the DFG priority program SPP 1104 and the BMBF project 13N8535.

References

- [1] Weitschies W, Kötitz R, Bunte T and Trahms L. Determination of relaxing or remanent nanoparticle magnetization provides a novel binding-specific technique for the evaluation of immunoassays. *Pharm. Pharmacol. Lett.* **7** (1997) 1-4
- [2] Lange J, Kötitz R, Haller A, Trahms L, Semmler W and Weitschies W. Magnetrelaxometry-a new binding specific detection method based on magnetic nanoparticles *J. Magn. Magn. Mat.* **252** (2002) 381-383
- [3] Grossman H L, Myers W R, Vreeland V L, Bruehl R, Alper M D, Bertozzi C R and Clarke J. Detection of bacteria in suspension by using a superconducting quantum interference device *PNAS* **101** (2004) 129 134
- [4] Eberbeck D, Wiekhorst F, Steinhoff U, Trahms L. submitted.
- [5] Lange J. Spezifisch bindende magnetische nanopartikel als Signalgeber in magnetischen Relaxationsmessungen. PhD-thesis, Greifswald, March 2001.

Magnetic enhancement of cellular nanoparticle uptake in tumour cells: Combination of magnetically based labelling and magnetic heating

M. Kettering¹, J. Winter¹, M. Zeisberger², S. Bremer-Streck³, C. Bergemann⁴,
C. Alexiou⁵, R. Hergt², W. A. Kaiser¹, I. Hilger¹

¹*Institute of Diagnostic and Interventional Radiology, University Hospital Jena, Erlanger Allee 101, 07747 Jena, Germany*

²*Institute for Physical High Technology, Postfach 100 239, 07702 Jena, Germany*

³*Institute of Clinical Chemistry and Laboratory Medicine, University Hospital Jena, Bachstraße 18, 07740 Jena, Germany*

⁴*chemicell GmbH, Wartburgstraße 6, 10823 Berlin, Germany*

⁵*Department of Otorhinolaryngology, Head and Neck Surgery, University Erlangen-Nürnberg, 91054 Erlangen, Germany*

Purpose: Magnetic nanoparticles (MNP) are known to be versatile tools in diagnostic and interventional radiology [1-8]. The motivation of this study was to assess if MNP could be used for multiple purposes: an increased MNP loading of tumour cells *in vitro* piloted by an external magnetic field (magnetic labelling) in combination with cell inactivation by exposure to an alternating magnetic field in order to generate heating (magnetic heating).

Material and Methods: Human adenocarcinoma cells were incubated with different amounts of MNP (10 to 30 mg) while exposed to an external magnetic field gradient (1 to 24 hrs; max. 56 mT (magnet A) and max. 83 mT (magnet B) labelling, respectively; control A: cells without MNP and without magnetic labelling; control B: cells with MNP, but without magnetic labelling). The combined effects of both magnetic labelling and magnetic heating (frequency, 400 kHz; amplitude, 24.6 kA/m) were assessed by the determination of the specific temperature increase of 0.5 to 5 x 10⁷ BT-474 cells. The amount of iron within these cells was determined by atomic absorption spectrometry.

Results: A significantly ($P \leq 0.05$) increased MNP cell uptake due to magnetic labelling with magnet B (e.g. 121.85 ± 7.09

pg Fe/cell; 2.5 x 10⁷ cells, 0.32 mg Fe/ml culture medium, 24 hrs incubation) could be observed over time and cell concentration, as compared to controls (e.g. control A: 0.0122 ± 0.0038 pg Fe/cell; control B: 99.86 ± 10.52 pg Fe/cell), showing a selective MNP accumulation. For this reason, an increased temperature during magnetic heating of labelled tumour cells was observed, for example, a temperature raise of 28.17 ± 0.35 K after magnetic labelling with magnet B compared to 19.39 ± 1.35 K of control B (control A: 2.50 ± 0.06 K). Furthermore, our data showed that the magnetic induction of magnet A was insufficient to enrich a significantly higher iron concentration within tumour cells and therefore to obtain a higher temperature rise in comparison to control B.

Conclusion: An additive, cytotoxic effect on tumour cells *in vitro* in dependence of incubation time and cell number was observed due to the combination of magnetic heating and magnetic labelling. Therefore, MNP are shown to be, in principle, valuable tools for the combination of magnetically based therapy modalities, magnetically induced labelling and magnetic heating, in the long term.

Acknowledgments

The present investigations were supported by the “Deutsche Forschungsgemeinschaft” within the frame of the DFG-priority program "Colloidal magnetic liquids" under contract number HI698/5-1 and HE2878/9-2. The technical assistance of Silvia Hein, Yvonne Heyne and Brigitte Maron is gratefully acknowledged.

References

- [1] I Hilger et al. (2001). Electromagnetic heating of breast tumors in interventional radiology: in vitro and in vivo studies in human cadavers and mice. *Radiol.* **218**,570-575
- [2] I Hilger et al. (2004). Magnetic nanoparticles for selective detection and heating of magnetically labeled cells in culture. *Nanotechnology* **15**, 1027-1032
- [3] R Hergt et al. (1998). Physical Limitations of Hyperthermia Using Magnetite Fine Particles. *IEEE Trans. Magn.* **34**, 3745-3754
- [4] R Hergt et al. (2004). Enhancement of AC-losses of magnetic nanoparticles for heating applications. *J. Magn. Mater.* **280**, 358-368
- [7] C Alexiou et al. (2005). In vitro and in vivo investigations of targeted chemotherapy with magnetic nanoparticles. *J. Magn. Mater.* **293**, 389-393
- [8] C Alexiou et al. (2005). Magnetic Drug Targeting – a new approach in locoregional tumorthrapy with chemotherapeutic agents. Experimental animal studies. *HNO* **53**, 618-622

Magnetic nanoparticles for combined hyperthermia and chemotherapeutic treatment of tumours

M. Kettering¹, M. Zeisberger², S. Dutz², R. Hergt², R. Müller², W.A. Kaiser¹, I. Hilger¹

¹Institut für diagnostische und interventionelle Radiologie, Klinikum der FSU Jena, Erlanger Allee, 07747 Jena

²Institut für Physikalische Hochtechnologie, Albert-Einstein-Str. 9, 07745 Jena

Introduction

Local hyperthermia using magnetic nanoparticles (MNP) comprises a promising technology for the highly selective therapy of tumours. In order to enhance the therapeutic effect, MNP can be used as multi-modal tools for both magnetic induced heating and chemotherapeutic approaches. Hereby, chemotherapeutics such as cisplatin are coupled to the shell of the MNP. The aim of the present study was to investigate the basic feasibility of the combined therapeutic modality.

Magnetic Properties

Starch coated MNP prepared by chemicell GmbH, Berlin were used in the present study. The first step of our investigations was the characterization of the magnetic properties of the original particles. The magnetization data obtained by VSM measurements showed superparamagnetic behaviour. We used the method of Chantrell [1] to calculate the mean particle size D and the distribution width σ of the lognormal distribution and obtained $D = 11.5$ nm and $\sigma = 0.42$. From the mean diameter and an anisotropy constant of 10^4 J/m³ a Néel relaxation time of $\tau = \tau_0 \exp(KV/kT) = 10^{-8}$ s [2] was estimated. The hydrodynamic diameter of the particles was determined by laser diffraction resulting in a mean value of $D_H = 71 \pm 3$ nm. From this value a Brown relaxation time $\tau_B = \pi\eta D_H^3/kT$ [3] of 0.27 ms was estimated.

In order to determine the behaviour of the material in ac fields, we used the ac sus-

ceptometry (ACS). Our set-up allows the measurement of the real (χ') and imaginary (χ'') part for frequencies from 20 Hz - 1 MHz and field amplitudes up to 60 A/m [4]. The $\chi''(f)$ obtained with our sample is nearly constant for frequencies above 10 kHz according to the fact that the Néel peak is outside of the measured frequency range. For 400 kHz which is a suitable frequency for medical hyperthermia [5] we obtained $\chi'' = 2.8$.

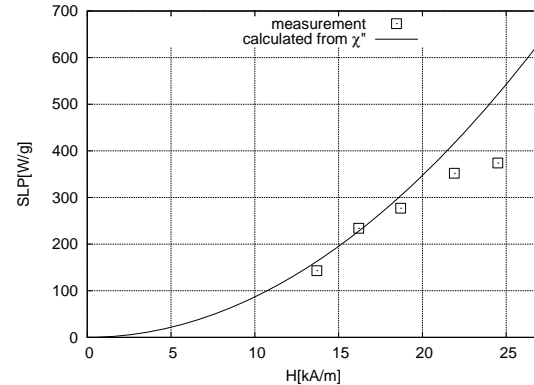


Fig. 1 Specific heating power of the fluid

In addition, we performed calorimetric measurements of the specific heating power (SHP) using a set-up as shown in [4]. An ac field with a frequency of 400 kHz and amplitudes of 11-25 kA/m can be applied to the sample. From the time dependence of the temperature $T(t)$ we can calculate the SHP. Fig. 1 shows the measured data as well as the SHP calculated from the χ'' according to the linear theory [6] by $SHP = \mu_0 \pi f H^2 \chi'' / \rho$. The data below 20 kA/m are in good accordance with the model. For higher amplitudes a saturation appears.

Cisplatin labelled MNP

Iron oxide MNP with different coatings were functionalized with the temperature-sensitive chemotherapeutic cisplatin. In this regard, we used the carbodiimide method [7] or just ionic binding. Up to now, we were able to bind a maximum of 27.36 mg cisplatin per g iron. In order to achieve distinct cytotoxic effects in SK-BR-3 cells emerging from the chemotherapeutic agent itself, coupling of higher cisplatin amounts is necessary.

Stability measurements of cisplatin labelled MNP

To evaluate the stability of cisplatin linked starch coated iron oxide MNP in ddH₂O, they were exposed to 26 °C over altered time periods (up to 20 weeks). Stability measurements were done by determining the mode of hydrodynamic diameters with laser diffraction and by quantitative determination of iron and platinum contents with atomic absorption spectrometry. The results demonstrated the stability of hydrodynamic diameters (71 ± 3 nm) up to 20 weeks. Cisplatin labelling was stable up to two weeks (85 – 100 %). After 20 weeks 51 ± 5 % of the cisplatin was still found to be linked with MNP.

Cytotoxic effects of cisplatin and cisplatin labelled MNP

In order to assess the therapeutic properties of MNP labelled with chemotherapeutics in the long term, the cytotoxicity on selected target cells was determined using the MTS assay as described previously [8]. Human cells (BT-474, HMEC-1, SK-BR-3) seeded in microtiter plates (1500, 4000, 9000 cells/ 0.34 cm^2) were incubated with cisplatin (0.5 μM to 100 μM) and cisplatin labelled MNP (0.5 μM to 20 μM cisplatin) at 37 °C for 24, 48 and 72 hrs. The effects due to hyperthermal temperatures (23, 47, 71 hrs at 37 °C and 1 hr at 42 °C) were also tested. The results showed that for cisplatin the IC₅₀ (concentration at which cell proliferation was reduced by 50 % as compared to untreated controls) was reached between

60 and 80 μM for BT-474 and SK-BR-3 (HMEC-1: > 150 μM). If cells were additionally exposed to heating, IC₅₀ was already achieved at a concentration of 25 to 35 μM cisplatin in BT-474 cells (HMEC-1: 150 μM).

Further on, incubation of SK-BR-3 cells with cisplatin labelled MNP (≈ 20 mg cisplatin per g iron; 24, 48, 72 hrs, 0.2 μM to 20 μM cisplatin, 3 to 350 μg Fe/ml culture medium) revealed the presence of intact cells or cells affected due to high MNP concentration itself (control). Therefore, a higher degree of functionalization of MNP with cisplatin should be performed.

Acknowledgments

The present investigations were supported by the "Deutsche Forschungsgemeinschaft" within the frame of the DFG-priority program "Colloidal magnetic liquids" under contract number HI698/5-1 and HE2878/9-2. The technical assistance of Silvia Hein, Yvonne Heyne and Brigitte Maron is gratefully acknowledged.

References

- [1] R. W. Chantrell, J. Popplewell, S. W. Charles, IEEE Trans. Mag., vol. MAG-14, no. 5 (1978) p. 975
- [2] E. Kneller, in Encyclopedia of Physics, vol. XVIII/2, Ferromagnetism, H. P. J. Wijn, Ed. New York: Springer-Verlag 1966, pp. 438-544
- [3] S. Chikazumi, Physics of Magnetism, Philadelphia, PA: Lippincott, 1964
- [4] M. Zeisberger, S. Dutz, R. Müller, R. Hergt, N. Matoussevich, H. Bönemann, submitted to J. Mag. Mag. Mat.
- [5] I. Hilger, R. Hergt, W. A. Kaiser, Investigative Radiology, 35 (2000), 170-179
- [6] L. D. Landau, E. M. Lifshitz, Electrodynamics of continuous media, London, UK, Pergamon 1960
- [7] J.C. Sheehan, and G.P. Hess (1955). A new method of forming peptide bonds. J. Am. Chem. Soc. 77 (1955), 1067-1068.
- [8] I Hilger, M Aufderheide, JW Knebel, S Fuchs, M Emura. Exp. Toxicol. Pathol. 48 (1996), 532.

Magnetosomes – Production, characterization and application

C. Lang, D. Schüler

Max-Planck-Inst. f. Marine Mikrobiologie, Celsiusstr. 1, 28359 Bremen

Introduction

The biomineralization of magnetosomes is one of the most intriguing examples for the biogenic synthesis of a hierarchical self-assembled nanostructure. In magnetotactic bacteria these membrane-enveloped particles serve as navigational tools for the orientation along geomagnetic field lines. Bacterial magnetic nanoparticles are of increasing interest for biotechnological and biomedical applications as they represent a novel class of small (20-45 nm), uniform particles with defined magnetic and crystal-line characteristics synthesized under controlled conditions (1).

In this project, the mass production of magnetosomes from the magnetic bacterium *Magnetospirillum gryphiswaldense* was established. Isolated suspensions of biogenic magnetite particles were thoroughly characterized with respect to their biochemical, physico-chemical, and magnetic characteristics. The discovery and characterization of the magnetosome membrane proteins and the corresponding genes facilitated the genetic modification of magnetosomes. Genetic engineering and *in vitro* modification of isolated magnetosomes is employed for the production of oligofunctional magnetosomes tailored for various biomedical applications.

Results and discussion

Production and characterization of magnetosomes

M. gryphiswaldense was routinely cultured in a mass fermentation procedure that was designed to maintain microaerobic conditions during bacterial growth. Continued optimization of the method of resulted in a further increased magnetosome yield (10 mg/l) magnetosomes equivalent to a productivity to approx. 9 mg per liter and day.

Beside wildtype cells, magnetosomes were additionally produced and isolated from several mutants with aberrant crystal morphologies and altered membrane properties. Of particular interest turned out to be magnetosome particles produced by a mutant strain (MSR-1K), which displayed not only a smaller size (25-30 nm), but also a narrower size distribution and thus predominantly fall into the superparamagnetic size range. As a consequence, aqueous suspensions of MSR-1K magnetosomes display a substantially higher stability and a lesser tendency to agglomerate compared to wild type magnetosomes.

Biochemical analysis revealed that the magnetosome membrane of isolated particles is stable in the presence of various compounds. The membrane can be completely solubilized by strong detergents (e. g. SDS), while treatment with various mild detergents as well as proteolytic digestion by trypsin resulted in the selective solubilization of individual magnetosome membrane proteins (2).

Magnetic properties of magnetosomes were characterized by several techniques including DC-susceptometry, magnetorelaxometry as well as atomic and magnetic force microscopy (Collab. D. Eberbeck, L. Trahms, M. Albrecht, PTB Braunschweig, Berlin). These studies revealed a high coercivity found by M(H) measurements and a dominance of Néel relaxation of the immobilized mono-domain particles, which was in accordance with blocked individual particles visible in MFM (3,4).

Isolated magnetosomes were prepared and evaluated for their use in magnetic particle hyperthermia (MPH) treatment of tumors (Collab. R. Hergt, I. Hilger, R. Hiergeist, Jena). A very large specific power loss up to 960 W/g at 410 kHz and a field amplitude of 10 kA/m was determined, revealing magnetosomes as very promising candi-

dates for biomedical applications in hyperthermia or thermoablation (5).

Functionalization of magnetosomes

The biotechnological potential of magnetosomes could be greatly extended if the particles can be functionalized, e. g. by the coupling with fluorophores, enzymes or linker molecules such as biotin, which can be harnessed to couple various biomolecules *in vitro* to the magnetosome surface. The chemical functionalization of magnetosomes from *M. gryphiswaldense* was demonstrated. Employing biotin-streptavidin chemistry it was possible to attach oligonucleotides, fluorescent dyes and gold particles to magnetosomes (6). In a collaboration with the Hilger group (Univ. Jena), M. Lisy and coworkers demonstrated that a fluorescent dye can be covalently attached to magnetosome membrane proteins in order to combine magnetic resonance and fluorescent imaging (7).

The identification of 18 magnetosome-specific proteins (collab. R. Reszka) and their genes provides a mean for genetic modification via the expression of heterologous proteins genetically fused to the native magnetosome proteins. Using green fluorescent protein (GFP) as a model fusion partner, we have identified magnetosome membrane proteins which can serve as membrane anchors. Using this system fluorescent magnetosomes were produced. After verification of the magnetosome membrane protein MamC as a functional membrane anchor, a MamC-GFP fusion was constructed resulting in magnetosome particles that displayed stable fluorescence both *in vivo* and *in vitro*. In a further genetic construct, GFP was replaced by the antibody-binding domain of staphylococcal protein A. This resulted in antibody-binding magnetosomes, which are currently evaluated for the purification of antibodies and for immunoassays. In addition, an intein domain was fused to MamC. This protein tag may facilitate the site-specific attachment of thiolated compounds to the magnetosome surface. Among other potential applications intein modified magnetosomes

could be employed for the attachment of oligonucleotides for nucleic acid extraction and detection.

In conclusion, these data show that bacterial magnetosomes can provide an alternative to synthetic magnetic nanoparticles for biomedical and biotechnological applications. The properties of magnetosome crystals are highly interesting for instance for hyperthermia applications and magnetic resonance imaging. In addition it has been shown that genetic engineering of magnetosome membrane proteins is a powerful tool to generate oligofunctionalized magnetosomes for various applications.

References

- [1] Lang, C. & Schüler, D. 2006. Biomineralization of Magnetosomes in Bacteria: Nanoparticles with potential applications. In: *Microbial Bionanotechnology: Biological Self-assembly Systems and Biopolymer-based Nanostructures*. Ed. Rehm B., Horizon Bioscience, Norfolk UK. p. 107-124
- [2] Grünberg, K., Müller, E.C., Otto, A., Reszka, R., Linder, D., Kube, M., Reinhardt, R., Schüler, D. 2004 Biochemical and proteomic analysis of the magnetosome membrane in *Magnetospirillum gryphiswaldense*. *Appl. Environ. Microbiol.* **70**:1040-1050.
- [3] Albrecht, M., Janke, V., Sievers, S., Siegner, U., Schüler, D., Heyen, U. Scanning Force Microscopy Study of Biogenic Nanoparticles for Medical Applications. *J. Magnetism Magnetic Materials* **290-291**:269-271.
- [4] Eberbeck, D., Janke, V., Hartwig, S., Heyen, U., Schüler, D., Albrecht, M., Trahms, L. Blocking of Magnetic Moments of Magnetosomes Measured by Magnetorelaxometry and Direct Observation by Magnetic Force Microscopy. *J. Magnetism Magnetic Materials* **289**:70-73.
- [5] Hergt, R. Hiergeist, R. Zeisberger, M. Schüler, D. Heyen, U. Hilger, I. Kaiser, W.A. Magnetic properties of bacterial magnetosomes as diagnostic and therapeutic tools. *J. Magnetism Magnetic Materials* **293**:80-86.
- [6] Ceyhan, B., P. Alhorn, C. Lang, D. Schüler, and C. M. Niemeyer. 2006. Semi-Synthetic biogenic magnetosome nanoparticles for the detection of proteins and nucleic acids. *Small* In press.
- [7] Lisy, M. R., A. Hartung, C. Lang, D. Schüler, W. Richter, J. R. Reichenbach, W. A. Kaiser, and I. Hilger. 2006. Fluorescent bacterial magnetic nanoparticles as bimodal contrast agents. *subm. to Nano Letters*

Loss investigations on dextran coated iron oxide nanoparticles

R. Müller¹, S. Dutz¹, R. Hergt¹, I. Hilger², M. Kettering², H. Steinmetz¹,
M. Zeisberger¹, W. Gawalek¹

¹ *Institut für Physikalische Hochtechnologie e.V., Albert-Einstein-Str. 9, 07745 Jena, Germany*

² *Institut für Diagnostische und Interventionelle Radiologie, FSU Jena, 07747 Jena, Germany*

Ferrofluids based on iron oxide particles (magnetite or maghemite) with enhanced anisotropy barrier lead to enhanced magnetic hysteresis losses in fluids. Losses may be used for application in magnetic particle hyperthermia proposed as a tumour therapy in ac-fields. (see contribution by M.Kettering)

Several types of losses which may appear (hysteresis losses, Néel- or Brown relaxation) depend strongly on the mean particle size, the size distribution width and magnetic field parameters [1]. To influence the size distribution of particles approaches in preparation are promising where nucleation and growth of particles can be influenced independently.

In hyperthermia a higher specific loss power (SLP) at lower fields would allow a reduction of the tissue load with magnetic material and improve the reliability of a therapy.

The preparation of magnetic iron oxide powder by crystallization from CaO-Fe₂O₃-B₂O₃-glass during a two-step temperature treatment for nucleation and particle growth and subsequent dissolving of the matrix was shown in [2]. The separated powders show magnetization values up to 70 Am²/kg close to literature values of γ -Fe₂O₃. Investigations by X-ray diffraction XRD show that there is a mixture of Fe₃O₄ and γ -Fe₂O₃. The mean particle size of the further investigated powder (powder 1) was ca. 16nm.

A water based charge stabilized ferrofluid (fluid 1) was prepared from powder 1 in connection with the dissolving of the borate by acetic acid [2]. The number of aggregates in the fluid was reduced by centrifugation. The particle concentration of the obtained fluid is \approx 1.0 mass-%.

In a second method [3] we prepared our particles by growing cycle by cycle on initial particles which were prepared by the usual wet precipitation method. A NaHCO₃-solution was added to a FeCl₂/FeCl₃ solution up to pH=7 what lead to the formation of a brownish precipitate. Then a new Fe²⁺/Fe³⁺-mixture was added and the precipitation was carried out again. This procedure was repeated three times. After that the solution was boiled for 10 minutes to form an almost black precipitate. Particles in the size range from 10 to 30nm could be prepared.

For medical in-vivo applications of iron oxide nanoparticles a biocompatible coating is necessary. We used carboxymethyl dextran (CMD) starting from initial material CMD sodium salt (Fluka). Typically, the nanoparticle dispersion was separated magnetically and washed with water. After adjusting the pH with diluted HCl to 3 - 4, the suspension was warmed to 45 °C and an aqueous solution of CMD was added. The mixture was homogenized by ultrasonic treatment for 1 min using a Sonopuls GM200 (Bandelin) device. The suspension was stirred for further 60 min at 45 °C and the coated nanoparticles were separated magnetically and washed once with water. Ferrofluids with particles < ca.17nm are stable concerning sedimentation. Typical dried fluid samples show a mass loss (at \approx 220°C) by thermogravimetry (Netzsch STA409) of 5-7% what can be interpreted as CMD amount. After about two weeks a considerable agglomeration could be observed in all samples what probably results from an aging effect of the CMD layer. Mean particle sizes by XRD measured on samples prepared by a three-cycle procedure with bigger iron oxide particles taken

from the sediment as well as from the stable supernatant after one day are 17.4 and 21nm, respectively. The mean size of the original sample (fluid 2) was 19.3nm. The distribution of the hydrodynamic diameter (number weighted) measured by dynamic light scattering has a mean value at about 80nm. The coercivity of the immobilised ferrofluid is 4.1kA/m.

Powder 2 was prepared by drying of fluid 2.

The specific hysteresis loss power at the usual field parameters (410kHz, 11kA/m) of the dried powder and the fluid is 21 and 43 W/g for sample 1, respectively, and 22 and 48 W/g for powder 2 and fluid 2.

Hysteresis loss investigations on ferrofluid samples with different mean sizes of 15.8 and 19.3nm (i.e. different sedimentation stability) revealed an interesting behaviour. Comparing losses versus applied field amplitude (Fig.1) from particles in immobilized state (dried powder) and in fluid state the latter show in some cases (like fluid 2) anomalous large losses at low magnetic fields whereas all powder samples show a similar behaviour as already found by [4].

In order to investigate whether there is a field dependent influence of an orientation of particles in the sample on specific hysteresis losses a Brown relaxation after texturing in a magnetic field of 39.8 and 796 kA/m, respectively, was reduced using a solid gel sample made from fluid 2. Magnetization loop measurements were performed in dependence on the direction of the external magnetic field (parallel or per-

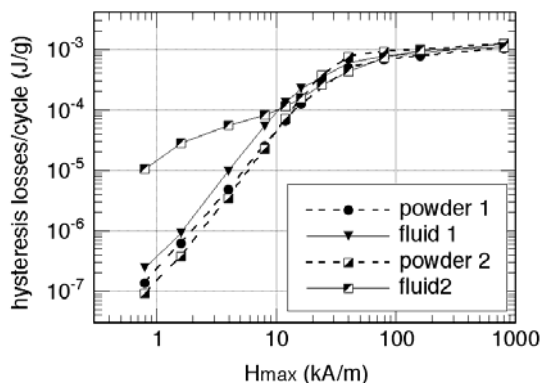


Fig. 1: Hysteresis losses of powder and fluid

samples in dependence on the applied field amplitude.

pendicular) with respect to the texture axis. Fig.2 shows the ratio of the values of the specific losses in both directions in dependence on the external magnetic field amplitude. The alignment effect of particle moments may be clearly seen at lower fields < ca. 80kA/m. The specific hysteresis losses vary by a maximum factor of more than two in case of the high texturing field but only by a factor of 1.16 for the low texturing field. There is only a weak effect at high measuring fields close to saturation. The influence of a texture could be confirmed by SLP measurements at 400kHz and 24.6kA/m. SLP-values of about 410 W/g and 345 W/g were measured parallel and perpendicular, respectively, to the texturing axis. The texturing field was ca. 400kA/m. The origin of the high losses of the fluid 2 is not clear up to now but may come from oriented particles or agglomerates, connected with interaction effects. Viscous effects of the fluid can't be excluded, too.

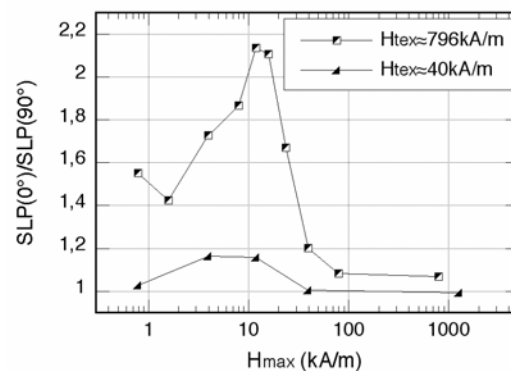


Fig. 2: Ratio of hysteresis losses at different directions with respect to the texture axis (0°) versus applied field strength

Acknowledgements

The authors thank Ch. Schmidt. The work was supported by DFG No. Ga662/3-1.

References

- [1] R. Hergt and W. Andrä, *Hyperthermia and Thermoablation In Magnetism in Medicine*, Second edition, W.Andrä and H. Nowak (Eds.) Wiley-VCH, Berlin (2006)
- [2] R. Müller, et al., *J. Magn. Magn. Mater.* **289** (2005) 13-16
- [3] R. Müller, et al., *Z. Phys. Chem.* **220** (2006) 51-57
- [4] S. Dutz, et al., *J. Magn. Magn. Mater.*, accept.

X-ray tomography as a tool for the analysis of magnetic particle distribution in tumor tissue

H. Rahn¹, Ch. Alexiou², I. Hilger³ and S. Odenbach¹

¹ TU Dresden, Professur für Magnetofluidynamik, 01062 Dresden

² Klinik und Poliklinik für Hals-, Nasen- und Ohrenkranke, Waldstr. 1, 91054 Erlangen

³ Inst. für Diagnostische und Interventionelle Radiologie, Klinikum F.S.U. Jena, Erlanger Alle 101, 07740 Jena

Introduction

The research activities in the field of biomedical applications of ferrofluids increased during the last years. In particular cancer treatment is in the actual focus of research. One of the related applications, the magnetic drug targeting (MDT) offers a possibility for local cancer treatment by directing magnetic nanoparticles which are enriched with a chemotherapeutic agent into a tumor region using a strong magnetic field gradient. In this case the efficiency and success of the therapeutic approach depends on the intratumoral distribution of the magnetic nanoparticles. The detection of the adsorption of magnetic nanoparticles within a tumor is usually done by histological cuts of the respective tissue and subsequent microscopic analysis of these sections [1]. This classical way provides only very local information about the distribution of the magnetic material in the tumor and it is limited to ex-situ examinations. A useful tool for three-dimensional, non destructive examination of intratumoral adsorbed magnetic nanoparticles is X-ray tomography. The following report will show the laboratory X-ray scanner, the image processing procedure and will discuss the advantages of synchrotron based tomography.

Physical background

As it was mentioned, X-ray tomography is a method for non destructive investigation of different objects. For a tomographic scan a set of X-ray absorption images of a sample at different projection angles θ

(\ominus) between 0° and 360° is needed. The whole absorption is determined by integration about the course of the linear attenuation coefficient μ as a function from x (ray direction) and y (sample cross-section) in ray direction.

The laboratory X-ray scanner

The laboratory setup is made up of a commercial cone beam X-ray source (Apogee 5000) with $40 \mu\text{m}$ focus size and a maximal acceleration voltage of 50 keV. In our case the X-ray source and the detector-system have a defined fixed position and the sample is mounted on a rotation stage.

Because of the divergent cone-beam characteristic of the X-ray tube it is possible to realize different magnifications of the sample by variation of the position between sample and detector and between source and sample.

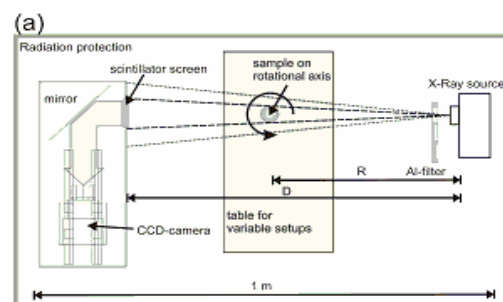


Figure 1: Schematic setup of the laboratory x-ray scanner.

Results

Until now some tomographic examinations of tumor samples after treatment with nanoparticles have been carried out with a laboratory tomography system as well as

using synchrotron microtomography at HASYLAB. Both experiments have shown that it is possible to determine the particle distribution in resected tumor samples [1]. Figure 2 shows as an example a comparison of the two tomography images which indicate clearly the advantages of the synchrotron measurements concerning spatial resolution and suppression of artifacts which enhance the difficulties of a quantitative analysis [2].

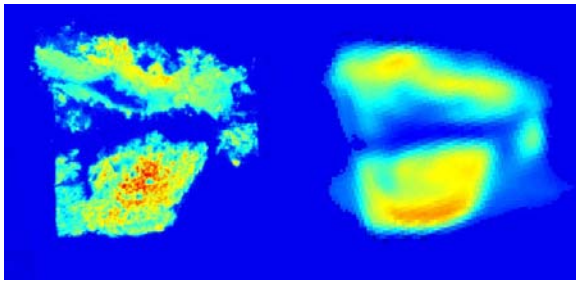


Figure 2: Two-dimensional cuts of a tumor treated with magnetic nanoparticles scanned by synchrotron tomography (left) and using laboratory equipment with a X-ray tube (right).

Further, tumour samples obtained using different preparation methods have been under examination:

- Sample tissue with intratumoural particle injection for hyperthermia (HT) resected from tumour-bearing mice.
- Sample tissue with intravascular particle injection for magnetic drug targeting (MDT) resected from tumour-bearing rabbits.

In both cases the tumours were resected from the animals after the respective therapy was finished. The tissue samples were fixated in formalin and subsequently embedded into paraffin.

The influence of the preparation method of the sample on the distribution of the particles within the tissue has been investigated.

Figure 3 shows a rendered 3d representation of the dataset of a tumour after intratumoural particle injection (HT sample). At the centre of the sample, the channel of the injection needle can be identified [2].

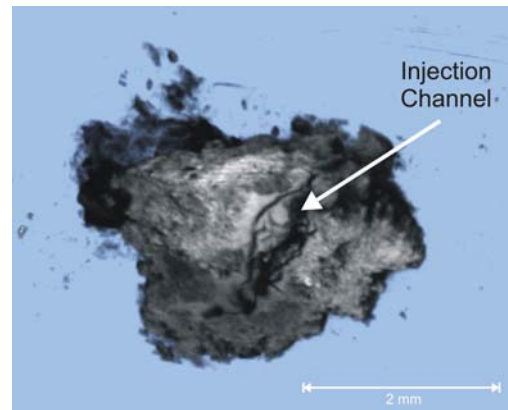


Figure 3: SR μ CT dataset of a tumour extracted from a mouse enriched with magnetic nanoparticles applied by means of intratumoural injection (HT-sample).

The Diffraction/Tomography system

The advantages of monochromatic synchrotron tomography lead to development and construction of a new tomography system, which will be installed at the new HARWI-2 beam line at HASYLAB. Due to the unique combination of properties of the HARWI-2 beam (energy range of 20 to 200 keV and a beam cross-section of up to 80x10 mm²) and the new tomography system (fast read-out rate of the detector) a wide range of experiments become possible. Large biomedical soft tissue samples can be analyzed. Due to the fast read-out rate, the scanning time for a whole tomogram can be reduced to 10 seconds, enabling also in-vivo experiments [2].

Acknowledgements

Financial support by DFG under grant OD18/9 within SPP1104 is gratefully acknowledged.

References

- [1] O. Brunke, S. Odenbach, C. Fritsche, I. Hilger, W. A. Kaiser (2005) Determination of magnetic particle distribution in biomedical applications by X-ray microtomography. *JMMM*, 289, 428-430.
- [2] O. Brunke, S. Odenbach, F. Beckmann (2004) Quantitative methods for the analysis of synchrotron- μ CT datasets of metallic foams, *European Physical Journal of Applied Physics*, 2005. 29: p. 73-81. DOI: 10.1051/epjap: 2004203

Temperature dependent Néel relaxation (TMRX) measurements for characterization of nanoparticle distributions

F. Schmidl¹, M. Büttner¹, T. Müller¹, S. Prass¹, T. Köttig¹, P. Weber¹, M. Mans¹, Christian Bocker², J. Heinrich³, K. Wagner³, M. Röder³, D.V. Berkov³, P. Görnert³, G. Glöckel⁴, W. Weitschies⁴, P. Seidel¹,

¹ *Institut für Festkörperphysik, Friedrich-Schiller-Universität Jena, D-07743 Jena Germany*

² *Otto-Schott-Institut für Glaschemie, Friedrich-Schiller-Universität Jena, D-07743 Jena Germany*

³ *Innovent Technologieentwicklung, Prüssingstraße 27B, D-07743 Jena Germany*

⁴ *Institut of Pharmacy, Ernst-Moritz-Arndt-University, D-17487 Greifswald Germany*

The magnetic properties of ferrofluids are strongly influenced by several parameters of the contained magnetic nanoparticles: their constituent material, their crystallographic structure, size, shape, as well as the particle size distribution. One way to obtain direct information about the distribution of the energy barrier E in such a complex particle system is through measurements of the Néel relaxation signal. The investigation of the temperature dependence of the Néel relaxation signal allows us to determine the particle size distribution of the investigated sample, assuming that the sample contains only non-interacting single domain magnetic nanoparticles [1].

The measurement setup for TMRX consists of a second-order low- T_C SQUID gradiometer to measure the magnetic relaxation signal in unshielded environment, an anticryostat with a heater for the sample and Helmholtz coils to magnetize the sample. The anticryostat was designed to minimize the distance between the SQUID gradiometer operating at 4.2 K and the sample holder which is at temperatures between 4.2 K and 315 K. For the measurements all samples must be lyophilized, thereby immobilizing the particle to avoid Brownian relaxation in the samples. The temperature dependence of the Néel relaxation signal depends for the immobilized nanoparticles directly on the magnetically active volume V and the anisotropy constant K of the

investigated nanoparticles. The bandwidth of our measurement system limits the measuring range of nanoparticles at different temperatures (figure 1).

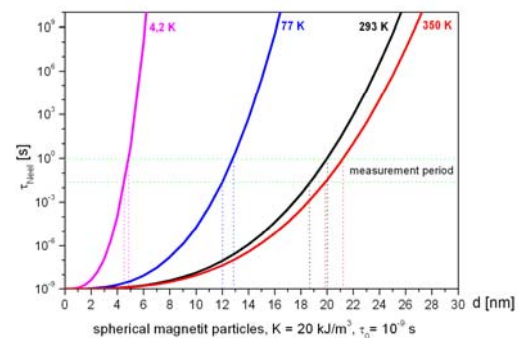


Figure 1: Néel relaxation time (calculated) as a function of the size of the magnetic nanoparticles

Given the anisotropy constant (for instance determined through coercivity measurements at low temperatures), we can determine the average particle diameter from the temperature at which we find the maximum signal.

We have investigated several types of ferrofluid samples to test the improved system for temperature dependent measurements [2], [3], [4], calibrate the measurement system for determination of the particle size distribution [5] and investigate the possibility of agglomeration [6]. Our method allows us also to investigate particle size distributions in more complicated

nanoparticle systems, for instance after crystallization of magnetic nanoparticles in a glas matrix (figure 2)

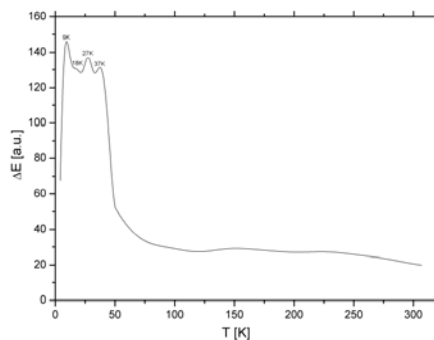


Figure 2: Energy barrier density distribution ΔE of Fe_2O_3 nanoparticles in a glas matrix as a function of the temperature T calculated from TMRX signal.

For comparison we have also carried out zero-field cooled measurements (ZFC). By low temperature coercitivity measurements we determine the magnetic anisotropy and the magnetization behaviour of the ferrofluids. We discuss the results of these investigations with regard to the possibilities and limitations of these methods for the characterization of ferrofluids for its applications.

All results have been compared to a mean physical particle size determination by transmission electron microscopy (TEM) investigations and the determination of the hydrodynamic particle size of the magnetic nanoparticles by magneto-optical relaxation measurements [7].

Acknowledgments

We gratefully acknowledge the European commission for financial support (project BIODIAGNOSTICS).

References

- [1] D.V.Berkov, R.Kötitz, J.Phys. Condens. Matter 8 (1996) 1257
- [2] E.Romanus, D.V.Berkov, S.Prass, C.Groß, W.Weitschies, P.Weber, Nanotechnology 14 (2003) 125
- [3] T.Köttig, P.Weber, S.Prass, P.Seidel, 20th International Cryogenic Engineering Conference (2004) Beijing China

- [4] E.Romanus, N.Matoussevitch, S.Prass, J.Heinrich, R.Müller, D.V.Berkov, H.Bönnemann, P.Weber, Appl. Organometal. Chem. 18 (2004) 548
- [5] E.Romanus, T.Köttig, G.Glöckel, S.Prass, J.Heinrich, D.V.Berkov, W.Weitschies, P.Weber, P.Seidel, will be submitted to Nanotechnology
- [6] F.Schmidl, P.Weber, T.Köttig, M.Büttner, S.Prass, C.Becker, J.Heinrich, M.Röder, K.Wagner, D.V.Berkov, P.Görnert, G.Glöckel, W.Weitschies, P.Seidel, submitted to J. Magn. Magn. Matter
- [7] E.Romanus, C.Groß, R.Kötitz, S.Prass, J.Lang, W.Weitschies, Magnetohydrodynamics No.2 (2000) 36

The modification of the dextran shell influences the interaction of magnetic nanoparticles with cells

Manuela Schwalbe, Marita Vetterlein, Tim Liebert*, Katharina Pachmann, Thomas Heinze, Klaus Höffken, Joachim H. Clement

Klinik für Innere Medizin II, Friedrich-Schiller-Universität Jena, Erlanger Allee 101, 07740 Jena
**Institut für Organische Chemie, Friedrich-Schiller-Universität Jena, Humboldt-Straße 10, 07743 Jena*

In hematology and oncology magnetic nanoparticles are used for labeling and detecting cells. During application the nanoparticles attach to the cell surface and could be incorporated into the cell. This attachment and subsequent incorporation is used for the separation of the cells in a magnetic field.

Our aim is the effective separation of tumor cells from leukocytes. It is known that most of the cancer patients do not die from the primary tumor but from distant metastases. Once the primary tumor is formed, cells may begin to break off from this tumor and travel to other parts of the body via the circulatory or lymph system. These disseminated tumor cells are able to form metastases. Our vision is to eliminate these cells quantitatively from the peripheral blood from tumor patients by magnetic separation to prevent metastasis formation.

The nanoparticles used in biomedical applications are covered with various coatings. The most popular is dextran and its derivatives. We used magnetic nanoparticles, which were coated with dextran (D), carboxy dextran (CD) and carboxymethyl dextran (CMD) in order to investigate the interaction of magnetic nanoparticles with tumor cells and leukocytes. We found, that nanoparticles with these shells interact with cells in a cell type specific manner. The tumor cells from the breast cancer cell line MCF and from the CML cell line K562 showed intense interaction with these particles whereas the leukocytes showed a lower tendency of interaction. Interestingly the differential interaction was intensified with the insertion of carboxy or carboxymethyl

groups in the dextran shell. These groups are charged and therefore the substitution of dextran with these residues alters the overall charge and in consequence may influence the interaction of the coated nanoparticles with cells. The application of CMD coated magnetic nanoparticles led to a better discrimination of tumor cells from leukocytes than D and CD coated particles. In order to optimize the charge of the CMD nanoparticles we investigated the role of the degree of substitution (DS) of dextran with carboxymethyl groups. We applied CMD nanoparticles with a DS of 0.8 and 1.6. With both types of CMD nanoparticles MCF-7 cells could be clearly discriminated from leukocytes after a 4 minute as well as 8 minute incubation and there was only a minor difference between these two preparations. But we found indices, that the molecular weight of the dextran and the pattern of functionalisation of the carboxymethyl groups have an influence on the interaction of the coated nanoparticles with the cells.

In conclusion we show that the CMD shell is an important prerequisite to separate tumor cells from leukocytes. We assume that the differential interaction of the used nanoparticles with the cells depends amongst others on the surface charge of the particles shell.

This work was supported by DFG priority program 1104, grant CL 202/1-2

Improvement of the separation of tumor cells from peripheral blood cells using magnetic nanoparticles

Manuela Schwalbe, Norbert Buske, Marita Vetterlein, Katharina Pachmann, Klaus Höffken, Joachim H. Clement

Klinik für Innere Medizin II, Friedrich-Schiller-Universität Jena, Erlanger Allee 101, 07740 Jena; MagneticFluids, Köpenicker Landstrasse 203; D-12437 Berlin

Circulating tumor cells are a key challenge in tumor therapy. Numerous approaches are on the way to achieve the elimination of these potential sources of metastasis formation. Antibody-directed magnetic cell sorting is supposed to enrich tumor cells with high selectivity, but low efficiency. The short term application of carboxymethyl dextran (CMD) coated magnetite/maghemite nanoparticles allow the discrimination of tumor cells from leukocytes. In the present work we show, that the interaction of CMD nanoparticles is cell-type specific and time-dependent. The breast cancer cell line MCF-7 and the CML cell line K-562 are characterized by a rapid and high interaction rate, whereas leukocytes exhibit a decelerated behavior. The addition of carboxymethyl dextran or glucose stimulated the magnetic labeling of leukocytes. The variation of the degree of substitution of dextran with carboxymethyl groups did not affect the labeling profile of leukocytes and MCF-7 cells. In order to verify the *in vitro* results whole blood samples from 13 cancer patients were analyzed *ex vivo* (Fig. 1). Incubation of the purified leukocyte fraction with CMD nanoparticles in the presence of low amounts of plasma reduced the overall cell content in the positive fraction. In contrast, the absolute number of residual tumor cells in the positive fraction was 90% of the initial amount.

This work was supported by DFG priority program 1104, grant CL 202/1-2

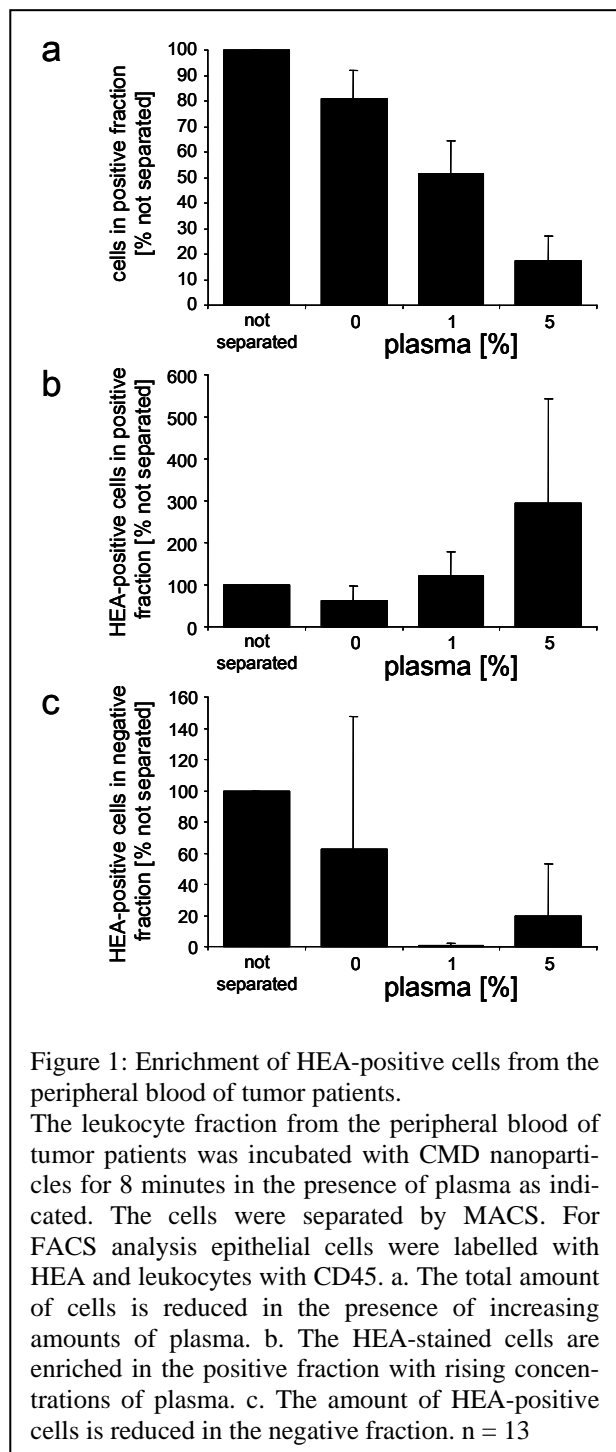


Figure 1: Enrichment of HEA-positive cells from the peripheral blood of tumor patients.

The leukocyte fraction from the peripheral blood of tumor patients was incubated with CMD nanoparticles for 8 minutes in the presence of plasma as indicated. The cells were separated by MACS. For FACS analysis epithelial cells were labelled with HEA and leukocytes with CD45. a. The total amount of cells is reduced in the presence of increasing amounts of plasma. b. The HEA-stained cells are enriched in the positive fraction with rising concentrations of plasma. c. The amount of HEA-positive cells is reduced in the negative fraction. n = 13

Quantitative magnetic assisted depletion of tumor cells from peripheral blood

Manuela Schwalbe, Marita Vetterlein, Katharina Pachmann, Klaus Höffken, Joachim H. Clement

Klinik für Innere Medizin II, Friedrich-Schiller-Universität Jena, Erlanger Allee 101, 07740 Jena;

Cancer is one of the main causes of death. Most of the cancer patients do not die from the primary tumor but from distant metastases which develop during the progression of cancer. Key events are the establishment of tumor vasculature and the invasion of tumor cells into the surrounding tissue and the circulation. These cells are suspected to be an origin of distant metastases. Therefore there is a need to eliminate these cells from the circulation especially from the peripheral blood.

We could show previously, that magnetic nanoparticles interact with human cells. The time-course of the labeling of tumor cells and leukocytes from peripheral blood differs dramatically within the first 20 minutes with a maximum discrepancy between 8 and 12 minutes. The difference could be further enhanced by addition of small amounts of human plasma (Schwalbe et al., 2005).

In order to verify the results obtained with tumor cell culture cells and isolated leukocytes we analyzed peripheral blood samples from 31 cancer patients (thereof 24 breast cancer). Leukocytes were prepared by erythrocyte lysis from whole blood samples from patients. Cells were inoculated with magnetic core/carboxymethyl-dextran nanoparticles with an average magnetite/maghemite core TEM-size varying between 3 and 15 nm for 8 minutes. The incubation medium (PBS/EDTA) contained 2.5% human plasma. Magnetically labeled cells were separated by MACS using a SuperMACS and MS columns. The separated cells were analyzed by FACS and Laser Scanning Cytometry (LSC). Tumor cells were detected with anti-human epithelium-antigen (HEA)-FITC.

The analysis of the patient samples showed that more than 80% of the total cell number was found in the flow through (negative fraction): breast cancer $80.3 \pm 9.5\%$, various tumors $80.6 \pm 7.4\%$. Next we determined the number of tumor cells in the flow through and the retained fraction (positive fraction) by HEA staining. Almost all tumor cells were held back in the separation column: breast cancer $97.1 \pm 5.9\%$, various tumors $95.6 \pm 6.4\%$. An important question is whether the leukocytes especially the lymphocytes are healthy and intact after incubation with magnetic nanoparticles and passage through the separation column. In a first attempt we studied the distribution and condition of the main subpopulations of leukocytes. The vast majority of lymphocytes was found in the negative fraction and was vital: breast cancer $91.9 \pm 5.6\%$, various tumors $84.0 \pm 9.1\%$.

In conclusion we show that our magnetic assisted tumor cell depletion procedure allows the effective labelling and quantitative separation of tumor cells from peripheral blood leukocytes.

This work was supported by DFG priority program 1104, grant CL 202/1-2

Schwalbe, M., Jörke, C., Buske, N., Höffken, K., Pachmann, K., Clement, J.H. (2005) *J. Magn. Mater.* 293: 433-437

Physiological and physical investigations concerning intraarterial Magnetic Drug Targeting

C. Seliger¹, R. Jurgons¹, S. Kolb¹, F. Wiekhorst², D. Eberbeck², L. Trahms², H. Iro¹, C. Alexiou¹

¹ *Department of otorhinolaryngology, head and neck surgery, University Erlangen-Nürnberg, Germany*

² *Physikalisch-Technische Bundesanstalt, Berlin, Germany*

Introduction

Magnetic drug targeting means the magnetic guided delivery of therapeutic agents to a specific body compartment [1,2]. Coated magnetic nanoparticles were used as carriers for this drug delivery system. The cytostatic drug mitoxantrone is bound to the active coating by an electrostatic binding. After intraarterial application of the drug loaded nanoparticle suspension these magnetic particles can be attracted by an external electromagnet positioned over the tumor region [3,4]. After a defined time the drug is released from the particle surface and infiltrates tumor tissue [5,6]. In an experimental tumor model total tumor remissions were achieved using only 20 % of the regular systemic drug concentration [1-3].

To avoid clearance of the majority of the carriers by the Retico-endothelial system the nanoparticles have to be applied via an intra-arterial injection in vivo [7-10]. This way of application is accompanied by a putative enhanced thrombotic risk. For the examination of potential thrombotic risk we evaluated an in vitro circulating vessel system, consisting of a circuit with blood like fluids and a intact bovine artery adjacent to the magnetic field. We performed our experiments with two different nanosized particle formulations. One consists of a magnetite core, covered by a phosphodextran shell. The second consists of citric acid as stabilising agent and as drug carrier molecule.

Material and Methods

This drug delivery system and its physiological compatibility is dependent on several physiological and physical parameters like the magnetic field gradient, blood flow or size, concentration and material of the particles. To examine these conditions we established an in vitro circulating system.

For his circulating system (figure 1) we used freshly isolated bovine femoral arteries. Small arteries outlets were ligated and the artery is mounted in a tempered circuit. As flow medium we used Krebs-Ringer buffer pH 7,4 substituted with 0,625 % Albumine. The arteries were placed near the tip of the electromagnet in the same manner as it was mounted for tumors. Nanoparticle suspension can be applied by a side inlet under pulsatile flow. Attraction of the particle on the vessel wall and in the vessel tissue was performed with a magnetic field gradient of 10 T/m.

After the magnetisation procedure the outflow was collected. Differences in particle agglomerate diameter were measured by Photon correlation spectroscopy. The particle concentration in different artery sections was examined by magnetorelaxometry and the infiltration of particles in the tissue was visualised by histological cross sections.

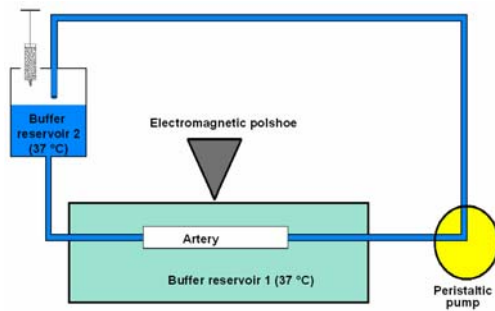


Figure 1: Schematic drawing of the in vitro circulating model

Results

Most of the particles were attracted in the artery wall segment next the magnetic tip, with a partial iron infiltration into the endothelium. Nevertheless for both particle formulation magnetic attraction under given conditions results in a significant particle diameter increase, indicating an adjustment of the applied magnetic field gradient for in vivo purposes.

Conclusions

This arterial in vitro model is a powerful tool for the investigation of nanoparticle suspension for pre-screening of different nanoparticle formulations and stability testing over given time period. Negative side effects are observable by this method before entering an animal model.

Acknowledgment

This research was supported by the priority program SPP1104 (AL 552/2) of the Deutsche Forschungsgemeinschaft.

References

- [1] Alexiou, C. et al., Locoregional cancer treatment with magnetic drug targeting. *Cancer Res*, 60: 6641-6648, 2000
- [2] Alexiou, C. et al., Magnetic drug targeting: Biodistribution and dependency on magnetic field strength in vitro. *Journal of*

Magnetism and Magnetic Materials 252:363-366, 2002

[3] Alexiou, C. et al., Magnetic Drug Targeting-Biodistribution of the magnetic carrier and the chemotherapeutic agent mitoxantrone after locoregional cancer treatment. *J Drug Target* 11:139-149, 2003

[4] Alexiou, C. et al., A high field gradient Magnet for Magnetic Drug Targeting. *IEEE Transactions on Applied Superconductivity*, 16:1527-1530, 2006

[5] Alexiou, C. et al., In vitro and in vivo investigations of targeted chemotherapy with magnetic particles. *Journal of Magnetism and Magnetic Materials* 252:363-366, 2005

[6] Alexiou C. et al., Targeting cancer cells: magnetic nanoparticles as drug carriers. *European Biophysics Journal with Biophysics Letters*, 35:446-450, 2006

[7] Alexiou, C. et al., Magnetic mitoxantrone nanoparticle detection by histology, x-ray and MRI after magnetic drug targeting. *Journal of Magnetism and Magnetic Materials*, 225:187-193, 2001

[8] Alexiou, C. et al., Therapeutic efficacy of ferrofluid bound anticancer agent. *Magneto hydrodynamics* 37:318-322, 2001

[9] Alexiou, C. et al., Magnetisches Drug Targeting – ein neuer Ansatz in der lokoregionären Tumorthherapie mit Chemotherapeutika. *HNO*, 53: 618-622, 2005

[10] C. Alexiou, C. et al., Magnetische Nanopartikel für die Chemotherapie. *Biomedizinische Technik* 49: 712-713, 2004

Quantification of magnetic nanoparticles in tissue demonstrated by magnetorelaxometry tomography

F. Wiekhorst¹, D. Eberbeck¹, U. Steinhoff¹, R. Jurgons², C. Seliger²
C. Alexiou², L. Trahms¹

¹Physikalisch-Technische Bundesanstalt, Berlin, Germany

²Head and Neck Surgery University Erlangen-Nürnberg, Germany

Introduction

Magnetic nanoparticles find wide application in medical diagnostics and therapy, examples are magnetic drug targeting, hyperthermia, magnetofection, and contrast agents in magnetic resonance imaging. For these applications it is of great importance to monitor and to control the accumulation of magnetic nanoparticles in the body regions of interest. In particular, quantitative information is essential for improving the therapeutic outcome.

Magnetorelaxometry (MRX) [1] is a technique to investigate with high sensitivity the properties of magnetic nanoparticle ensembles [2]. In the present work we describe a method to quantify the amount of magnetic nanoparticles in biological tissue by magnetorelaxometry. We illustrate the method by an application in magnetic drug targeting [3], where we determine the amount of magnetic nanoparticles in a squamous VX-2 carcinoma of a rabbit treated by locoregional chemotherapy using magnetic nanoparticles.

Magnetorelaxometry

In a typical magnetorelaxometry measurement, the sample containing magnetic nanoparticles is magnetized by a magnetic field of defined strength and duration. After the field is switched off, the decay of the sample magnetization is measured by a SQUID magnetic field sensor. The unwanted remanent background does not contribute to the relaxation signal. Usually, both relaxation mechanisms of the nano-

particle magnetization, the Brownian and the Néel relaxation, are present and the process with the shortest relaxation time will dominate the relaxation signal. After immobilizing the sample (freeze drying) the Brownian relaxation is suppressed, so that bound particles can be identified by their relaxation behavior [4].

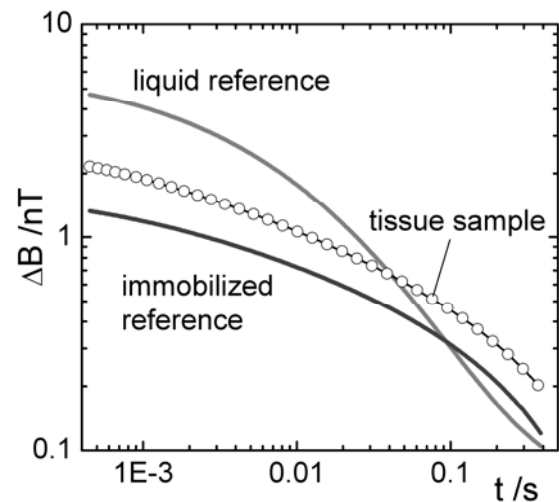


Fig. 1 MRX relaxation curves of liquid, immobilized reference, and tissue sample, respectively. Note the logarithmic scaling of the axes.

Quantification method

The basic procedure to quantify the amount of magnetic nanoparticles in tissue starts with the preparation of a set of reference samples and the characterization of their relaxation behavior in liquid and freeze dried state. Then, the relaxation curve of the tissue sample is compared to the shape of the reference curves in order to decide whether the particles in the tissue sample are immobilized or in solution. Accordingly, the quantification of the amount of

magnetic nanoparticles in the tissue sample is carried out by amplitude comparison with the corresponding reference curve.

In order to illustrate the method, we quantified the amount of magnetic nanoparticles in a squamous VX-2 carcinoma induced in a rabbit after magnetic drug targeting [5]. One ml of magnetic nanoparticles (target-MAG, chemicell, Berlin) in suspension were intraarterially administered and then attracted and concentrated by a high magnetic field gradient focused at the tumor region. After sacrificing the animal, the tumor was extracted and magnetorelaxometry of the tumor tissue was performed.

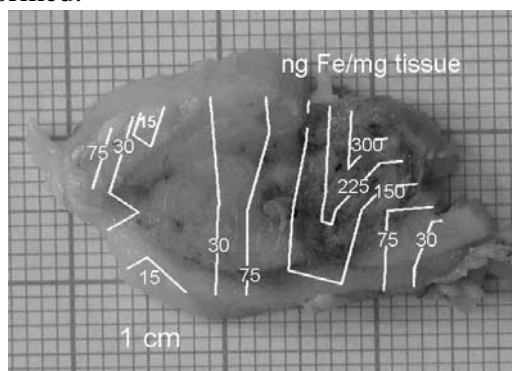


Fig. 2 Relative mass of magnetic nanoparticles throughout a slice of VX-2 squamous carcinoma.

Results

Figure 1 shows the different relaxation signals of the liquid and the immobilized reference sample, and of the tissue sample. From the shape of the tissue sample curve we can see that the magnetic nanoparticles in the tissue are immobilized.

We quantified the distribution of magnetic nanoparticles within a small slice of the extracted tumor by dividing the slice into a number of small pieces and investigating the magnetic relaxation piece by piece. According to the procedure described above, the amount of magnetic nanoparticles in each piece was quantified.

The results were used to reconstruct a map of the magnetic nanoparticle concentration across the tumor slice as shown in Fig. 2. The relative mass of magnetic nanoparticles could be resolved down to 10 ng per mg tissue.

Conclusion and Outlook

Magnetorelaxometry is a fast and integral technique for quantification of the relative mass of magnetic nanoparticles in tissue. Quantification is reached by relating the tissue relaxation curves to reference curves with identical relaxation behavior.

In general, this method is not limited to in-vitro samples, but suited for in-vivo applications as well. For this purpose, we presently develop a dedicated magnetorelaxometry device for in-vivo measurements in small animals [6]. This device contains an integrated superconducting Niobium shield against magnetic distortions and a multichannel SQUID sensor array for the localization and quantification of magnetic nanoparticle accumulations. First magnetorelaxometry experiments with this device could successfully be performed in a real laboratory environment.

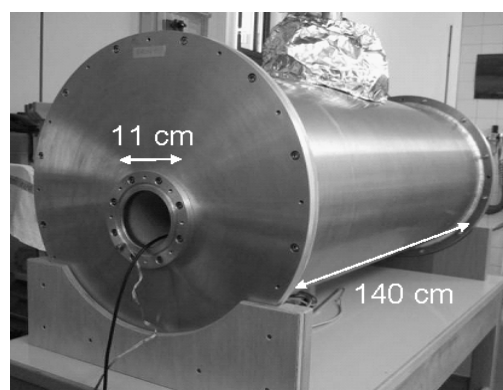


Fig. 3 Dedicated magnetorelaxometry device for in-vivo measurements in small animals.

Acknowledgments

This research is partially funded by the BMBF project Nanomagnetomedizin (FKZ 13N8535) and the DFG priority program 1104. Animal experiments were approved by the local ethics committee.

References

- [1] R. Koetitz et al. *JMMM* **149** (1995), 42-46
- [2] D. Eberbeck et al. *MHD* **39** (2003), 77-83
- [3] C. Alexiou et al. *HNO* **53** (2005), 618-622
- [4] D. Eberbeck et al. *Appl Organometal Chem* **18** (2004), 542-547
- [5] C. Alexiou et al. *J Drug Target* **11** (2003), 139-149
- [6] F. Wiekhorst et al. *Biomed Tech* **50** (1/1) (2005), 609-610

Temperature limited heating by magnetic nanoparticles

M. Zeisberger, R. Müller, H. Steinmetz, R. Hergt, W. Gawalek

Institut für Physikalische Hochtechnologie, Albert–Einstein–Str. 9, D–07745 Jena

Introduction

The effect of heating of magnetic nanoparticles in an ac magnetic field can be used for medical and technical applications, e. g. hyperthermia for cancer treatment or hardening of glue. In all applications a well defined and homogeneous temperature distribution is required. However, with particles of constant specific heating power (SHP) this requirement is hard to fulfill if the particle distribution is not homogeneous or the object to be heated has a complicated geometry rather than a spherical volume fraction. A possible solution to this problem is to use particles having a Curie temperature T_C close to the operation temperature [1], e. g. substituted La-manganese, which provides a limitation of the heating process to $T \leq T_C$.

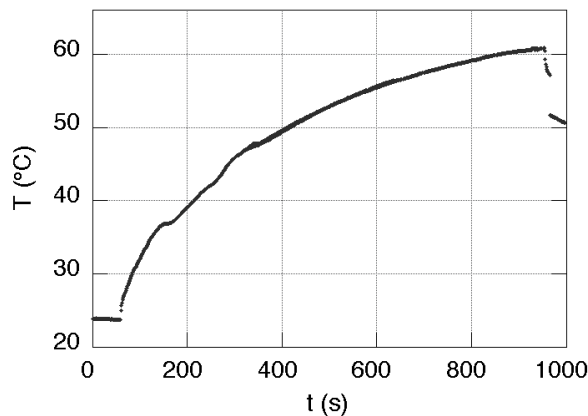


Figure 1: Heat up curve of the fluid

Preparation and Measurements

The preparation of $\text{La}_{0.7}\text{Sr}_{0.3}\text{MnO}_3$ -powder

was carried out by crystallization from La_2O_3 - SrO-MnO_4 - B_2O_3 -glass during a temperature treatment and subsequent dissolving of the matrix [2]. The separated powders show magnetization values up to $49 \text{ Am}^2/\text{kg}$. The mean particle size of the used powder (powder 1) was about 45 nm calculated from the specific surface value assuming spheres. The Curie temperature is about 93°C .

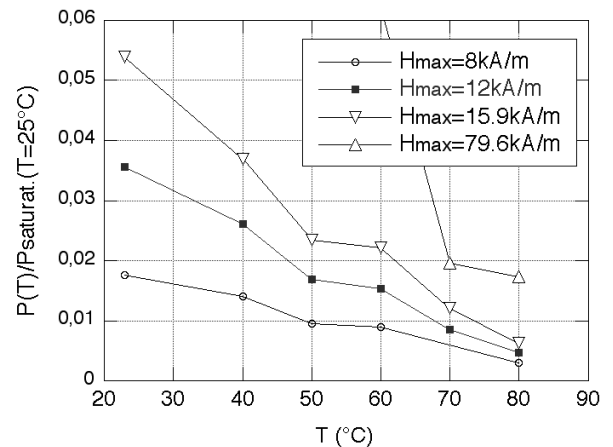


Figure 2: Normalized hysteresis losses vs. temperature of the particles

An ethylene glycol based ferrofluid was prepared from powder 1 to avoid influences of an evaporation on the heating near the Curie temperature by dispersing a freeze dried powder in the carrier liquid by ultrasonic treatment. The ferrofluid was stable over a period of some hours. In order to investigate the heating effect the fluid was placed into a coil generating an ac field of 400 kHz and 24.5 kA/m and the temperature was measured using a thermocouple. The measured

data are shown in Fig. 1. The SHP obtained from these data is 21 W/g.

Investigations of hysteresis losses at different temperatures and different maximum fields were done on $\text{La}_{0.7}(\text{Sr},\text{Ba})_{0.3}\text{MnO}_3$ powder prepared by conventional solid state reaction method from La_2O_3 and Sr-, Ba- and Mn-carbonates. The data are shown in Fig. 2. A Curie temperature of about 82°C can be estimated from these data.

Simulation of the temperature distribution

In order to get information about the required SHP and particle concentrations for T_C limited heating we use a model similar to that presented in [3], but we will use a temperature dependent heating power here. In a medium with homogeneous heat conductivity λ , a certain mass per volume C_m of magnetic particles with the SHP $P_m(T)$ being homogeneously distributed inside a spherical volume of radius R_0 . The stationary equation of heat transport for this system is

$$\frac{1}{R^2} \frac{\partial}{\partial R} \left(R^2 \frac{\partial T}{\partial R} \right) = \begin{cases} -P_V(T)/\lambda & \text{if } R \leq R_0 \\ 0 & \text{if } R \geq R_0 \end{cases} \quad (1)$$

where T is the absolute temperature and $P_V = P_m C_m$ the heating power per volume. For the temperature dependence of the SHP we assume a linear relation which is in agreement with the experimental data (Fig. 2)

$$P_m(T) = P_{m0} \frac{T_C - T}{T_C - T_0} \quad (2)$$

where T_0 and T_C are the initial and the Curie temperature and P_{m0} is the SHP at T_0 . In order to obtain a more general numerical solution we will use a reduced temperature $t = (T_0 - T)/(T_0 - T_C)$ and a reduced radius coordinate $r = R/R_0$. With this substitutions we get the following equations for the problem

$$\frac{1}{r^2} \frac{\partial}{\partial r} \left(r^2 \frac{\partial t}{\partial r} \right) = \begin{cases} -S(1-t) & \text{if } r \leq 1 \\ 0 & \text{if } r \geq 1 \end{cases} \quad (3)$$

with the heat source parameter

$$S = \frac{R_0^2 P_{m0} C_m}{(T_C - T_0) \lambda} \quad (4)$$

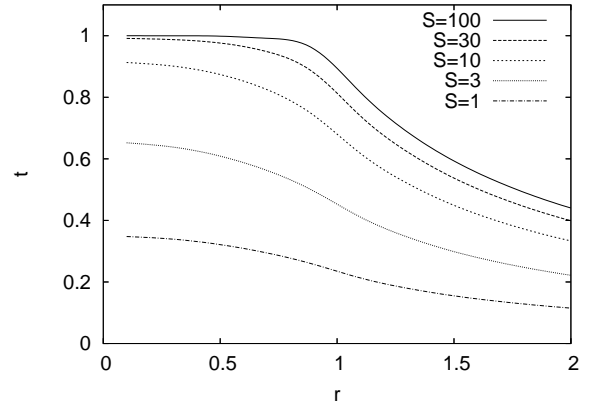


Figure 3: Reduced temperature vs. reduced radius for different values of the source parameter S

Equation 3 was numerically solved for different source parameters S using the FEM-LAB software. The result is shown in Fig. 3.

Acknowledgments

The work was supported by the DFG under contract no. Ga 662/3-1 and HE 2878/9-2.

References

- [1] S. Vasseur et al., J. Magn. Magn. Mater., 302 (2005) 315-320
- [2] R. Müller et al., J. Europ. Cer. Soc. 21 (2001) 1941-1944
- [3] W. Andrä et al., J. Mag. Mag. Mat. 194 (1999) 197-203

List of Participants

Christoph Alexiou

Klinik und Poliklinik für
Hals-, Nasen- und Ohrenkrankhe
Waldstr. 1
91054 Erlangen
Tel.: 09131-8534769
Fax: 09131-8534828
E-mail: C.Alexiou@web.de

Bastian Arlt

Institut für Theoretische Physik
TU Berlin
Hardenbergstr. 36
10623 Berlin
Tel.: 030-31423461
Fax: 030-31421130
E-mail: basti@itp.physik.tu-berlin.de

Konstanze Aurich

Institut für Pharmazie der EMAU
Biopharmazie und Pharmazeutische
Technologie
Friedrich-Ludwig-Jahn-Str.17
17487 Greifswald
Tel.: 03834-864808
Fax: 03834-864886
E-mail: aurich@uni-greifswald.de

Achim Beetz

Experimentalphysik 5
Universität Bayreuth
95440 Bayreuth
Tel.: 0921-563340
Fax: 0921-563647
E-mail: Achim.Beez@uni-bayreuth.de

Dmitri Berkov

INNOVENT e.V.
Prüssingstr. 27B
07745 Jena
Tel.: 03641-282537
Fax: 03641-282530
E-mail: db@innovent-jena.de

Stefan Bohlius

MPI für Polymerforschung
Postfach 3148
55021 Mainz
Tel.: 06131-379147
Fax: 06131-379340
E-mail: bohlius@mpip-mainz.mpg.de

Valter Böhm

Technische Universität Ilmenau
Technische Mechanik
PF 100565
98684 Ilmenau
Tel.: 03677-691845
Fax: 03677-691823
E-mail: valter.boem@tu-ilmenau.de

Jens Bolle

Institut für Technische Chemie,
Bereich Wasser- und Geotechnologie
Forschungszentrum Karlsruhe
Herrmann-von-Helmholtz-Platz 1
76344 Eggenstein-Leopoldshafen
Tel.: 07247-822836
E-mail: Jens.Bolle at itc-wgt.fzk.de

Dmitry Borin

Technische Universität Dresden
Fakultät Maschinenwesen
Lehrstuhl für Magnetofluidynamik
01062 Dresden
Tel.: 0351-46332037
Fax: 0351-46333384
E-mail: Dmitry.Borin@tu-dresden.de

Norbert Buske

MagneticFluids
Köpenicker Landstr. 203
12437 Berlin
Tel.: 030-53007805
E-mail: n.buske@magneticfluids.de

Joan J. Cerda

FIAS
JW Goethe - Universität
Max-von-Laue Strasse 1
D-60438 Frankfurt/Main
Tel.: 069-79847536
Fax: 069-79847611
E-mail: j.cerda@fias.uni-frankfurt.de

Nelica Ciobanu

Physik-Department E17 der TU München
James Franck Straße
85747 Garching
Tel.: 089-28912558
Fax: 089-28912548
E-mail: nciobanu@ph.tum.de

Joachim Clement

Klinik für Innere Medizin II
Friedrich-Schiller-Universität Jena
Erlanger Allee 101
07740 Jena
Tel.: 03641-9325820
Fax: 03641-9325822
E-mail: Joachim.Clement@med.uni-
jena.de

Eric Coquelle

Institut für Theoretische Physik
TU Berlin
Hardenbergstr. 36
10623 Berlin
Tel.: 030-31425225
Fax: 030-31421130
E-mail: coquelle@itp.physik.tu-berlin.de

Silvio Dutz

IPHT
Albert-Einstein-Str. 9
07745 Jena
Tel.: 03641-206136
Fax: 03641-206199
E-mail: silvio.dutz@iph-t-jena.de

Dietmar Eberbeck

Physikalisch-Technische Bundesanstalt
Berlin
Abbestr. 2-12
10587 Berlin
Tel.: 030-34817208
Fax: 030-34817361
E-mail: Dietmar.Eberbeck@ptb.de

Harald Engler

Technische Universität Dresden
Fakultät Maschinenwesen
Lehrstuhl für Magnetofluidynamik
01062 Dresden
Tel.: 0351-46334353
Fax: 0351-46333384
E-mail: Harald.Engler@tu-dresden.de

Amir Fahmi

Senior Research Fellow
School of Mechanical, Materials and
Manufacturing Engineering
The University of Nottingham
University Park
Nottingham NG7 2RD
UK
Tel.: 1159514066
Fax: 1159514140
E-mail: amir.fahmi@nottingham.ac.uk

Ubbo Felderhof

Institut für Theoretische Physik A
RWTH Aachen
Templergraben 55
52056 Aachen
Tel.: 0241-8027019
Fax: 0241-8022188
E-mail: ufelder@physik.rwth-aachen.de

Birgit Fischer

Experimentalphysik 5
Universität Bayreuth
95440 Bayreuth
Tel.: 0921-563336
Fax: 0921-563647
E-mail: Birgit.Fischer@uni-bayreuth.de

Danielle Franke

Schering AG
CRBA Diagnostics &
Radiopharmaceuticals
13342 Berlin
Germany
Tel.: 030-46818960

Natalia Frickel

Institut für Organische und
Makromolekulare Chemie II
Heinrich-Heine-Universität Düsseldorf
Gebäude 26.33 Raum 00.30
Universitätsstr. 1
D-40225 Düsseldorf
Tel.: 0211-8124820
Fax: 0211-8125840

Stefan Fruhner

Institut für Theoretische Physik
TU Berlin
Hardenbergstr. 36
10623 Berlin
Tel.: 030-31423461
Fax: 030-31421130
E-mail: stefan@itp.physik.tu-berlin.de

Nicole Gehrke

Schering AG
CRBA Diagnostics &
Radiopharmaceuticals
13342 Berlin
Germany
Tel.: 030-46818960
E-mail: Nicole.Gehrke@schering.de

Thorsten Gelbrich

Institut für Organische und
Makromolekulare Chemie II
Heinrich-Heine-Universität Düsseldorf
Gebäude 26.33 Raum 00.35
Universitätsstr. 1
D-40225 Düsseldorf
Tel.: 0211-8114822
Fax: 0211-8115840
E-mail: juppschwupp@gmx.de

Gunnar Glöckl

Institut für Pharmazie der EMAU
Biopharmazie und Pharmazeutische
Technologie
Friedrich-Ludwig-Jahn-Str.17
17487 Greifswald
Tel.: 03834-864857
Fax: 03834-864886
E-mail: gunnar.gloeckl@uni-
greifswald.de

Christian Gollwitzer

Experimentalphysik 5
Universität Bayreuth
95440 Bayreuth
Tel.: 0921-553337
Fax: 0921-553647
E-mail: Christian.Gollwitzer@uni-
bayreuth.de

Peter Görnert

INNOVENT e.V.
Prüssingstr. 27B
07745 Jena
Tel.: 03641-282515
Fax: 03641-282530
E-mail: pg@innovent-jena.de

Stefan Grandner

Institut für Theoretische Physik
TU Berlin
Hardenbergstr. 36
10623 Berlin
Tel.: 030-31424410
Fax: 030-31421130
E-mail: grandner@physik.tu-berlin.de

Jan Magnus Guldbakke

Technische Universität Braunschweig
Institut für Werkzeugmaschinen und
Fertigungstechnik
Langer Kamp 19b
38106 Braunschweig
Tel.: 0531-3917158
Fax: 0531-3915842
E-mail: jm.guldbakke@iwf.ing.tu-bs.de

Wolfgang Haase

TU Darmstadt
Institut für Physikalische Chemie
Petersenstraße 20
64287 Darmstadt
Tel.: 06151-163398
Fax: 06151-164924
E-mail: haase@chemie.tu-darmstadt.de

Urs Hafeli

Division of Pharmaceutics and
Biopharmaceutics
Faculty of Pharmaceutical Sciences
The University of British Columbia
Room 63, 2146 East Mall
Vancouver, B.C. V6T 1Z3 CANADA
Tel.: 001-604-8227133
Fax: 001-604-8223035
E-mail: uhafeli@interchange.ubc.ca

Sebastian Heidenreich

Institut für Theoretische Physik
TU Berlin
Hardenbergstr. 36
10623 Berlin
Tel.: 030-31424253
Fax: 030-31421130
E-mail: sebastian@physik.tu-berlin.de

Erik Heim

TU Braunschweig
Institut für Elektrische Messtechnik
und Grundlagen der Elektrotechnik
Hans-Sommer-Strasse 66
38106 Braunschweig
Tel.: 0531-3913876
Fax: 0531-3915768
E-mail: e.heim@tu-bs.de

Dirk Heinrich

Institut für Festkörperphysik
Technische Universität Berlin
Hardenbergstr. 36
10623 Berlin
Tel.: 030-31422476
Fax: 030-31427705
E-mail: dhein@physik.TU-Berlin.DE

Rolf Hempelmann

Universität des Saarlandes
Physikalische Chemie
Gebäude 9.2
D-66123 Saarbrücken
Tel.: 0681-3024750
Fax: 0681-3024759
E-mail: hempelmann@rz.uni-sb.de

Rudolf Hergt

IPHT
Albert-Einstein-Str. 9
07745 Jena
Tel.: 03641-206133
Fax: 03641-206799
E-mail: rudolf.hergt@ipht-jena.de

Siegfried Hess

Institut für Theoretische Physik
TU Berlin
Hardenbergstr. 36
10623 Berlin
Tel.: 030-31423763
Fax: 030-31421130
E-mail: s.hess@physik.tu-berlin.de

Ingrid Hilger

Institut für Diagnostische und
Interventionelle Radiologie
Klinikum der F.S.U. Jena
Erlanger Alle 101
07740 Jena
Tel.: 03641-9325921
Fax: 03641-9325922
E-mail: ingrid.hilger@med.uni-jena.de

Michael Hipper

TU Berlin
Institut für Werkzeugmaschinen
und Fabrikbetrieb
Pascalstr. 8-9
10587 Berlin
Tel.: 030-31421791
Fax: 030-31424456
E-mail: hipper@iwf.tu-berlin.de

Christian Holm

FIAS
JW Goethe - Universität
Max-von-Laue Strasse 1
D-60438 Frankfurt/Main
Tel.: 069-79847505
Fax: 069-79847611
E-mail: C.holm@fias.uni-frankfurt.de

Verena Holzapfel

Organische Chemie III -
Makromolekulare Chemie
Universität Ulm
Albert-Einstein-Allee 11
89081 Ulm
Tel.: 0731-5022871
Fax: 0731-5022883
E-mail: verena.holzapfel@uni-ulm.de

Patrick Ilg

Institut f. Polymere
Wolfgang-Pauli-Str. 10
ETH Zürich, HCI H 541
CH-8093 Zürich
Tel.: (41) 44-632839
Fax: (41) 44-6321076
E-mail: patrick.ilg@mat.ethz.ch

Larisa Iskakova

Ural State University
Department of Mathematical Physics
620083, Lenin Av. 51
Ekaterinburg, Russia
Tel.: 007-3433507541
Fax: 007-3433507401
E-mail: Larisa.Iskakova@usu.ru

Alexej Ivanov

Ural State University
Department of Mathematical Physics
620083, Lenin Av. 51
Ekaterinburg, Russia
Tel.: 007-3433507541
Fax: 007-3433507401
E-mail: Alexey.Ivanov@usu.ru

Roland Jurgons

Klinik und Poliklinik für
Hals-, Nasen- und Ohrenkrankheiten
Waldstr. 1
91054 Erlangen
Tel.: 09131-8534769
Fax: 09131-8534828
E-mail: roland_jurgons@web.de

Andreas Kaiser

Institut für Organische und
Makromolekulare Chemie II
Heinrich-Heine-Universität Düsseldorf
Gebäude 26.33 Raum 00.35
Universitätsstr. 1
D-40225 Düsseldorf
Tel.: 0211-8114822
Fax: 0211-8115840
E-mail: andreaskaiser1@gmx.de

Martin Kammel

Hahn-Meitner-Institut Berlin
Glienickestr. 100
14109 Berlin
Tel.: 030-80623099
Fax: 030-80623059
E-mail: kammel@hmi.de

Sofia Kantorovich

Ural State University
Department of Mathematical Physics
620083, Lenin Av. 51
Ekaterinburg, Russia
Tel.: 007-3433507541
Fax: 007-3433507401
E-mail: sue_kantorovich@yahoo.com

Melanie Kettering

Institut für Diagnostische und
Interventionelle Radiologie
Klinikum der F.S.U. Jena
Erlanger Alle 101
07740 Jena
Tel.: 03641-9325920
Fax: 03641-9325922
E-mail:
MELANIE.KETTERING@med.uni-
jena.de

Holger Knieling

Experimentalphysik 5
Universität Bayreuth
95440 Bayreuth
Tel.: 0921-553338
Fax: 0921-553647
E-mail: holger.knieling@uni-bayreuth.de

Robert Krauß

Experimentalphysik 5
Universität Bayreuth
95440 Bayreuth
Tel.: 0921-553311
Fax: 0921-553647
E-mail: Robert.Krauss@uni-bayreuth.de

Marina Krekhova

Universitaet Bayreuth, Makromolekulare
Chemie I
D-95440 Bayreuth, Germany
Tel.: 0921-552530
Fax: 0921-552788
E-mail: Marina.Krehova@uni-
bayreuth.de

Walter Lachenmeier

DFG
Kennedyallee 40
53175 Bonn
Tel.: 0228-8852281
Fax: 0228-8852777
E-mail: walter.lachenmeier@dfg.de

Katharina Landfester

Organische Chemie III -
Makromolekulare Chemie
Universität Ulm
Albert-Einstein-Allee 11
89081 Ulm
Tel.: 0731-5022870
Fax: 0731-5022883
E-mail: katharina.landfester@uni-ulm.de

Claus Lang

MPI für Marine Mikrobiologie
Celsiusstr. 1
28359 Bremen
Tel.: 0421-2028740
Fax: 0421-2028580
E-mail: clang@mpi-bremen.de

Adrian Lange

Fraunhofer Institute for Material and
Beam Technology
Winterbergstrasse 28
D-01277 Dresden
Tel.: 0351-2583328
Fax: 0351-2583300
E-mail: Adrian.Lange@iws.fraunhofer.de

Günter Lattermann

Universitaet Bayreuth, Makromolekulare
Chemie I
D-95440 Bayreuth, Germany
Tel.: 0921-553290
Fax: 0921-553206
E-mail: g.lattermann@uni-bayreuth.de

Andreas Leschhorn

Institut für Theoretische Physik
Universität des Saarlandes
66041 Saarbrücken
Germany
Tel.: 0681-3024217
Fax: 0681-3024316
E-mail: andy@lusi.uni-sb.de

Manfred Lücke

Universität des Saarlandes
Theoretische Physik, Geb. 38
66041 Saarbrücken
Tel.: 0681-3023402
Fax: 0681-3024316
E-mail: luecke@lusi.uni-sb.de

Frank Ludwig

TU Braunschweig
Institut für Elektrische Messtechnik
und Grundlagen der Elektrotechnik
Hans-Sommer-Strasse 66
38106 Braunschweig
Tel.: 0531-3913863
Fax: 0531-3915768
E-mail: f.ludwig@tu-bs.de

Christian Märkert

Universität des Saarlandes
Physikalische Chemie
Gebäude 9.2
D-66123 Saarbrücken
Tel.: 0681-3023850
Fax: 0681-3024759
E-mail: c.maerkert@mx.uni-saarland.de

Nina Matoussevitch

Division of Chemical-Physical
Processing
Institut für Technische Chemie (ITC-
CPV)
Forschungszentrum Karlsruhe GmbH
Herman-von-Helmholtz-Platz 1
76344 Eggenstein-Leopoldshafen,
Germany
Tel.: 7247-824320
Fax: 7247-822244
E-mail: nina.matoussevitch@itc-
cpv.fzk.de

Pascal Matura

Institut für Theoretische Physik
Universität des Saarlandes
66041 Saarbrücken
Germany
Tel.: 0681-3023442
Fax: 0681-3024316
E-mail: pama@lusi.uni-sb.de

Michael Meier

DFG
Kennedyallee 40
53175 Bonn
Tel.: 0228-8852281
Fax: 0228-8852777
E-mail: michael.meier@dfg.de

Vladislav Mekhonoshin

Institut für Theoretische Physik
Universität des Saarlandes
PF 151150
D-66041 Saarbrücken
Tel.: 0681-30264017
Fax: 0681-3024316
E-mail: vladik@lusi.uni-sb.de

Markus Mertz

Institut für Theoretische Physik
Universität des Saarlandes
66041 Saarbrücken
Germany
Tel.: 0681-3024217
Fax: 0681-3024316
E-mail: maggu@lusi.uni-sb.de

Robert Müller

IPHT
Albert-Einstein-Str. 9
07745 Jena
Tel.: 03641-206109
Fax: 03641-206199
E-mail: robert.mueller@ipht-jena.de

Arnim Nethe

BTU-Cottbus
Universitätsplatz 3-4
03044 Cottbus
Tel.: 0355-694139
Fax: 0355-694137
E-mail: arnim.nethe@tet.tu-cottbus.de

Stefan Odenbach

Technische Universität Dresden
Fakultät Maschinenwesen
Lehrstuhl für Magnetofluidynamik
01062 Dresden
Tel.: 0351-46332062
Fax: 0351-46333384
E-mail: stefan.odenbach@tu-dresden.de

Katharina Pachmann

Klinik für Innere Medizin II
Friedrich-Schiller-Universität Jena
Erlanger Allee 101
07740 Jena
Tel.: 03641-9325820
Fax: 03641-9325822
E-mail: katharina.pachmann@med.uni-jena.de

Jens Patzke

Technische Thermodynamik
Universität Bremen, Fachbereich 4
Badgasteiner Str. 1
D-28359 Bremen
Tel.: 0421-2187855
Fax: 0421-2187555
E-mail: jpatzke@uni-bremen.de

Harald Pleiner

MPI für Polymerforschung
Ackermannweg 10
55128 Mainz
Tel.: 06131-379246
Fax: 06131-379340
E-mail: pleiner@mpip-mainz.mpg.de

Jana Popp

Technische Universität Ilmenau
Technische Mechanik
PF 100565
98684 Ilmenau
Tel.: 03677-691845
Fax: 03677-691823
E-mail: jana.popp@stud.tu-ilmenau.de

Sylvain Prévost

Institut für Chemie - Technische
Universität Berlin
Strasse des 17. Juni 124
D-10623 Berlin
Tel.: 030-31422750
Fax: 030-31426602
E-mail: prevost.sylvain@gmail.com

Helene Rahn

Technische Universität Dresden
Fakultät Maschinenwesen
Lehrstuhl für Magnetofluidynamik
01062 Dresden
Tel.: 0351-46332068
Fax: 0351-46333384
E-mail: Helene.Rahn@tu-dresden.de

Bernd Rathke

Technische Thermodynamik
Universität Bremen, Fachbereich 4
Badgasteiner Str. 1
D-28359 Bremen
Tel.: 0421-2183334
Fax: 0421-2187555
E-mail: brathke@uni-bremen.de

Matthias Reindl

Technische Universität Dresden
Fakultät Maschinenwesen
Lehrstuhl für Magnetofluidynamik
01062 Dresden
Tel.: 0351-46339868
Fax: 0351-46333384
E-mail: Matthias.Reindl@tu-dresden.de

Reinhard Richter

Experimentalphysik 5
Universität Bayreuth
95440 Bayreuth
Tel.: 0921-553351
Fax: 0921-553647
E-mail: reinhard.richter@uni-bayreuth.de

Dennis Rührmer

TU Braunschweig
Institut für Elektrische Messtechnik und
Grundlagen der Elektrotechnik
Hans-Sommer-Str. 66
38106 Braunschweig
Tel.: 0531-3913879
Fax: 0531-3915768
E-mail: d.ruehmer@tu-bs.de

Andrey Ryskin

MPI für Polymerforschung
Ackermannweg 10
55128 Mainz
Tel.: 06131-379165
Fax: 06131-379340
E-mail: ryskin@mpip-mainz.mpg.de

Annette Schmidt

Institut für Organische und
Makromolekulare Chemie II
Heinrich-Heine-Universität Düsseldorf
Gebäude 26.33 Raum 00.30
Universitätsstr. 1
D-40225 Düsseldorf
Tel.: 0211-8114820
Fax: 0211-8115840
E-mail: Schmidt.Annette@uni-duesseldorf.de

Rudi Schmitz

Institut für Theoretische Physik C
RWTH Aachen
Templergraben 55
52056 Aachen
Tel.: 0241-8027023
Fax: 0241-8022188
E-mail: rschmitz@physik.rwth-aachen.de

Dirk Schüller

MPI für Marine Mikrobiologie
Celsiusstr. 1
28359 Bremen
Tel.: 0421-2028746
Fax: 0421-2028580
E-mail: dschuele@mpi-bremen.de

Manuela Schwalbe

Klinik für Innere Medizin II
Friedrich-Schiller-Universität Jena
Erlanger Allee 101
07740 Jena
Tel.: 03641-9325820
Fax: 03641-9325822
E-mail: manu.schwalbe@med.uni-jena.de

Christian Seliger

Klinik und Poliklinik für
Hals-, Nasen- und Ohrenkranke
Waldstr. 1
91054 Erlangen
Tel.: 09131-8544769
Fax: 09131-8544828
E-mail: cseliger2004@yahoo.de

Hamid Shahnazian

Technische Universität Dresden
Fakultät Maschinenwesen
Lehrstuhl für Magnetofluidynamik
01062 Dresden
Tel.: 0351-46334353
Fax: 0351-46333384
E-mail: hamid.shahnazian@tu-dresden.de

Klaus Stierstadt

Ludwig-Maximilians Universität München
Sektion Physik
Schellingstr. 4
80799 München
Tel.: 089-21802762
Fax: 089-21803391
E-mail: geschaefsstelle@physik.uni-muenchen.de

Detlef Stock

INNOVENT e.V.
Prüssingstr. 27B
07745 Jena
Tel.: 03641-282537
Fax: 03641-282530
E-mail: DS@innovent-jena.de

Andre Thess

TU Ilmenau
Maschinenbau
Postfach 100565
98684 Ilmenau
Tel.: 03677-692445
Fax: 03677-691281
E-mail: thess@tu-ilmenau.de

Lutz Tobiska

Otto-v.-Guericke Universität Magdeburg
Institut für Analysis und Numerik
PF 4120
39016 Magdeburg
Tel.: 0391-6718650
Fax: 0391-6718073
E-mail: tobiska@mathematik.uni-
magdeburg.de

Lutz Trahms

Physikalisch-Technische Bundesanstalt
Berlin
Abbestr. 2-12
10587 Berlin
Tel.: 030-34817213
Fax: 030-34817361
E-mail: lutz.trahms@ptb.de

Sylvia Türk

Technische Universität Dresden
Fakultät Maschinenwesen
Lehrstuhl für Magnetofluidynamik
01062 Dresden
Tel.: 0351-46334819
Fax: 0351-46333384
E-mail: Sylvia.Türk@tu-dresden.de

Kerstin Wagner

INNOVENT e.V.
Bereich Biomaterialien
Prüssingstr. 27b
07745 Jena
Tel.: 03641-282555
Fax: 03641-282530
E-mail: KW@innovent-jena.de

Joachim Wagner

Universität des Saarlandes
Physikalische Chemie
Gebäude 9.2
D-66123 Saarbrücken
Tel.: 0681-3023229
Fax: 0681-3024759
E-mail: j.wagner@mx.uni-saarland.de

Albrecht Wiedenmann

Hahn-Meitner-Institut Berlin
Glienickestr. 100
14109 Berlin
Tel.: 030-80622283
Fax: 030-80623059
E-mail: wiedenmann@hmi.de

Frank Wiekhorst

Physikalisch-Technische Bundesanstalt
Berlin
Abbestr. 2-12
10587 Berlin
Tel.: 030-34817347
Fax: 030-34817361
E-mail: Frank.Wiekhorst@ptb.de

Stefan Will

Technische Thermodynamik
Universität Bremen, Fachbereich 4
Badgasteiner Str. 1
D-28359 Bremen
Tel.: 0421-2182229
Fax: 0421-2187555
E-mail: swill@uni-bremen.de

Igor Zeidis

Technische Universität Ilmenau
Technische Mechanik
PF 100565
98684 Ilmenau
Tel.: 03677-692474
Fax: 03677-691823
E-mail: igor.zeidis@tu-ilmenau.de

Matthias Zeisberger

IPHT
Albert-Einstein-Str. 9
07745 Jena
Tel.: 03641-206107
Fax: 03641-206199
E-mail: matthias.zeisberger@ipht-
jena.de

Klaus Zimmermann

Technische Universität Ilmenau
Technische Mechanik
PF 100565
98684 Ilmenau
Tel.: 03677-692474
Fax: 03677-691823
E-mail: klaus.zimmermann@tu-
ilmenau.de

Andrey Zubarev

Ural State University
Department of Mathematical Physics
620083, Lenin Av. 51
Ekaterinburg, Russia
Tel.: 007-3433507541
Fax: 007-3433507401
E-mail: Andrey.Zubarev@usu.ru

The workshop is sponsored by

**Deutsche
Forschungsgemeinschaft**

DFG

within the frame of the
priority program 1104
"Colloidal Magnetic Fluids"

